RELATIONS BETWEEN MICROSTRUCTURAL DEVELOPMENT AND RHEOLOGICAL PROPERTIES IN POLYMER NANO-COMPOSITES

Thèse

MAHI HASSANABADI HOJJAT

Doctorat en génie chimique
Philosophiae Doctor (Ph.D.)

Québec, Canada

Résumé

Cette thèse porte principalement sur la compréhension des relations entre la microstructure et les propriétés rhéologiques des nano-composites à base d'un copolymère d'éthylène-acétate de vinyle (EVA).

La première partie de l'étude concerne les nano-composites d'EVA avec de la cellulose nanocrystalline (NCC). Cette partie cherche à inférer la structure d'échantillons inconnus à l'aide de mesures rhéologiques. En analysant les propriétés obtenues par des mesures rhéologiques en cisaillement et en élongation, les principaux mécanismes étant à l'origine du renforcement de ces nano-composites sont étudiés en détail.

Dans la deuxième partie du travail, on s'intéresse aux nano-composites contenant des particules isométriques ($CaCO_3$) et anisométrique (argile). L'objectif est de déterminer l'effet de variables structurelles comme les interactions polymère-particule et particule-particule, l'état de dispersion, et en particulier la forme des particules sur les propriétés finales. Les mécanismes par lesquels ces paramètres influencent les propriétés rhélogiques ont été abordés en lien avec les prédictions par un modèle de fonction moléculaire de contrainte (MSF). Il a été constaté que plus les particules sont non-isométriques, plus les interactions polymère-particule et les interactions entre les particules sont élevées. Ainsi, l'effet de l'argile est beaucoup plus important que celui du $CaCO_3$, et ce pour presque tous les comportements rhéologiques étudiés. La plupart des paramètres rhéologiques ont montré une divergence autour du seuil de percolation. Par conséquent, les modèles basés sur la dynamique des chaînes (modèle MSF) ne peuvent prédire le comportement après la percolation. Pour les systèmes percolés, les modèles basés sur le réseau fractal, qui considèrent les interactions entre les particules, ont été utilisés.

Abstract

The main objective of this thesis is to understand the relations between microstructure and rheological properties of polymer nano-composites based on ethylene vinyl acetate (EVA) copolymer.

The first part of the study is related to EVA-nano crystalline cellulose (NCC) composites. As a first step, determination of the unknown structure of the samples using rheological methods was investigated. By analyzing the properties obtained under shear and extensional deformations, the mechanisms leading to polymer reinforcement were investigated in details.

In the second part, nano-composites containing isometric ($CaCO_3$) and anisometric (clay) particles were used. The focus here was to determine the effect of structural variables such as polymer-particle and particle-particle interactions, state of dispersion, and in particular particle shape on the final properties of these nano-composites. The mechanisms involving these parameters were investigated through rheological properties and discussed with respect to experimental data. Predictions via the molecular stress function (MSF) model are also presented. It was found that higher particle anisomety led to greater polymer-particle and particle-particle interactions. Therefore, the effect of clay was much higher than $CaCO_3$ on almost all the rheological parameters studied. But, lower predictability was found around the percolation concentration. Consequently, while a model based on chain dynamics could predict the behavior below percolation, such model failed to predict the response at higher concentrations. For percolated systems, models based on fractal networks, which include particle-particle interactions, were used.

Foreword

This dissertation is composed of six chapters. In the first chapter, a general introduction on nano-composites and rheology is presented. The importance of rheological analysis for understanding structure-property relationships of nano-composites is highlighted and reviewed according to the literature. Then, Chapters 2-5 report on the results of the project which were published as four scientific articles as follows:

Chapter 2

H. Mahi, D. Rodrigue, "Linear and non-linear viscoelastic properties of ethylene vinyl acetate/nanocrystalline cellulose composites, Rheol. Acta, 51, 127-142 (2012).

In this part of the work, for the first time, the linear and non-linear rheological behavior of melt blended cellulosic nano-composites was discussed with the aim to get some information about the structure of nano-composites by rheological measurements. Because of the carbon-based structure of both nano-cellulose and polymeric matrix, it was not possible to distinguish the particles and the matrix by typical microscopic techniques like TEM and SEM. Therefore, rheological analysis was used to capture some structural parameters and to discuss on the molecular origin of the observed responses under different deformations.

Chapter 3

H. Mahi, D. Rodrigue, "Relationships between linear and non-linear shear response of polymer nanocomposites", Rheol. Acta, 51, 991-1005 (2012).

While in chapter 2, rheology was used for a system in which nano-particles and matrix were indistinguishable by typical microscopic methods, the rheology of two nano-composites (based on clay and $CaCO_3$) for which the particles are distinguishable inside the polymer matrix (EVA) was studied. Three main objectives were achieved in this work. First, since the structure of the systems was analysed by TEM and SEM, investigations relating rheology to structure were validated by morphological analyses. Second, the effect

of particle shape on the rheological properties was studied with an emphasis to distinguish the effect of particle-particle and polymer-particle interactions. Finally, the relations between nano-composite structure (data under SAOS) and material flow (data obtained in shear transient tests) were studied in detail.

Chapter 4

H. Mahi, D. Rodrigue "Effect of nano-particles on flow and recovery of polymer nanocomposites in the melt state", Int. Polym. Proc., 28, 151-158 (2013).

This part of the work is a continuation of the work presented in chapter 3. In chapter 3, the effect of two geometrically different nano-particles was studied and discussion about the importance of particle-particle network was made. In this chapter, in order to validate the statements in chapter 4, as well as to study the recovery behavior of the nano-composites, the behavior of the pre-sheared systems was studied.

Chapter 5

H. Mahi, M. Abbasi, M. Wilhelm, D. Rodrigue "Validity of the modified molecular stress function theory to predict the rheological properties of polymer nanocomposites", J. Rheol., 57, 881-899 (2013).

Considering the wide applicability of models based on the tube concept to predict the rheological properties of polymeric systems, it was tried to examine to what extent a model based on the tube theory can predict the rheology of nano-composites. In this context, a modified version of the molecular stress function (MSF) theory was used to predict the non-linear flow behavior under extension and shear. The validity and the limits of the tube theory for polymer nano-composites were investigated. In order to better understand the molecular origin of the behavior observed for nano-composites, the observed response of the systems under LAOS was quantified by FT-rheology.

Finally, in **chapter 6**, the general conclusions are given and completed by suggestions for future works.

It should be mentioned that for all papers, I performed the experimental work including data analysis and wrote the first draft of the papers which were revised by all co-authors. In chapter 5, the MSF calculations were performed by M. Abbasi.

Furthermore, in addition to the above mentioned papers, some other results in this work were presented in conferences/presentations as:

H. Mahi, D. Rodrigue, "Rheology, and microstructure in polymer nanocomposites", Karlsruhe Institute for Technology (KIT), Karlsruhe, **Germany**, **(2013/06)**.

H. Mahi, D. Rodrigue, "Effect of MWNTs on Rheological Properties of Polymer Nanocomposites: A Comparison between Different Nano-Particle Shapes", SoR 84th Annual Meeting, Pasadena, California, **USA (2013/02)**.

H. Mahi, M. Abbasi, M. Wilhelm, D. Rodrigue, "Effect of Nano-Particle Geometry on Rheological Properties of Nanocomposites Using SAOS and LAOS Deformations", XVIth International Congress on Rheology, Lisbon, **Portugal (2012/08)**.

H. Mahi, D. Rodrigue, "Effect of nano-particles on the recovery of polymer nanocomposites in the melt state", PPS Regional meeting, Kish Island, **Iran (2011/10)**.

H. Mahi, D. Rodrigue, "Effect of nano-particle shape on linear and non-linear rheological properties of polymer nano-composite", SoR 83rd Annual Meeting, Cleveland, Ohio. **USA (2011/09)**.

H. Mahi, D. Rodrigue, "Shear rheology of nanocomposites based on cellulose, clay and $CaCO_3$", Karlsruhe Institute for Technology (KIT), Karlsruhe, **Germany**, **(2011/09)**.

H. Mahi, D. Rodrigue, "Rheological analysis as a tool to understand structure-property relation in polymer nanocomposites", CERMA meeting, Université Laval, QC, **Canada (2011/07)**.

H. Mahi, D. Rodrigue, "Rheological properties of ethylene-vinyl acetate and nanocrystalline cellulose composites", SoR 82nd Annual Meeting, New Mexico, **USA (2010/10)**.

Acknowledgements

First and foremost, my highest gratitude goes to my supervisor Prof. Denis Rodrigue for his support and his unique way of leadership. I am grateful for all his considerations, help and the amount of time he spent regarding this work.

I would like to thank Mr. Yann Giroux, our group technician, who from the beginning until the end of the project had kind concern and collaboration regarding the required equipments.

I would like also to thank all my colleagues and staff in the chemical engineering Department in Université Laval.

I would like to thank all the group member of Prof. Manfred Wilhelm at Karlsruhe Institute for Technology in Germany for their help and support during my two stays in Germany.

I would like to thank Dr. Jennifer Kuebel for her revision on the introduction part.

I acknowledge the financial support of the Natural Sciences and Engineering Research Council of Canada (NSERC), and Fonds Québécois de la Recherche sur la Nature et les Technologies (FQRNT).

Ultimately, I would like to highly specify my appreciation to all my family members for their encouragement in the whole period of my life, more specially my wife Zahra for her support and apprehension during this long way.

"You are not a drop in the ocean; you are the entire ocean in a drop" "Let the beauty of what you love be what you do" –Rumi-

Table of Content

List of tables

List of figures

Nomenclature

A_G	The terminal slope of storage modulus in the plot of modulus vs. frequency
a_0	tube diameter at equilibrium
a_2	Parameter related to the overshoot degree in transient shear
a_{pq}	In-phase expansion coefficients under nonlinear oscillatory regime (p, q=1, odd)
a_T	Temperature shift factor
B	Finger tensor in eq. (5-4)
B_G	Terminal slope of loss modulus in the plot of modulus vs. frequency
b_{pq}	Out-of-phase expansion coefficients under nonlinear oscillatory regime (p, q=1, odd)
b_T	Shift factor
$\boldsymbol{C}$	Cauchy tensor in eq. (5-4)
$CaCO_3$	Calcium carbonate
C_{ij}	Taylor or polynomial expansion coefficient, i, j=1,2, 3, · · ·
c	Mass of polymer per unit volume
D	Diameter
De	Deborah number
d_f	Fractal dimension
EVA	Ethylene vinyl acetate
FT	Fourier transformation
$\boldsymbol{F}_{t,t'}^{-1}$	Displacement gradient tensor between t and t'
$f(t-t')$	Molecular stress function
f_{max}	Maximum stretch of polymer chain before slipping
$G(;$	Shear modulus in shear transient test
G (s)	Relaxation modulus
G(t,γ)	Relaxation modulus in the nonlinear region
G'(ω)	Storage modulus
G"(ω)	Loss modulus
G*(ω)	Complex modulus
h_{clay}	Thickness of clay layers
I_n/I_1	Relative intensities from FT-Rheology (n=3,odd)
iPP	Isotactic polypropylene
k_B	Boltzmann constant
L	Length
LAOS	Large amplitude oscillatory shear
M	Molecular weight
MAOS	Medium amplitude oscillatory shear
MI	Melt index
MMT	Montmorillonite
MWNT	Multi walled nano-tubes

M_w	Weight average molecular weight
m	Mass fraction
m_c	Threshold rheological percolation
$m(t\text{-}t')$	Memory function
N_1	First normal stress growth function
N_2	Second normal stress growth function
N6	Nylon 6
NCC	Nanocristalline cellulose
n	Power-law exponent
PCC	Precipitated calcium carbonate
PCL	Poly(ε-caprolactone)
Pe	Peclet number
PEO	Poly(ethylene oxide)
PI	Poydispersity index
PMMA	Poly(methyl-methacrylate)
PP	Polypropylene
PS	Polystyrene
Q	Nonlinear parameter from FT-Rheology
Q_0	Zero-strain nonlinear parameter or intrinsic nonlinear parameter from FT-Rheology
R	Gas constant
R_g	Radius of gyration
R_h	Radius of clay platelet
$\boldsymbol{S}$	Orientation tensor
SAOS	Small amplitude oscillatory shear
SAXS	Small angle x-ray scattering
SEM	Scanning electron microscopy
SHR	Strain-hardening ratio
SWNT	Single wall nano-tubes
$\boldsymbol{S}_{DE}^{IA}(t,t')$	Strain measure with independent alignment assumption
TEM	Transmission electron microscopy
Tg	Glass transition temperature
TTS	Time-temperature superposition
t	Time
t_{peak}	Time for maximum stress in sher transient test
WAXD	Wide-angle X-ray diffraction
Wi	Weissenberg number
w_{per}	percolation threshold for clay particles
α	Slope of storage modulus at high frequency region in the plot of modulus vs. frequency
$\Gamma(n)$	Gamma function
γ	Shear strain
$\gamma_{at\sigma max}$	Strain at maximum stress in shear transient test
$\dot{\gamma}$	Shear rate

δ	Phenomenological parameter in eqs. (2-6 and 4-2)
δ_n	n^{th} phase angle from shear stress under nonlinear regime (n=1, odd)
ε	Strain
$\dot{\varepsilon}$	Elongation rate
η_0	Zero shear viscosity
η^*	Complex viscosity
η'	Real component of complex viscosity
η''	Imaginary component of complex viscosity
$\eta^+(t)$	Shear stress growth coefficient
$\eta_E^+(t, \dot{\varepsilon})$	Extensional viscosity
λ	Relaxation time
ν	Critical exponent in eq. (1-10)
ρ_{org}	Density of the polymer
ρ_{clay}	Density of the Clay
σ	Stress
σ^+	Shear stress growth function
σ_c	Electrical conductivity
σ_E	Extensional stress
σ_∞	Steady state shear stress
σ_0	Shear rate dependent elastic modulus
τ_1	Time scale related with the rearrangement of the structure under shear
τ_2	Time scale related to the network break-up under shear
τ_e	Retraction relaxation time
τ_R	Longest rouse relaxation time
φ_{per}	Percolation volume fraction for spherical particle
ω	Frequency

Chapter 1 Introduction

Polymer nano-composites provide a way for achieving great improvement in various properties such as mechanical (Crosby and Lee 2007; Ci et al. 2008; Paul and Robeson 2008; Jancar et al. 2010), thermal (Moniruzzaman and Winey 2006; Han and Fina 2011), dielectric (Ma et al. 2009; Yoonessi and Gaier 2010; Zhou et al. 2011), barrier (Takahashi et al. 2006; Matteucci et al. 2008; Introzzi et al. 2012), flammability resistance (Bourbigot et al. 2006; Morgan 2006; Mi et al. 2013), polymer blend compatibilization (Khatua et al. 2004; Goffin et al. 2012; Ojijo et al. 2012) and rheological (Krishnamoorti and Giannelis 1997; Krishnamoorti and Yurekli 2001; Knauert et al. 2007; Utracki et al. 2010) to mention a few. With nanoparticles, these property improvements can be achieved at much smaller particle contents in comparison to traditional micrometer-sized particles. This is associated with the specific surface properties arising from the very small size of the nano-particles.

However, in order to take full advantage of the nano-structured particles in polymeric systems, the structure-property relations for these advanced systems must be understood. It is necessary to understand polymer/particle interactions (mobility, conformation and crystallinity), and particle/particle interactions, the state of dispersion, particle morphology and the chemistry as a way to control these parameters for designing tailored nano-composites. Despite the diversity of published literature on the relationships between structural parameters and final properties of polymer nano-composites over the last years, the origin of these impressive property improvements is still not well understood. One reason is that the word “nano-composite”, which refers to any polymer composites in which the particle size in at least in one dimension lower than 100 nm, is general and can encompass a wide range of compositions and morphologies. Within this framework, changes to the polymer chain/particle size ratio are important resulting in additional critical length scales affecting the final composition. Furthermore, particle shape, state of dispersion and energetic attraction present in each system is unique. These multiple factors

lead to a wide diversity in this field of research and cause some discrepancies in the results reported so far.

The two main methods generally used to understand these relations are structure analysis and property analysis (Koo 2006). Typically, structure analysis is carried out using various techniques such as wide-angle X-ray diffraction (WAXD), transmission electron microscopy (TEM), scanning electron microscopy (SEM) and small angle x-ray scattering (SAXS). Because of the complexity of polymer nano-composites, each of these techniques has some limitations (Koo 2006; Paul and Robeson 2008) and no single technique can provide enough information to fully describe the structure. In addition, analysis of the material properties is very important since they are highly dependent on their structure. Furthermore, while structural analyses are generally more qualitative methods, material properties can be modeled and used for quantitative analysis. Because of the possibility to achieve thermodynamic equilibrium conditions and due to the ease and precision of rheological analysis, rheology is known as a very reliable method to understand such relations in complex systems. For polymer composites, all the structural variables such as filler morphology, particle-particle and particle-polymer interactions and the state of dispersion can strongly influence both the linear and non-linear viscoelastic behavior. Furthermore, rheological analysis is an important first step in any melt processing operation. In order to optimize processing conditions, rheological properties, especially non-linear ones, must be understood. Therefore, rheological analysis is important not only for processing, but also to provide a deep understanding of the material structure. Considering the above mentioned advantages for rheological analysis, rheology was selected as the main experimental tool in this work to study the behavior of various nano-composites containing different nano-particles. In this context, this thesis is organized such that following a brief introduction on rheological analysis, a focus is made on nano-composites using specific deformations of interest. Then, experimental results are presented and discussed in the following chapters.

1-2 Rheological analysis

The main objective of this work is to investigate how parameters related to the nano-composite structure can influence the rheological properties. Even though both polymer and particle characteristics are important for property investigation (scheme 1), to avoid complexities the focus of this work is mainly on particle characteristics. Issues related to polymer structure (chemistry, size, and topology) are not included here and therefore only one polymer was used to prepare different nano-composites. Thus, the parameters of interest in this work include structural variables related to particles such as shape and size, dispersion, and interfacial phenomena. Hence, this work investigates how these structural parameters influence the final rheological behavior.

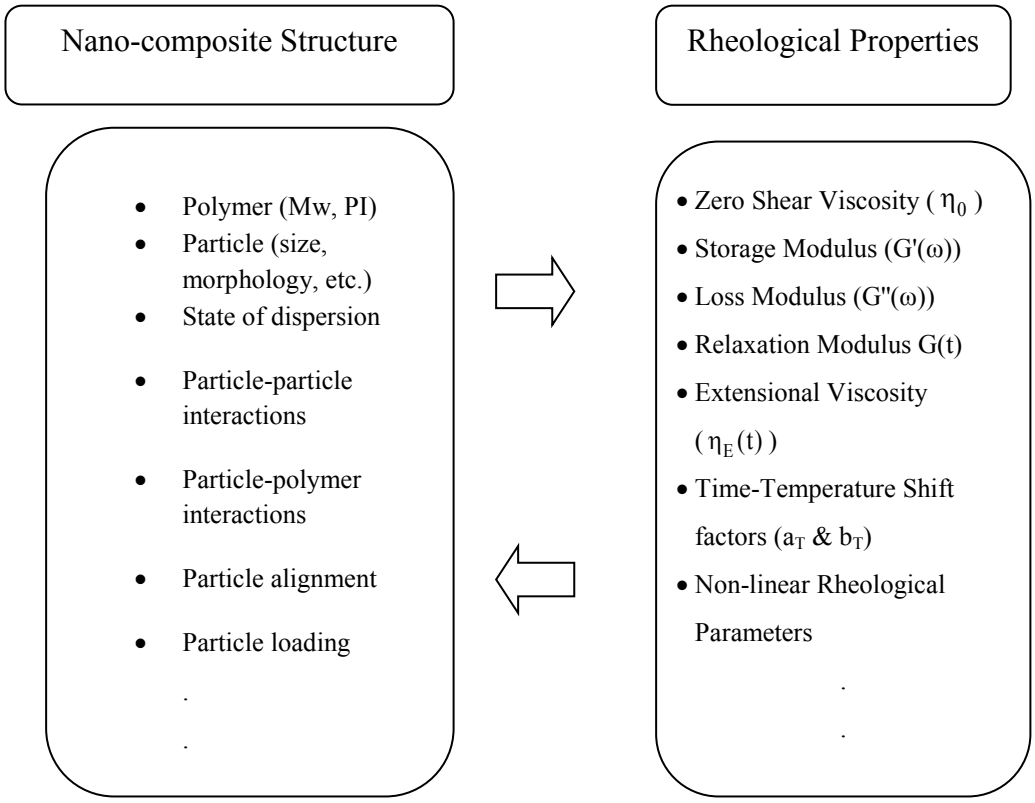

Scheme 1. Rheological parameters as a method to assess nano-composite structure.

The general principle behind the use of rheology as a tool to understand structure-property relationships is very simple: the idea is to apply a deformation to the structure of interest

and then track the response of the material. Then, the resulting viscoelastic properties of the materials can be entirely described by relating the deformation to the response of the material. Depending on the applied deformation and on the material structure, the type of response would vary, which can be used for material classification. Using this simple outline, very complex structures can be studied by rheological measurements. This is the main principle used in this thesis where even small, but known, differences in material structure can be studied by changing the type/amplitude of the deformation applied. The deformations used in this work include oscillatory shear tests (small and large amplitude oscillatory shear (SAOS and LAOS)) and step wise tests (shear and extension). These deformations are quite common in polymer science and, since most of the details related to them are known, they can be used as a first step to investigate nano-composite behavior. Next, the general features and observations related to these tests will be discussed. Since the main objective of this work is to use rheology for material characterization, only issues related to structure will be highlighted.

1-3 Oscillatory Shear

In this test, a sinusoidal deformation in the form of equation (1-1) is applied to the sample and the response as a function of time is measured:

$$\gamma = \gamma_0 sin(\omega t) \tag{1-1}$$

where γ_0 is the amplitude and ω is the frequency. The common experimental testing devices for performing these deformations are in general strain or stress controlled devices. In strain controlled systems (e.g. ARES rheometers shown in figure 1-1) by applying the strain or rotation, the torque (stress) is measured. In stress controlled devises (e.g. AR-G2) however, torque (stress) is applied and strain or rotation is measured. Nowadays, feedback loops are fast enough that most rheometers can operate properly in both modes. Depending on the value of γ_0, the material response is divided into two different regions (see figure 1-2). At low strains (small amplitude oscillatory shear (SAOS)) the behavior is linear meaning that the material properties are not function of the applied strain amplitude, and at high strains (large amplitude oscillatory shear (LAOS)), the response is non-linear and values for the

material properties vary with the applied strain amplitude. The non-linear region can also be subdivided in to two sub-regions: MAOS (medium amplitude oscillatory shear) and LAOS (Hyun et al. 2011) where the MAOS regime is the transition region between SAOS and LAOS. However here, MAOS and LAOS are considered together as the LAOS regime. Although the data obtained in both regions (SAOS and LAOS) are used for material characterization, the analysis of the response in these two regions is completely different and must, therefore, be treated separately.

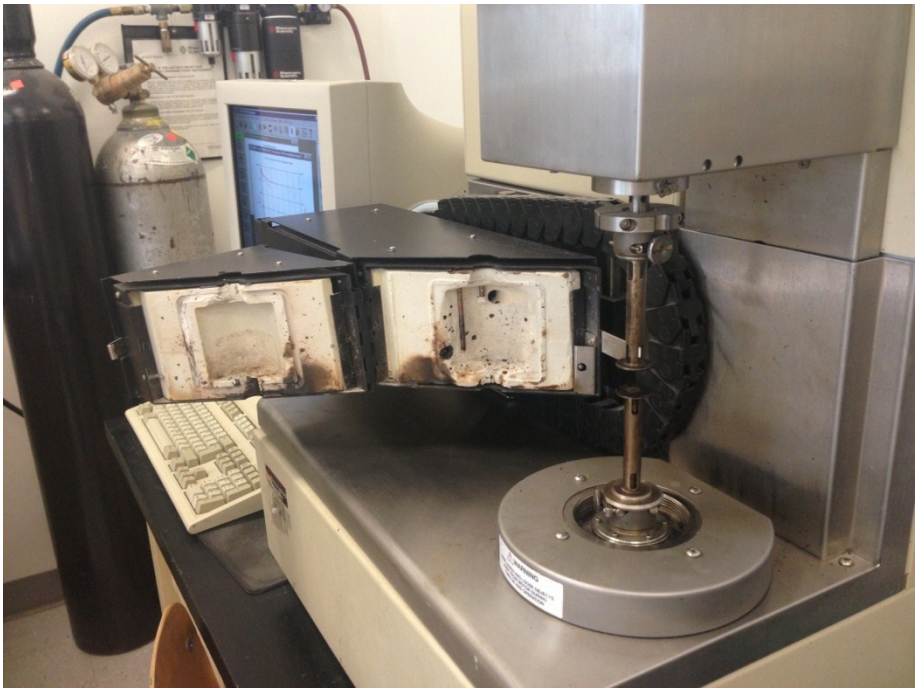

Figure 1-1: A typical ARES rheometer used for much of the common rheological tests in this work including SAOS, step-wise shear and extension tests.

1-3-1 Small amplitude oscillatory shear (SAOS)

The response of a viscoelastic material to a SAOS test is within the linear viscoelastic regime. Generally, this type of behaviour is observed when the deformation is sufficiently small so that the molecules are only slightly stressed. It is important to note that most of the deformations used in polymer processing do not fit in this category leading to the question

why these tests are of interest. The answer lies in the fact that the principles behind these methods are used for characterizing the molecules in their equilibrium state. Therefore, the most commonly applied rheological methods in the field of nano-composites and polymer systems in general are SAOS tests. As previously mentioned, the experiment involves measuring the unsteady response of a system while it is subjected to sinusoidal deformations with small strain amplitudes. Generally, the response of a polymer system is complicated. However, as the applied deformation in SAOS is very low, the relationship between stress and strain is linear and for a linear behavior the stress-strain relation can be written in the form of (Dealy and Larson 2006):

$$\sigma = \int_{-\infty}^{t} \frac{\partial G(t-t')}{\partial t'} \left(\gamma(t) - \gamma(t')\, dt' \right. \tag{1-2}$$

and, using the Boltzman superposition principle, can be written as:

$$\sigma = \int_{-\infty}^{t} G(t-t')\dot{\gamma}(t')dt' \tag{1-3}$$

This means that in the linear region, the constitutive equation can be described by only one material function: *G(t)*. Next, using the expression for the applied deformation in the form of equation (1-1), equation (1-3) for SAOS deformations results in:

$$\sigma = \gamma_0(G' \sin(\omega t) + G''(\omega) \cos(\omega t) \tag{1-4}$$

with

$$G'(\omega) = \omega \int_0^{\infty} \sin(\omega t)\, G(t)dt \tag{1-5}$$

$$G''(\omega) = \omega \int_0^{\infty} \cos(\omega t)\, G(t)dt \tag{1-6}$$

where G' and G'' are the storage and loss moduli, respectively. Analysis of how these two parameters are related to structure is very basic and, at the same time, very important in polymer systems.

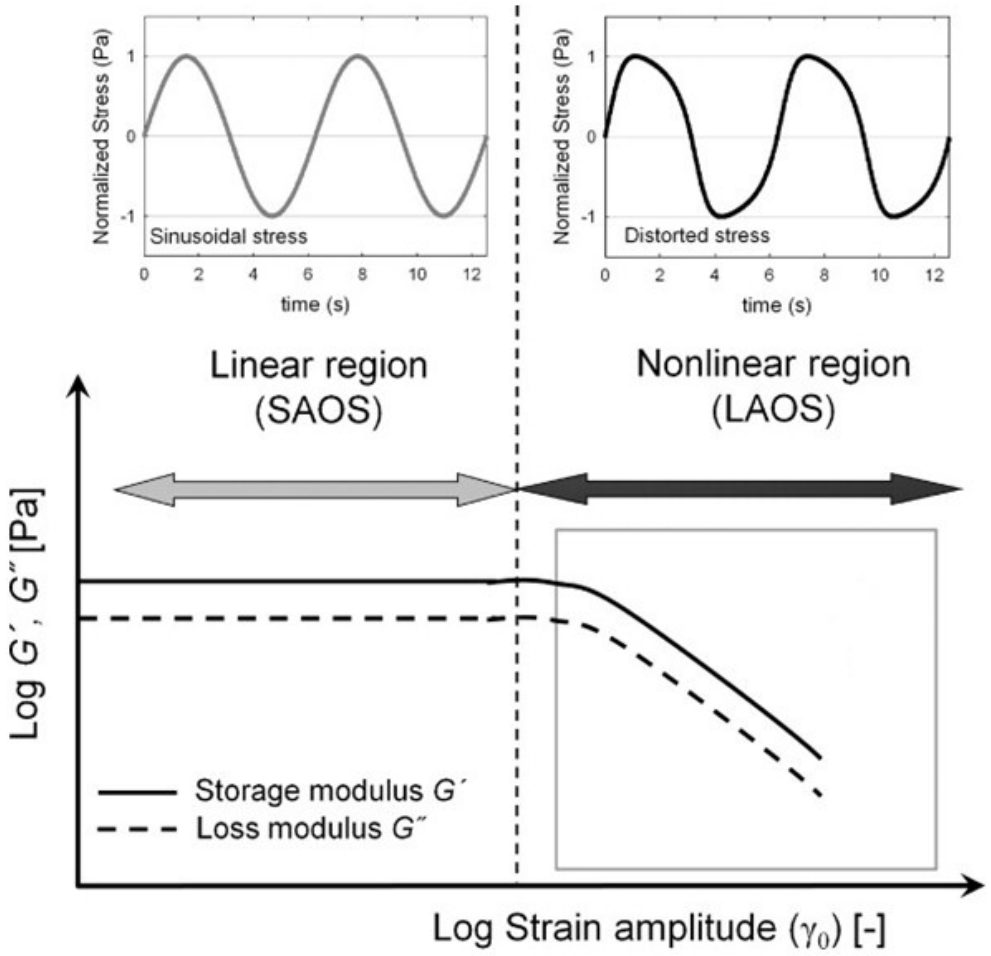

Figure 1-2: Schematic illustration of an oscillatory shear test containing both linear and non-linear behaviour of a polymer. At low strains (SAOS), the response to a sinusoidal deformation is also sinusoidal and the storage (G′) and loss (G″) moduli are independent of the applied strain. However, at high strains (LAOS), the response is not sinusoidal and the moduli are function of the strain amplitude (Hyun et al. 2011).

Thanks to the long history of polymer science, relationships between these two variables and material structure is quite well understood for polymers. However, for nanocomposites, the situation is less clear. Before discussing the literature on the SAOS response of nanocomposites, it would be first interesting to show how the polymer matrix material used in this thesis (ethylene vinyl acetate (EVA)) responds to SAOS deformation. This would help first to better understand the general features observed in a linear viscoelastic region

and also to better assign features caused by the presence of the nano-particles. For this reason, the moduli and viscosity of the neat polymer under SAOS is shown in figure 1-3.

The SAOS response as shown in figure 1-3 is divided into two regions: a high frequency region where the slope for both G' and G'' is 0.5 and a low frequency region where the slopes for G' and G'' change to 2 and 1, respectively. In polymer science, these two distinct behaviors are well described by the two main relaxations called reptation (Doi and Edwards 1989) and Rouse (Rouse 1953) dynamics.

In the Rouse model, the molecule is considered as beads which are connected to each other by springs and, based on this proposition, the relationship between G' and G'' in the Rouse region is defined as (Dealy and Larson 2006):

$$G'(\omega) = G''(\omega) = \sqrt{\frac{3\rho RT\eta_0}{4M}}\omega^{1/2} \equiv C\omega^{1/2} \tag{1-7}$$

where η_0 is the viscosity and M is the molecular weight of the polymer. The agreement between the data at high frequencies and the Rouse predictions is not surprising because, in the high frequency region, the polymer response is dominated by vibration, which is well described by the bead-spring scheme proposed in the Rouse theory. It is noteworthy that the Rouse description of chain dynamics was proposed for polymers having chains with molecular weights lower than the molecular weight for entanglement. But even for entangled systems, when the length scale of the motion is small, the entanglement effect is not significant (Doi and Edwards 1989), that is why the high frequency region also follows Rouse scaling behavior. On the other hand, in the low frequency region, the behavior is well predicted instead by reptation dynamics. Based on the tube model (Doi and Edwards 1989), reptation relaxation is related to the movement of a chain within an enclosing imaginary tube, which represents the effect of entanglements on chain motion. As at low frequency a test chain has enough time to escape from its surrounding imaginary tube, therefore this region of the test includes reptation relaxation.

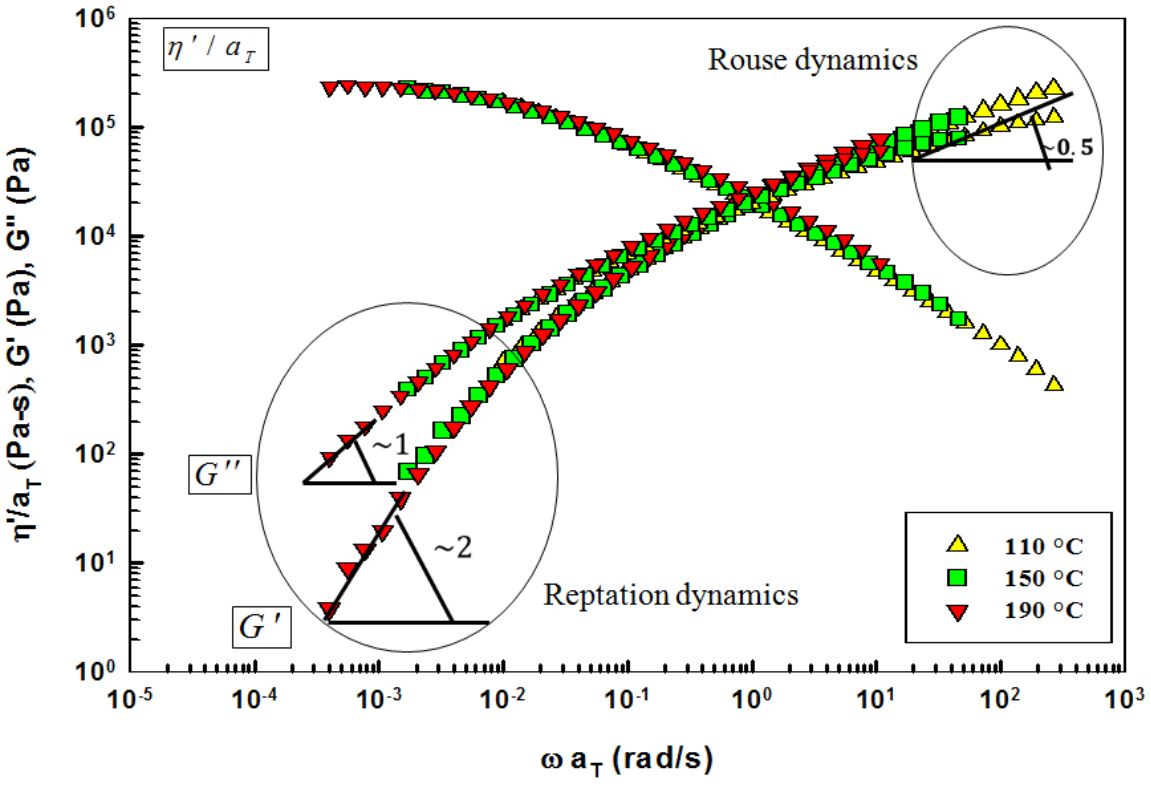

Figure 1-3: Observed behavior of ethylene vinyl acetate (EVA) from SAOS measurements at different temperatures where the data are shifted to 110 °C using the time-temperature superposition principle (TTS).

By considering the reptation mechanism, one can obtain (Doi and Edwards 1989):

$$G'(\omega) \sim A_G \omega^2 (when\ \omega \to 0) \tag{1-8}$$

$$G''(\omega) \sim B_G \omega^1 (when\ \omega \to 0) \tag{1-9}$$

where A_G and B_G are constants. By these two equations, the longest relaxation τ_d, which is related to the time that a chain can escape from its surrounding tube, can be calculated by $\tau_d = A_G/B_G$. The scaling properties obtained for G' and G'' in figure 1-3 is clearly the same as predicted from the reptation theory. Based on this general framework, the effect of nano-particles on SAOS data can be studied and analyzed.

1-3-2 SAOS data for nano-composites

A frequent experimental observation for nano-composites is that, although common polymers exhibit terminal behavior that approximately scales as $G' \sim \omega^2$ and $G'' \sim \omega$, introduction of nano-particles reduce the terminal slope of the storage modulus and, at high concentrations, the nano-composite storage modulus shows a plateau at low frequencies (figure 1-4). Krishnamoorti and Giannelis (1997) first investigated such flow behavior in nano-composites based on poly(ε-caprolactone) (PCL) and nylon 6 (N6) with organically modified MMT and this report was then followed by a large number of other publications (Krishnamoorti and Yurekli 2001; Du et al. 2004; Cassagnau 2008; Akcora et al. 2009; Chen et al. 2010).

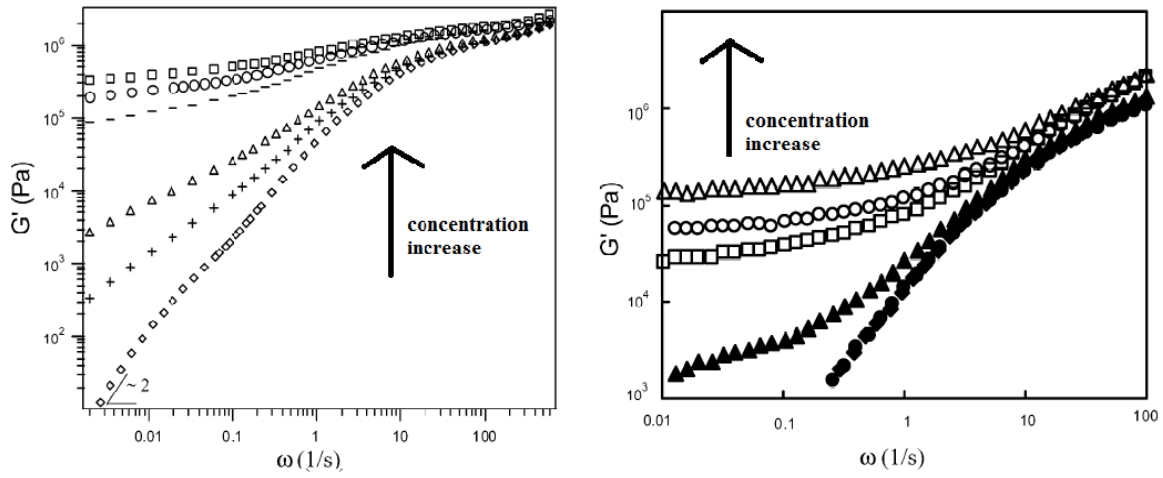

Figure 1-4: Storage modulus vs. frequency for PEO-clay (left) (Zhang and Archer 2002) and PMMA-carbon nanotubes composites (right) (Du et al. 2004) at various nano-particle loadings.

Two different mechanisms have been proposed for this behavior (Akcora et al. 2010a) including those based on particle-particle interactions (percolation) and those based on particle-polymer interactions (coupling). The first mechanism, which is also called the percolation mechanism (Nan et al. 2010), states that, at a specific volume fraction of nano-particles, the particles create a network dominating the behavior, which is also referred to as "jamming". These connected networks provide a pathway for stress propagation and, therefore, the storage modulus increases significantly (Chatterjee and Krishnamoorti 2008;

Akcora et al. 2009; Akcora et al. 2010a; Dykes et al. 2012). On the other hand, according to the second mechanism, the improvement in the modulus is the result of the formation of constrained glassy layers around the particles (Sternstein and Zhu 2002; Picu and Rakshit 2007; Robertson and Roland 2008; Zhou et al. 2011). The constrained chains are thought to be unable to relax under shear because they are confined, therefore causing the modulus to show a plateau at low frequencies. Surprisingly, there are evidences supporting both mechanisms, indicating the complex nature of this phenomenon in nano-composites.

Referring to the first mechanism, for example, it was observed that composites having aggregated structures of nano-particles show better property improvements compared to those where the particles are separated by chemical modification (Akcora et al. 2009). The reason for this could be that the stress distribution by particle fractal structures inside the polymer is more efficient for aggregated structures. Another evidence for the particle-particle based scenario is the observation that the rheological properties are independent of temperature (Wagener and Reisinger 2003). Structurally, this result indicates that the behaviour is dominated by a solid network rather than by viscoelastic chains, which have temperature dependant behavior. Another observation related to filler based mechanism is that, for some nano-composites, the glass transition temperature (Tg) did not change significantly (Böhning et al. 2003; Pluta et al. 2007; Robertson and Roland 2008). This indicates that fillers do not affect the local motion of the polymer chains. Also, for many systems, the effect of nano-particles on the rheological properties at high frequencies is not significant suggesting that nano-particles do not change the short-range behavior of the polymeric chains considerably, but instead on size scales equivalent to the entanglement length (Du et al. 2004).

For the mechanisms based on polymer-particle attraction, there is also supports found in the literature (Sternstein and Zhu 2002; Picu and Rakshit 2007; Robertson and Roland 2008; Zhou et al. 2011). Previous works have shown that by improving the interfacial attractions between filler and polymer (coupling), liquid-like rheological behavior was changed to solid-like behaviour (Krishnamoorti and Giannelis 1997; Manitiu et al. 2009; Xu et al. 2009). Even for systems with the same dispersion quality, increased properties have been

reported by improving the coupling characteristics (Xu et al. 2009). For the second mechanism to occur, polymer-particle coupling must be strong enough to allow for the particles to be uniformly dispersed in the polymer matrix. In this case, solid-like behavior is observed where surrounding chains around particles are immobilized leading to an increase in Tg with filler addition.

Generally speaking, improved rheological properties for each system are the result of both particle-particle interactions and a polymer-based network where both phenomena simultaneously participate in the reinforcement of the composite. Complex interfacial interactions (polymer and particles) reduce the molecular dynamics relaxation processes and suppress relaxation, thus affecting the performance of the nano-composites and the nano-dispersion. Also, particle fractals inside the polymer can propagate stress and influence the system dynamics strongly. However, it seems that the role of particle-particle interactions in inducing solid-like behavior is the more dominant effect relative to constrained layers especially at high concentrations and most notably for particles with active surfaces. Even if the polymer-particle interactions are strong, at concentrations higher than the threshold concentration, it is instead the formation of a filler network that provides the pseudo-solid rheological behaviour at low frequencies. The percolation threshold depends on various parameters including the morphology of the nano-particles, the state of dispersion, the polymer molecular weight distribution and processing methods. Therefore, different values for percolation thresholds have been reported for different systems (Sinha Ray and Okamoto 2003; Hussain et al. 2006; Habibi et al. 2010).

It should be noted that a particle network is not necessarily the result of direct physical contacts between the fillers (similar to electrical percolation threshold). Therefore, the reported rheological percolation threshold can be lower than the electrical percolation threshold (figure 1-5). This indicates the association of chain confinement (glassy layer) with the appearance of solid-like behaviour in SAOS tests.

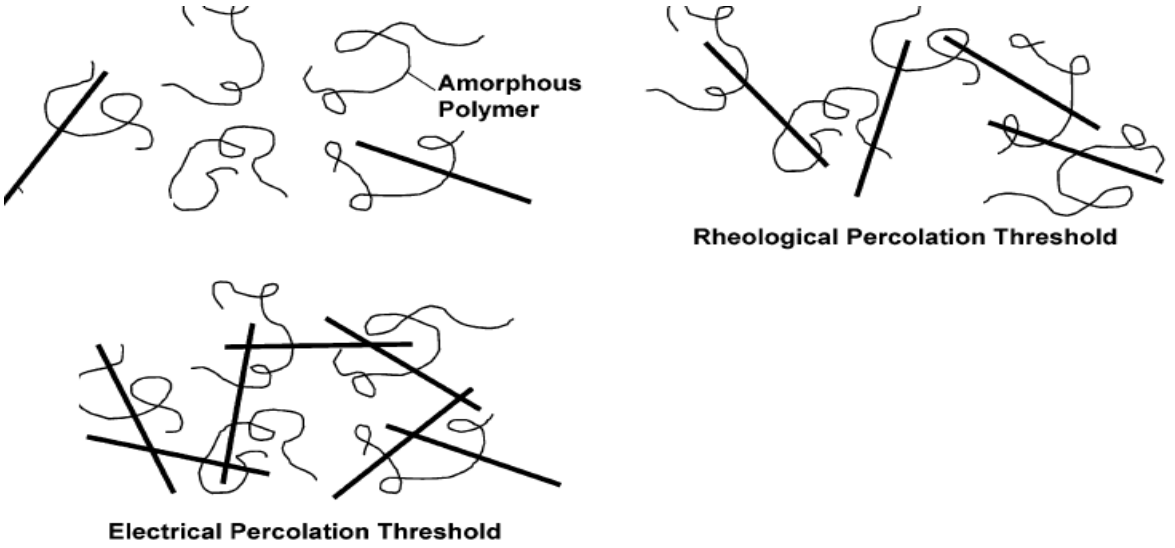

Figure 1-5: Schematic representation showing the differences between electrical and rheological percolations (Du et al. 2004).

1-3-3 Viscosity

From a rheological perspective, a direct result of filler incorporation in molten polymers is a significant change in the resulting viscosity. The existence (or not) of yield stress is an important issue in polymer micro-composites (Hornsby 1999) and therefore, plays a key role in nano-composites as these have even higher surface area. A formal definition of yield stress is that a minimum stress is required for certain materials to flow. Below that specific stress, materials show solid-like behavior (i.e. they deform elastically) and, at stresses higher than the yield stress, the material behaves like a liquid. Most of the literature related to this phenomenon shows that, in a manner similar to the dynamic modulus, yield phenomena can also be correlated with the degree of interaction between the particles or the interfacial interactions between the polymer and particles. In addition, as mentioned for the solid-like behavior in the storage modulus, the exact mechanism for yield stress in viscosity is also complicated. For example, a paradox has been reported by Jancar et al. (2010) for fumed silica and clay nano-composites (see figure 1-6). For clay, the percolation threshold was reduced and the modulus and viscosity at yield increased with increasing dispersion quality; while for silica, the behavior followed the opposite trend. This again reflects the

complexity of the interactions and indicates that depending on the system studied the mechanism for solid-like behavior changes accordingly.

1-3-4 Effect of nano-particle loading, percolation

From a practical perspective, the percolation threshold concentration is very important in a variety of applications such as mechanical reinforcement, electrical conductivity, flame retardancy and permeability. Since the relaxation patterns change very strongly at percolation, rheological analysis is a very sensitive technique to detect this concentration. At low particle loadings, the chain can relax with ease. With increasing filler concentration, the relaxation gets longer and longer and at percolation, a solid-like behaviour in which the stress is not relaxed is observed (see figure 1-4). Therefore, at percolation, a divergence can be observed in many viscoelastic properties. An example of such a divergence for viscosity and modulus is shown in figure 1-7. The zero shear viscosity increases as concentration increases until percolation is reached and, at higher concentrations, no zero shear viscosity is observed due to the yield phenomenon. On the other hand, the storage modulus at low concentrations shows typical terminal behaviour and, above percolation, a plateau is observed which increases with concentration.

Near this transition (around percolation), the rheological properties of the composites can be described by simple power-law equations (Winter and Mours 1997) as:

$$\eta_0 \sim (m_c - m)^{-\beta} \text{ when } m < m_c \tag{1-10}$$

$$G_e \sim (m - m_c)^{-\delta} \text{ when } m_c < m \tag{1-11}$$

where G_e and η_0 are the plateau dynamic modulus and zero shear viscosity, respectively. m is the mass fraction of nano-particles, m_c is the rheological percolation threshold, while β and δ are the critical exponents. Such divergence can occur for many other properties. Therefore, these power-law equations and the trends observed in figure 1-7 may be relevant in describing the loss modulus, tan δ or electrical conductivity (σ_c). However, the sensitivity of each property to the mass fraction is different. For example, it was shown that

the complex viscosity (η^*) and viscous modulus (G'') are less sensitive to percolation than either G', G'/G'' or σ_c (Kota et al. 2007). On a microstructural level, this indicates that elastic load transfer and electrical conductivity are much more sensitive to the creation of a percolated network than the dissipation mechanisms, which are instead associated with viscous properties.

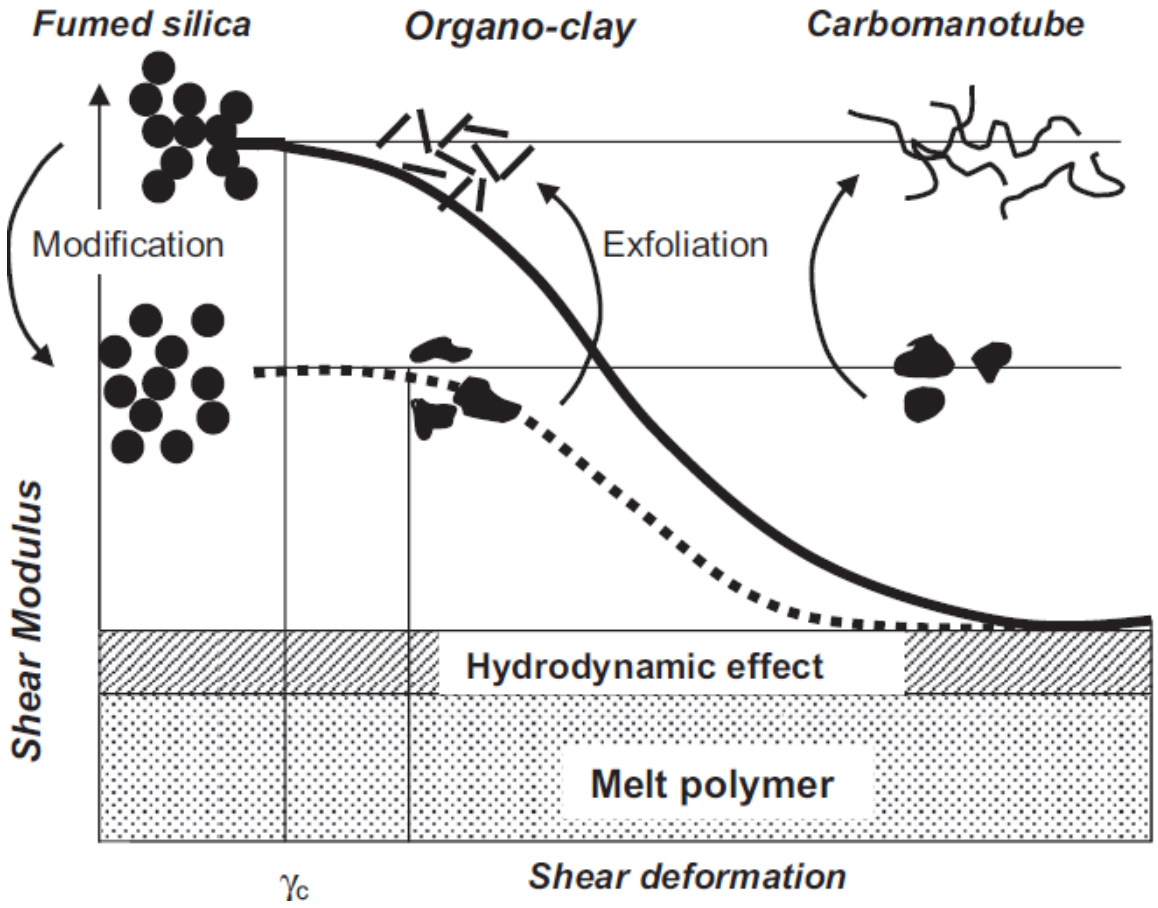

Figure 1-6: Paradox observed for the dispersion dependency of the shear modulus where, for spherical silica particles, the modulus decreased with improving dispersion quality and, for clay platelets, the trend was inversed (Jancar et al. 2010).

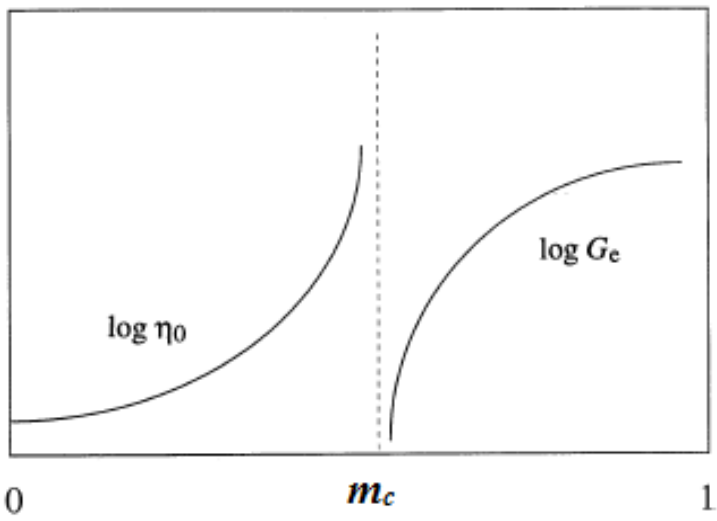

Figure 1-7: Schematic representation of the divergence of the zero shear viscosity and storage modulus at the percolation threshold (Winter and Mours 1997).

1-3-5 Effect of particle size

Using the word "nano" automatically emphasizes the size characteristics of a material. It is the specific size of nano-materials that results in outstanding property improvement. While filler size effects have been observed in different polymeric systems, the possible underlying mechanisms are complicated. When considering the proposed mechanisms for solid-like behaviour in the resulting rheological properties (polymer-particle and particle-particle interactions), it is obvious that both possible interactions increase as the size of the particles is reduced. Clearly, with decreasing filler size and increasing surface area, the particles tendency to interconnect increases accordingly. In addition, increasing surface area increases the likelihood of interfacial chain interactions. Therefore, micro-mechanical models cannot predict the resulting properties. Indeed, particles with smaller sizes generally create stronger nano-composites. However, the best parameter to address the effect of size scale is the aspect ratio. In fact, the smaller the size and the higher the aspect ratio, the stronger is the resulting material. Because of the diversity of particle morphology, the aspect ratio for each specific morphology must be defined accordingly (Kagarise et al. 2008).

1-3-6 Effect of polymer matrix

Referring back to particle–particle and polymer–particle interactions, the latter is directly related to the phenomena at the chain/filler interface and, therefore, highlights the role of the polymer nature on rheological properties. Even when particle-particle attractions are dominant, the matrix effect on viscoelastic properties is significant. Some structural variables such as coupling characteristic, particle to polymer size ratio and the degree of polymerizations which are directly related to polymer matrix have an important effect on rheological properties. The roles played by nano-particle size were mentioned, but it is clear that not only nano-filler size must be considered, but the relative size of the particle to the polymer chains is also a critical parameter influencing considerably the viscoelastic properties. It was reported that when the radius of gyration of the tracer polymer (R_g) is higher than the radius of the nano-particle (R_p), the resulting reinforcement is much larger relative to situations where R_g is shorter than the radius of the nano-particles (Mu and Winey 2007; Nusser et al. 2010). Two main mechanisms can explain this phenomenon. First, when the length of a polymeric chain is large, it can easily entangle with particle and thereby increase the relaxation time of the polymer chain relative to a shorter chain for which no entanglement with the particle is possible (figure 1-8). In many studies, the degree of reported constraint is higher for higher molecular weight polymers compared to lower ones (Du et al. 2004; Picu and Rakshit 2007; Anderson and Zukoski 2009; Anderson and Zukoski 2010). The second mechanism in which longer chains can contribute to higher reinforcement is that the local fractals of nano-particles can also be linked together through long polymer chains. This phenomenon, which is called the chain bridging mechanism, has been reported mainly in filled rubbers (Zhang and Archer 2002; Zhu et al. 2005; Merabia et al. 2008). Another important parameter regarding the chain size is the diffusivity of a chain, which can influence the dispersion quality. With respect to diffusion, shorter chains can better wet the particle surface, which can then improve the dispersion quality.

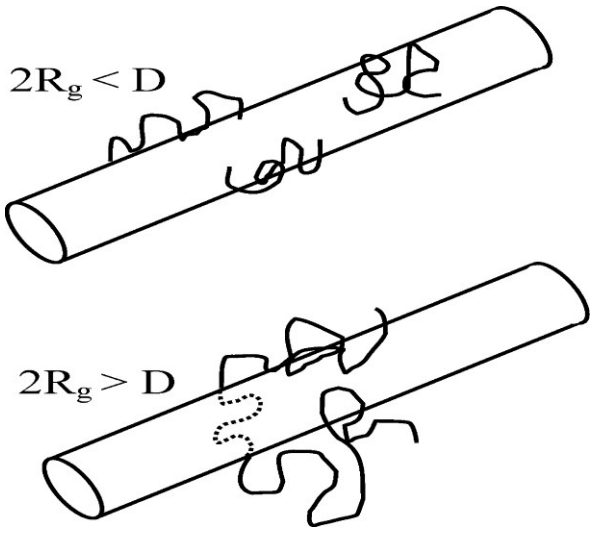

Figure 1-8: Schematic representation of particle-polymer interactions for different size ratios of the nano-particle to the polymer chain (Mu and Winey 2007).

For example, a better exfoliation structure for clay nano-composites is observed for polymers with low M_W compared to those with high M_W (Koo et al. 2002). As a final point, the polymer chemical structure, and therefore its affinity to particle surface, is important as the reinforcement is best when there is a strong energetic attraction between the polymer and particle.

1-3-7 Large amplitude oscillatory shear (LAOS)

Although linear viscoelasticity, which can be studied with SAOS deformation, is very useful for material characterization, understanding non-linear viscoelasticity is also very important for a variety of reasons. First, most of the deformations actually used in material processing are within the non-linear regime. Therefore, understanding non-linear parameters is essential. Second, even if the focus is solely on understanding structure property relations, many of the structural variables can also be accessed from non-linear experiments. Finally, many theories based on linear behaviour can be examined and expanded with an understanding of non-linear viscoelasticity. Therefore, in order to have a better understanding of the structure, it is better to study the non-linear behavior in parallel with the linear behavior. One of the tests that can be used for such an analysis is a LAOS

test where the sample is subjected to a sinusoidal deformation in the form of equation (1-1) with a very high amplitude. Even though LAOS measurements have a long history in polymer science, due to precision limitations during testing and the complexity of the calculations, the main progress in this field is quite recent and coincided with improvements in transducer resolution and software power. Different quantitative methods are used to analyze LAOS data (Hyun et al. 2011). Among these methods, Fourier Transformation (FT) rheology is one of the most important ones (Wilhelm et al. 1998; Wilhelm et al. 1999). Since only FT-rheology was used for LAOS analysis in this work, only the aspects related to FT-rheology will be reviewed briefly.

When a sinusoidal deformation in the form of equation (1-1) is applied to a sample, if the amplitude is low, the stress response will also be sinusoidal. However, in the non-linear region (high deformation), the stress response is no longer sinusoidal (see figure 1-2), but can be written as (Hyun et al. 2011):

$$\sigma(t) = \sum_{i=0} \sum_{j=0} C_{ij} \gamma^i(t)\, \dot{\gamma}^j(t) \tag{1-12}$$

where C_{ij} are mathematical constants for the expansion of the nonlinear stress as a function of the strain and strain rate (Hyun et al. 2011).

In FT-rheology, the time dependent stress response is analysed using Fourier transformation. Generally speaking, a Fourier transform is an operation which converts functions from the time to the frequency domain as shown in equation (1-13) and figure 1-9.

$$S(\omega) = \int_{-\infty}^{+\infty} S(t) e^{-i\omega t} dt = \int_{-\infty}^{+\infty} S(t) \lfloor \cos(\omega t) - i sin(\omega t) \rfloor dt \tag{1-13}$$

Equation (1-12) can then be expanded to (Hyun et al. 2011):

$$\sigma(t) = \gamma_0 [a_{11} sin\, \omega t + b_{11} cos\omega t] + {\gamma_0}^3 [a_{31} sin\, \omega t + b_{31} cos\omega t + a_{33} sin\, 3\omega t + b_{33} cos 3\omega t] + O({\gamma_0}^5) + \cdots \tag{1-14}$$

where

$$a_{11} = C_{10}|_{\gamma\to 0} = G'(\omega) \qquad b_{11} = C_{01}|_{\gamma\to 0} = G''(\omega)$$

$$a_{31} = \frac{1}{2}(C_{10} + C_{12}\omega^2) \qquad b_{31} = \frac{1}{4}(-C_{21}\omega + 3C_{03}\omega^3)$$

$$a_{33} = \frac{1}{4}(-C_{30} + C_{12}\omega^2) \qquad b_{33} = \frac{1}{4}(-C_{21}\omega + C_{03}\omega^3)$$

$$\vdots \qquad\qquad \vdots$$

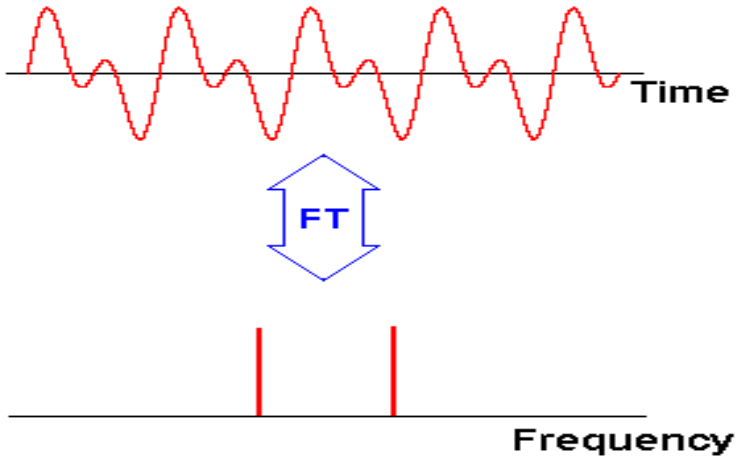

Figure 1-9: A simple representation of the way that a Fourier transformation operates to convert a function from time to frequency (image from: ttp://www.cis.rit.edu/htbooks/nmr/inside.html).

In the linear domain, only the first part of the right side of equation (1-14) is considered, while the other components are also important in the non-linear region.

Considering equation (1-12), a different notation for the non-linear stress can be used (Hyun et al. 2011):

$$\sigma(t) = \sum_{n=1,odd} \sigma_n \sin(n\omega t + \delta_n) \qquad (1\text{-}15)$$

These equations (1-12 to 1-15) are the basis for FT-rheology to quantify LAOS data. More details regarding how these equations were developed and used can be found elsewhere (Wilhelm et al. 1998; Wilhelm 2002; Hyun et al. 2011). In order to be able to analyse the stress data, the raw oscillatory waveforms should be obtained with special care (Wilhelm et al. 1999). The setup for such measurements is shown in figure 1-10 in which the raw torque and normal stress data are digitized by an analog-to-digital converter (ADC) card. The set-up can be installed on most equipments performing SAOS measurements (as in figure 1-1).

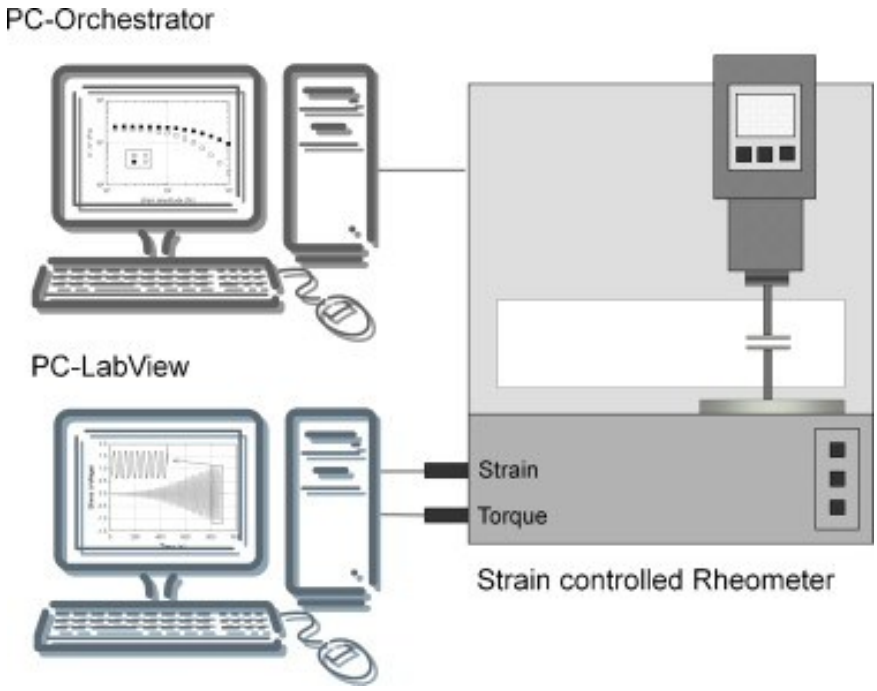

Figure 1-10: Experimental set-up for common LAOS experiments in which the strain, torque and normal forces are digitized via a stand-alone PC (Hyun et al. 2011).

In material characterization, among the higher harmonics which are observed in a LAOS experiment, it was shown that the ratio of the relative intensity of the third harmonic to the first harmonic ($I_3/I_1 = I_{3/1}$) is very sensitive to structural variables. The ratio I_3/I_1 is defined as (Hyun et al. 2011):

$$I_{3/1} = \frac{I_3}{I_1} = \frac{\sigma_3}{\sigma_1} = \frac{\sqrt{(\sigma_3 cos\delta_3)^2 + (\sigma_3 sin\delta_3)^2}}{\sqrt{(\sigma_1 cos\delta_1)^2 + (\sigma_1 sin\delta_1)^2}} \quad (1\text{-}16)$$

Based on this equation, Hyun and Wilhelm (2009) recently proposed a new non-linear parameter defined as:

$$Q \equiv {I_3}/{I_1}\Big/{\gamma^2} \tag{1-17}$$

They also defined a zero-strain non-linearity or intrinsic non-linearity, Q_0 (ω), as:

$$Q_0(\omega) = \lim_{\gamma_0 \to 0} Q(\omega, \gamma_0) = \frac{|G^*_{33}(\omega)|}{|G^*_{11}(\omega)|} \tag{1-18}$$

These two parameters (Q and I_3/I_1) in FT-rheology are the two main parameters to analyze the non-linearity of a material and consequently understand its structure. Although, due to the novelty of the method, very few works (Hyun et al. 2012; Lim et al. 2013) have been published using this characterization method for nano-composites structure, this method has the potential to be a powerful technique for this application.

1-4 Transient tests

In addition to LAOS measurements, other tests can be used to analyze the nonlinear behaviour, but not based on oscillatory deformations. The most popular method in this context is to apply a stepwise deformation and track the stress response as a function of time. This can be done with two different deformation types: shear and extension.

1-4-1 Shear transient

In transient shear tests, a sample in its equilibrium state is subjected (at time t=0) to a constant shear rate ($\dot{\gamma}$) and the rheological functions (σ^+, η^+, N_1, N_2) are measured:

$$\eta^+(t, \gamma) = \frac{\dot{\sigma}^+(t, \dot{\gamma})}{t} \tag{1-19}$$

The equipment for such test is the same as for SAOS and LAOS measurements. In the limit of low shear rate, $\eta+$ becomes equal to the related material function from linear viscoelasticity:

$$\lim \eta^+(t,\dot{\gamma}) \tag{1-20}$$

At sufficiently long time, the stress reaches steady state and the value of the material function would be equal to the viscometric function:

$$\lim_{t\to\infty} \eta^+(t,\dot{\gamma}) \tag{1-21}$$

Experiments on viscoelastic systems show that, regardless of the mechanism, at high shear rates the start-up of shear flow is accompanied by stress overshoots (figure 1-11). After a certain time, which appears to be related to the relaxation time of the system and the applied strain rate, the stress recovers to a plateau value.

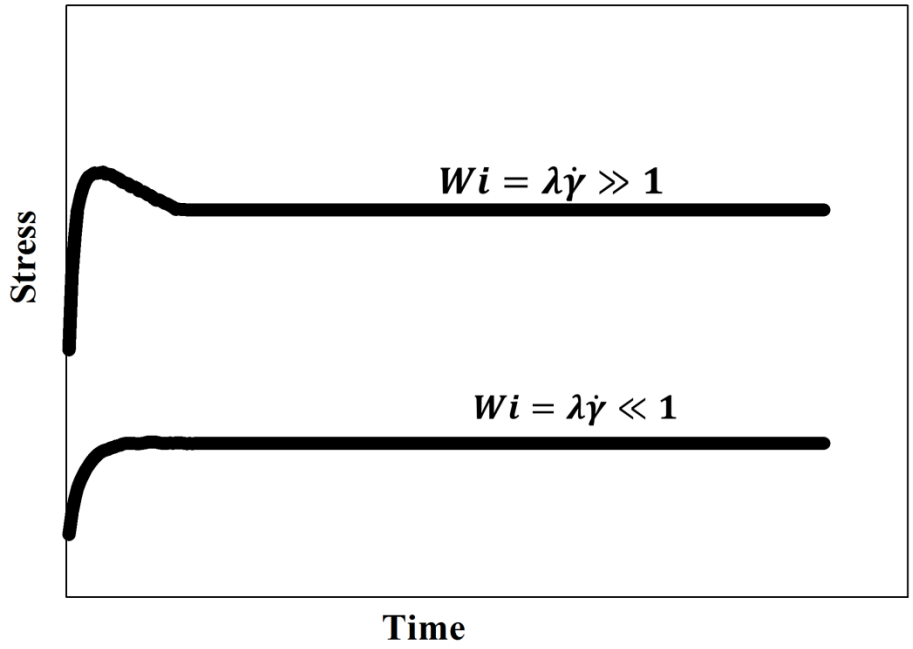

Figure 1-11: Typical curves for shear stress as a function of time for polymer systems where depending on the Weissenberg number, the material shows or not an overshoot.

For low shear rates, this approach occurs gradually while at high shear rates, the time for relaxation is too short and a high stress is needed for deformation (figure 1-11). Consequently, at high shear rates, viscoelastic materials normally show a yield stress or

stress overshoot. Therefore, two types of behaviors can be obtained: data sets with or without stress overshoots. One criterion to express this transition depends on both material characteristics and the testing rate. The influence of both parameters can be addressed by the Weissenberg number (Dealy 2010), which is defined as:

$$Wi = \lambda \dot{\gamma} \tag{1-22}$$

where λ is the relaxation time of the material and $\dot{\gamma}$ is the applied shear rate. Normally, for entangled polymers, an overshoot is observed for $Wi \geq 1$ (Pearson et al. 1991). While data at low shear rates are suitable for determining linear parameters, data at high shear rates (with stress overshoot) are very useful in understanding the material structure. For nano-composites, the overshoot is very important because it contains information about the structure. However, relatively fewer studies in comparison to dynamic tests in the field of nano-composites have used this method. Regarding the stress overshoot two main features are important: first, whether it appears or not, and second, the degree of overshoot. Since the appearance (or not) of an overshoot depends on chain dynamics, by analyzing the variation in the starting shear rate for the overshoot, the effect of a specific nano-particle on chain dynamics (chain confinement) can be assessed. To our knowledge, this issue has not been previously considered in the literature and, in the next sections (chapters 3 and 5), this phenomenon will be analyzed in details. Another aspect of the overshoot, which was discussed previously in the literature, is the degree of overshoot. The main observation in this context is that, regardless of the mechanism, the amount of overshoot increases with nano-particle concentration. The nature of this overshoot in filled systems is mainly related to particle-particle interactions and the formation of a particle network. When shear is applied to the nano-composites, in addition to the stress needed for polymer to start to flow, the particle network must also be broken and then reorganized in the flow direction. This requires a higher stress, which is observed as an overshoot in the stress curve. The importance of this orientation distribution was extensively discussed for percolated systems formed by spherical (Whittle and Dickinson 1997; Mohraz and Solomon 2005), plate-like (Letwimolnun et al. 2007; Dykes et al. 2012) and tubular (Pujari et al. 2009) particles. However, since the impact of particle orientation is more important for anisometric

particles (Pujari et al. 2009; Dykes et al. 2012) at concentrations higher than the percolation threshold, stress overshoot is expected to be lower for particles having a low aspect ratio than for those having a high aspect ratio.

1-4-2 Extensional rheology

Similar to transient shear, transient extension tests also subject the material (at time t = 0) to a constant elongation rate ($\dot{\varepsilon}$). The elongational viscosity growth function, $\eta_E^+(t,\dot{\varepsilon})$, is defined by:

$$\eta_E^+(t,\dot{\varepsilon}) = \frac{\sigma_E}{\dot{\varepsilon}} \qquad (1\text{-}23)$$

where σ_E is the extensional stress (Dealy and Wissbrun 1990). The test can be done on the ARES rheometer shown in figure 1-1. However, an appropriate testing fixture, as shown in figure 1-12, must be used to apply extensional deformation (Sentmanat 2004).

The extensional viscosity, in the linear viscoelastic regime, can be determined by:

$$\lim_{\dot{\varepsilon}\to 0} \eta_E^+(t,\dot{\varepsilon}) = 3\eta^+(t) = 3\int_0^t G(s)ds \qquad (1\text{-}24)$$

where *G(s)* is the relaxation modulus.

For small and slow deformations, linear viscoelastic theory provides relations between the material functions. Thus, for small deformations, no new data is obtained from extensional flow and all the extensional properties can be calculated from shear data. On the other hand, at large deformations due to the contribution of non-linear phenomena, extensional data cannot be predicted from shear data. However, the comparison of extensional properties with linear properties is useful as it provides a practical test of the validity of the non-linear properties. Furthermore, deviation from the linear behavior can be assessed and used for non-linear properties analysis. For these reasons, a plot of $\eta_E^+(t,\dot{\varepsilon})$ is usually compared with the value of $3\eta^+(t)$. This ratio is normally referred to Trouton ratio (*TR*).

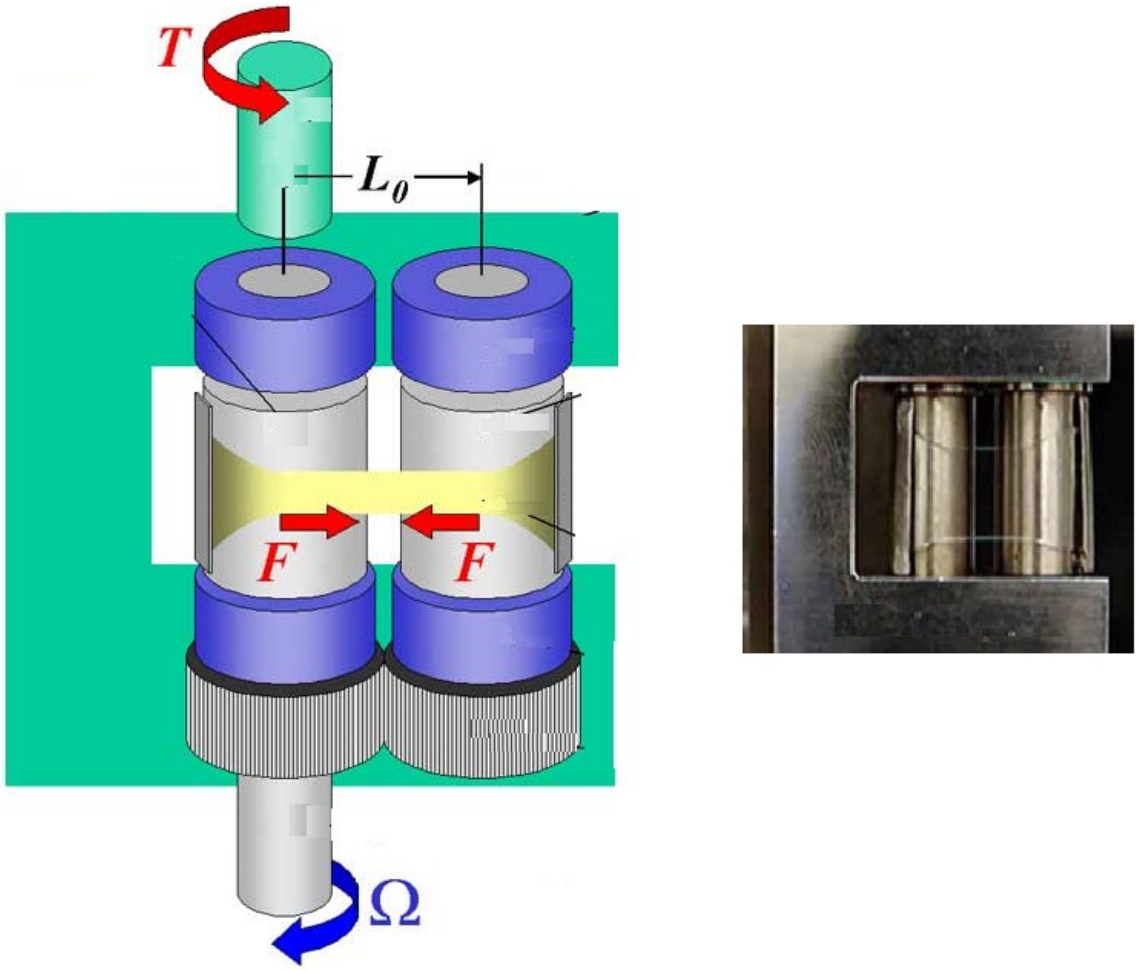

Figure 1-12: Testing fixture to perform uniaxial extensional measurements on an ARES rheometer (images are from: http://www.xinst.com).

At short times, the extensional viscosity slowly increases with time and, in this region, the curve presents linear viscoelastic properties and the viscosity is only a function of time ($\eta_E^+(t)$) as calculated from equation (1-24). On the other hand, at longer times, the extensional viscosity increases rapidly and the data deviates from the linear behavior. In this region, the viscosity is a function of both time and strain rate ($\eta_E^+(t, \dot{\varepsilon})$). This region of rapid increase in extension is called strain-hardening. There are advanced models for describing the molecular origin of this hardening effect in polymeric systems (Wagner et al. 2000; Marrucci and Ianniruberto 2004) and some of these topics will be mentioned in chapter 5.

For nano-composites, in contrast to dynamic data, there is a limited amount of information in the literature on their extensional behavior. However, similar to linear properties, it is well agreed that extensional properties are also sensitive to structural variables such as polymer-particle interactions, particle-particle interactions and the state of dispersion.

Increased extensional viscosity in the linear regime as a result of nano-filler introduction is a general feature of nano-composites. This is expected from both the linear viscoelastic properties and equation (1-24) where an increase in the storage modulus was discussed in detail as part of the discussion on the SAOS data. However, the existence and extent of strain-hardening in nano-composites is highly dependent on the structure. Similar to other types of deformations, polymer and particle characteristics, as well as particle spatial distribution inside the polymer, are important in determining extensional properties. Due to the type of deformation, the extensibility of a material is very sensitive to polymer-particle interactions (coupling) and the state of dispersion.

Reduction in strain-hardening was observed for systems in which the polymeric chain was not properly coupled with the nano-particle (Park et al. 2006; Lee et al. 2009). Similar results were also reported when the dispersion quality was reduced (Gupta et al. 2005).

Normally, addition of nano-particles reduces extensibility. However, an interesting phenomenon where strain-hardening increased as a result of nano-particle introduction was reported for PP-clay nano-composites (Okamoto et al. 2001a; Okamoto et al. 2001b). Okamoto and coworkers found that a complex internal structure was created under elongational flow. As a result of the creation of this network, strong strain-hardening was observed for nano-composites while, for the neat polymer (PP), no strain-hardening was observed. Specifically, $\eta_E^+(t,\dot{\varepsilon}$ of the nano-composites was more than 10 times larger than $3\eta_0$ for the neat polymer and the elongational viscosity of the nano-composites increased continuously with time. By analyzing the structure, it was found that extensional flow led to a stronger structure than the unstretched one. As a result of stretching, new clay surface was exposed and exfoliation increased accordingly.

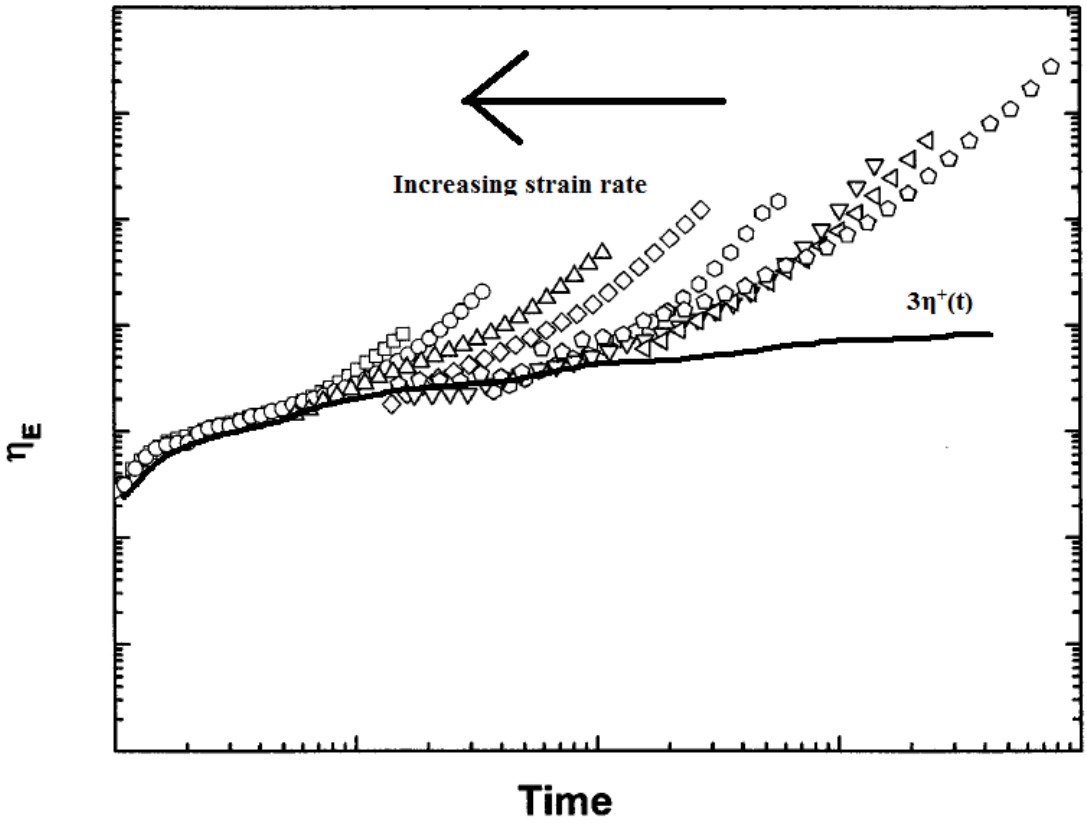

Figure 1-13: Typical extensional viscosity curve for a polymer showing strain-hardening (Okamoto et al. 2001a).

These few examples show that in addition to processes such as blow-molding and foaming, where elasticity and maximum extension must be carefully controlled, extensional data can also be used to study the structure of nano-composites.

1-5 Rheological modeling for nano-composites

Although the main objective of this work is to experimentally relate the rheological properties to the nano-composite structure, rheological modeling is used in chapter 5 for the shear and extensional properties of the nano-composites. Therefore, before ending the introduction part a brief review on the modeling of nano-composites rheological properties is presented. Generally speaking, the models are categorized based on the length scale they consider. In this context, three main categories can be mentioned: models on molecular

scale, macro scale, and a length scale between these which is micro scale (Zeng et al. 2008).

In the first category (molecular scale) the atoms, molecules or their small collections are considered as the basic units and the dynamics are discussed based on the size scale comparable to these units. The two main methods are molecular dynamics (MD) and Monte Carlo simulations which have been used repeatedly in polymer nano-composites (Boek et al. 1997; Huh and Balazs 2000; Smith et al. 2002; Starr et al. 2003; Kairn et al. 2005; Sarvestani 2008; Zeng et al. 2008; Batistakis et al. 2012).

These models have some limitations. First, due to the atomic size scale involved, the number of mathematical operation is high which can result in complexity while modeling. Another problem is also related to the small size involved in the modeling. Normally, the nano-fillers used in polymer nano-composites contain sizes larger than the molecular level involved in these simulations. Therefore, these models cannot be properly applied for nano-composites that are practically used. Consequently, these models cannot provide useful information regarding the nature of the interfacial interactions or particle-particle interactions and some other structural parameters at the nano scale dimension (Allegra et al. 2008).

The second category (macro scale models) does not consider discrete molecular structure and suppose that the material is continuously distributed in its volume. In this case, the rules of continuum mechanics are used (Zeng et al. 2008). These modeling are normally used by people having a mechanical engineering background. Some classical models like Halpin-Tsai, Einstein, Guth-Gold, or other models based on the rules of mixture can all be considered in this category which has been used frequently in composite science (Tandon and Weng 1984; Tucker III and Liang 1999; Huber 2002; Odegard et al. 2004; Greco et al. 2007).

Although these models are appropriate to describe macroscopic properties, they provide less information about the microstructure and the importance of structural variables at the micro scale level.

Finally, micro scale models are an intermediate (from the size scale involved) between molecular methods and continuum methods. The focus of these models is to study the microstructure related dynamics. In polymer science, this range characterizes the length scale at which molecular details are averaged, but the material cannot yet be considered as a homogeneous continuum (Allegra et al. 2008). Since these models do not consider very short length scales, the mathematical complexity is highly reduced compared to molecular simulations. On the other hand, these models consider micro scale dynamics which can be used to study the structure of nano-composites. Therefore, these models are very interesting in the field of nano-composites rheology, especially when the focus is to capture the roles of structural variables. Most of the models in this category contain adjustable parameters and therefore special attention should be considered when interpreting the physical significance of these parameters. Starting from a polymer, the most appreciated models are based on the tube concept which was first proposed by Doi and Edwards (1989). In this concept the effect of molecules on a test chain is averaged in an imaginary tube which represents the effect of entanglement and therefore by this averaging the situation is much easier to be studied particularly from a modeling point of view. Considering the applicability of this concept, few works tried to study the effect of nano-particles also based on this framework where the relaxation mechanisms proposed for the polymer were modified in the presence of nano-particles (Dong and Youn 2007; Jancar 2009; Kabanemi and Hétu 2013).

The main problem for tube based models is that these models mainly consider the polymer characteristics and partly some interfacial phenomena. However, for nano-composites the situation is more complex. First, chain relaxation is strongly influenced by the presence of particles and particle jamming (networking), especially at high concentrations (higher than percolation), has an important effect in composite dynamics; a phenomena which is not considered in tube based models.

In this situation many models based on fractal dynamics have been proposed (Shih et al. 1990). Based on these models the composite (typically percolated systems) is considered as a combination of local fractals, and property changes are related to the characteristics of

these fractals. Considering that normally in polymer nano-composites, the situation is in the percolated state, these fractal models have been used repeatedly to interpret the rheological behavior of polymer nano-composites (Mobuchon et al. 2007; Vermant et al. 2007; Cassagnau 2008; Mobuchon et al. 2009). In chapter 3, some of the aspects related to these models have been used to interpret the rheological behavior observed for nano-composites. More details on modeling of polymer nano-composites can be found in different reviews such as Allegra et al. (2008), Zeng et al. (2008), as well as Kabanemi and Hétu (2013).

1-6 Thesis objective and organization

Thus far, the applicability of rheological experiments to understand the effects of introducing nano-particles into polymer systems was reviewed. Two important deformations were discussed including oscillatory (SAOS and LAOS) and stepwise (shear and extension) deformations. Their importance and applicability to understanding the structure of nano-composites was discussed in detail. Due to the diversity of results in the literature, very different interpretations can be made leading to possible uncertainty when studying the physical principles controlling nano-composite properties.

The main objective of this work is thus to get a deeper understanding of the relations between microstructure and final rheological properties of polymer nano-composites. In this context, this thesis focuses on polymer nano-composites based on ethylene vinyl acetate (EVA) containing three geometrically and chemically different nano-particles: nano-crystalline cellulose (NCC), clay, and $CaCO_3$. The choice of EVA was based on three main issues. First, EVA has a low melting temperature (~80°C) and melt blending could be performed at low temperature. This is particularly important for NCC to limit thermal degradation of the material while processing. Also, EVA has a polar nature and therefore the affinity of the polymer towards hydrophilic particles (the three particles used here and mainly NCC) is appropriate. So good coupling is expected for these nano-composites even without using a third component as coupling agent. Finally, EVA is a common industrial polymer having properties similar to polyolefins, more specially polyethylene (PE). So understanding the effect of structural variables for EVA based nano-composites will not

only help to understand the situation for this polymer, but also the data can be extended to other similar structures which are very common in the plastic industry.

The compositions were prepared by melt blending and then compression molded. The obtained materials were subjected to a wide range of deformation including small and large amplitude oscillatory shear (SAOS and LAOS), as well as transient deformations in shear and extension. The results are then discussed in the next chapters.

The first part of the study (chapter 2) is related to NCC nano-composites for which, due to the chemical structure of cellulose, it was not possible to distinguish between the polymer and particles by common image analyses. Thus this part seeks to infer the unknown structure of the samples by rheological measurements. After determining the percolation threshold by linear viscoelasticity, structural changes for concentrations lower and higher than a threshold are discussed based on linear and non-linear rheological properties. In particular, the nano-composites response under shear transient tests is discussed in detail based on a model considering the effect of NCC interactions.

In the second part of the work (chapters 3-5), a study on the effect of particle shape is performed via linear and nonlinear viscoelastic properties of nano-composites containing isometric (spherical $CaCO_3$) and anisometric (clay platelet) particles is performed in a concentration range between 2.5 and 15 wt%. For these systems, since the particles and the polymer are distinguishable, morphological analyses through SEM and TEM are used to strengthen the interpretations.

More especially in chapter 3, the relation between linear and non-linear shear response of nano-composites based on clay and $CaCO_3$ is discussed. The effect of particle-polymer interactions which are related to the relaxation phenomena happening at the chain-particle interface and particle-particle interactions which are related to the particles tendency to form a network structure inside the polymer is discussed. The role of other structural variables, in particular particle shape, in affecting these interactions and hence the final properties is highlighted as well. This is done by analyzing the scaling properties of the storage modulus (G') in SAOS and stress overshoot (σ_{max}) in step shear.

In chapter 4, the same analysis as in chapter 3 is discussed for the same nano-composites, but on pre-sheared samples. The effect of particle orientation, which happens mainly for anisometric particles, is discussed with the aim of highlighting the effect of particle-particle interactions on the final rheological properties.

To validate the findings of chapters 3 and 4, and also to have a deeper understanding of the mechanisms involved in rheological properties, chapter 5 deals with the rheological properties of nano-composites containing clay and $CaCO_3$ under transient shear and extension. The mechanisms related to particle shape affecting the linear and mainly the nonlinear behavior are discussed in relation with rheological predictions by a molecular stress function (MSF) model. The validity and limits of such model to predict the nonlinear rheological properties of the nano-composites is investigated. In order to better address the limitation of the MSF model, quantification via LAOS data and FT-rheology is used to address the nonlinearity resulting from a nano-particle network.

Finally, in chapter 6, by combining the rheological properties of different nano-composites, the microstructural development at concentrations lower than percolation, at percolation, and higher than percolation is discussed, and a more comprehensive picture for the rheological behavior of the nano-composites is presented.

Chapter 2 Linear and non-linear viscoelastic properties of ethylene vinyl acetate/nano crystalline cellulose

H. Mahi and D. Rodrigue, Rheol. Acta, 51, 127-42 (2012).

Résumé

Cet article présente les propriétés rhéologiques à l'état fondu de l'éthylène-acétate de vinyle contenant entre 0 et 10% (en poids) de nanocellulose cristalline (NCC). Un ensemble complet de tests rhéologiques comprenant des balayages en fréquence, des cisaillements transitoires et des élongations uniaxiales a été effectué. Les balayages en fréquence ont montré que, dans les basses fréquences, un comportement du type pseudo-solide a été obtenu pour des concentrations en NCC supérieures à 5%. Ce comportement est lié à la liaison hydrogène entre les particules de la NCC et la création de réseaux de particules résultant d'interactions entre les particules. Pour les tests de cisaillement transitoire, toutes les compositions ont présenté un dépassement de contrainte pour des vitesses de cisaillement élevées avant d'atteindre un état d'équilibre. Il a été constaté que l'amplitude de ce dépassement dépend à la fois du contenu en NCC et du taux de cisaillement. D'autre part, il ressort que le temps pour atteindre le maximum de contrainte dépend fortement du taux de cisaillement, mais faiblement de la concentration. Pour une déformation en extension uniaxiale, la viscosité élongationnelle augmente avec l'augmentation de la concentration en NCC. D'autre part, il a été constaté que le caractère rhéo-épaississant diminue avec l'augmentation de la teneur en NCC.

Abstract

This paper reports on the melt rheological properties of Ethylene Vinyl Acetate (EVA) containing between 0 and 10% wt. of Nanocrystalline Cellulose (NCC). A complete set of rheological tests including frequency sweeps, shear transients and uniaxial elongations was performed. Frequency sweeps showed that at low frequencies, a pseudo solid-like behavior was obtained for NCC concentrations higher than 5%. This behaviour was related to hydrogen bonding between NCC particles and the creation of particle networks as the result of particle-particle interactions. For transient shear tests, all compositions presented a stress overshoot at high shear rates before reaching a steady state. It was found that the amplitude of this overshoot depends on both NCC content and shear rate. On the other hand, the time to reach the maximum was found to be highly shear rate dependent but concentration dependence was rather weak. For uniaxial extensional flow, higher extensional viscosity was observed with increasing NCC content. On the other hand, strain-hardening was found to decrease with increasing NCC content.

2-1 Introduction

In the last few years, polymer nano-composites have been the focus of extensive research efforts. To this end, different nano-particles like nano-clays, carbon nano-tubes, carbon nano-fibers, graphite, silica, and nano-metals have been studied. Recently, the potential of nanocrystalline cellulose (NCC) for the production of improved nano-composites was presented (Favier et al. 1995). Since then, because of its renewability, bio-structure, high surface area, light weight and unique morphology, NCC has attracted great interest in the nano-composite field and has been used in various polymeric matrices like polyethylene (Menezes et al. 2009), polycaprolactone (Siqueira et al. 2009, Habibi et al. 2008), polyvinyl coloride (Chazeau et al. 2000), polyurethane (Marcovich et al. 2006), polymethylmethacrylate (Liu et al. 2010), polyethylene-co-vinyl acetate (Chauve et al. 2005), polypropylene (Gray 2008), ethylene oxide–epichlorohydrin (Schroers et al. 2004), polyvinyl alcohol (Shweta et al. 2008) poly(oxyethylene) (Azizi et al. 2004a), polystyrene (Capadona et al. 2007), and poly(lactic acid) (Mathew et al. 2006). Also, a review on the subject was prepared by Habibi et al. (2010).

Among these works, few studies used extrusion to prepare NCC-based nano-composites. Mathew et al. (2006) for the first time used this method for the production of polylactic acid NCC nano-composite. Also, extrusion processing of modified NCC with low density polyethylene was attempted by Menezes et al. (2009). The main challenges in melt processing are low thermal stability of NCC, as well as availability of the material in large quantities and processing conditions optimization.

Another challenge which is not specific to NCC nano-composites but for most nano-composites is to characterize the nano-structure. Generally, two main methods are used: structure analysis and property analysis. Structure analysis is carried out using various techniques like wide-angle X-ray diffraction (WAXD), transmission electron microscopy (TEM), scanning electron microscopy (SEM) and small angle x-ray scattering (SAXS). Because of the specific properties of nano-structured materials, each of these techniques has some limitations (Paul and Robeson 2008) and no single technique can provide adequate information related to the structure of nano-composites. Another possibility is property analysis. The properties of nano-composites highly

depend on their structure. Therefore, property analysis is an appropriate method for the assessment of the nano-structure. While structural analyses are qualitative methods, properties can be modeled easily and used for quantitative analysis. For NCC nano-composites, different tools like TEM (Menezes et al. 2009, Liu et al. 2010, Morin and Dufresne 2002), SEM (Liu et al. 2010, Azizi et al. 2004b) and AFM (Kloser and Gray 2010) have been used. But, it is difficult to have a complete representation of polymer nano-composites due to limited contrast with most polymer matrices because of the carbon based structure of NCC. This is why property analysis would be very informative in understanding the structure-property relations of these nano-composites. Up to date, the studies mostly focused on solid state properties like mechanical (Liu et al. 2010, Morin and Dufresne 2002), dynamic mechanical (Favier et al. 1995, Morin and Dufresne 2002, Dalmas et al. 2006) and thermal properties (Morin and Dufresne 2002, Gray 2008, Habibi and Dufresne 2009).

To our knowledge, there is no melt rheological analysis of NCC nano-composites. Rheological analysis is an important first step in any melt processing operation. In order to optimize processing conditions, rheological properties, especially non-linear ones, must be understood. Furthermore, rheological properties (linear and non-linear) are very sensitive to the nano-structure (Utracki and Jorgensen 2002, Muenstedt et al. 2008, Xu et al. 2005).

To date, several studies used linear rheology as a mean to assess the state of dispersion of nano-fillers (Zhao et al. 2005, Du et al. 2004, Huang et al. 2006, Xu et al. 2009). Parameters like particle orientation, exfoliation degree, as well as particle-particle and particle-polymer interactions have also been assessed by rheological studies (Du et al. 2004, Kagarise et al. 2010, Handge and Pötschke 2007, Akcora et al. 2010a). Furthermore, transient studies have been used to understand the non-linear viscoelastic properties and to assess the structure of nano-composites (Gupta et al. 2005, Letwimolnun et al. 2007, Chatterjee and Krishnamoorti 2008). So, in addition to processing issues, rheology can be used to understand the structure of nano-composites. A good review regarding this issue has been recently prepared by Utracki et al. (2010).

Therefore, the main objective of this work is to perform rheological studies on NCC nano-composites to get detailed information on the processing issues of these nano-composites. The

study also provides appropriate information about the structure-properties of these advanced nano-composites. As a first step, ethylene vinyl acetate (EVA) is used as the matrix. EVA has a low processing temperature minimizing possible NCC degradation in the blending, molding and characterization steps. Also, this polymer is highly polar which is believed to improve dispersion and compatibility between the matrix and the reinforcement.

2-2 Experimental

Ethylene vinyl acetate (EVA) was used as the matrix: ELVAX 360 from DuPont which contains 25% of vinyl acetate. This polymer has a melt index of 2 dg/min, a density of 948 kg/m^3 and a melting point of 78°C. The nanocellulose (NCC) was produced based on acid hydrolysis of softwood.

Before blending, NCC was dried at 60°C for 8 h. To prepare the nano-composites, EVA was melt blended with different NCC contents as described in Table 2-1. Blending was performed in a batch mixer (Rheocord 40 from Haake Büchler) for a total time of 15 min at a speed of 70 rpm and a temperature of 110°C. At first, the polymer was introduced to get a homogeneous melt. When the torque became stable (normally after 2 min), the selected amount of NCC was added slowly to the mixer. In order to have similar processing history, the neat polymer (0% NCC) was also processed under the same conditions to impose a similar thermo-mechanical history for the matrix. The compounds were then compression moulded at 150°C under 2300 kg (5000 lb) of force in a rectangular mold having dimensions of 100 x 100 x 1.8 mm3 for 3 min. Finally, the samples for rheological testing were directly cut in the molded plates.

2-2-1 Scanning electron microscopy

A scanning electron microscope (SEM) JEOL JSM 840A from JEOL USA Inc. was used for morphological investigations. The samples were first frozen in liquid nitrogen before being fractured to expose the structure which was then coated with Pd/Au prior to SEM observation.

Table 2-1. Compositions of the nano-composites produced.

Sample	EVA (% wt.)	NCC (% wt.)
EVA 0	100	0
EVA 2.5	97.5	2.5
EVA 5	95	5
EVA 7.5	92.5	7.5
EVA 10	90	10

2-2-2 Dynamic shear tests

All the shear rheological tests were performed on a strain controlled TA Instruments rheometer (ARES) with a torque transducer (0.02-2000 g-cm) and a normal force transducer (2-2000 g). All measurements were done using a 25 mm diameter parallel plate geometry with a gap between 1.5 and 2 mm. At first, strain sweep tests were performed at a frequency of 1 rad/s to determine the linear viscoelastic range of each sample. A deformation of 2% was then chosen to perform frequency sweeps in the range 0.01-300 rad/s. The tests were performed at different temperatures: 110, 150 and 190°C. But due to space limitation, only the data at 190°C will be presented here because at this temperature the terminal behaviour of the composites can be better studied.

2-2-3 Transient shear tests

The shear viscosity growth function $\eta^+(t,\dot{\gamma})$was obtained with the same geometry as for dynamic tests (25 mm plates). The shear rates used were: 0.005, 0.01, 0.03, 0.05, 0.1, 0.5 and 1 s^{-1}. In order to study shear induced alignment, the same procedure as Letwimolnun et al. (2007) was used. The sample was first sheared during a preset time (300 s) and the test was stopped allowing the sample to rest for a determined time period (200 s). Next, the test was started again at the selected shear rate in the same (Clockwise, CL) direction. Then, the material was allowed

to rest again (200 s) and the same rate was applied in the opposite (Counter-clockwise, CCL) direction. In order to examine the no slip boundary condition, shear tests with different gap distances (1.2-2.4 mm) was performed and it was found that wall slip does not happen within the conditions tested (see Appendix A).

2-2-4 Transient elongational tests

To perform uniaxial elongation deformation, the SER HV-A01 model of the SER universal testing platform from Xpansion instrument (Sentmanat 2004) was used as in our previous studies (Twite-Kabamba and Rodrigue 2008). The tests were performed at a temperature of 110ºC on rectangular samples with dimensions of 17 x 10 mm2 with thicknesses between 0.8 and 1.0 mm. The deformation rates were set between 0.05 and 5 s-1. In order to determine the dimensions of the sample at the testing temperature, PVT data for EVA were used (Wohlfarth 2001).

2-3 Results and Discussion

2-3-1 Morphology

A SEM image of the original NCC particles (before blending) is shown in Figure 2-1a. Agglomerates with different sizes (the maximum being around 1 mm) are observed. These agglomerates are created by hydrogen bonding between cellulosic particles. From the processing point of view, the agglomerates are a challenge and, in order to have a good dispersion, these agglomerates must be broken. On the other hand, from a mechanical point of view, the hydrogen bonds between the particles in the cellulosic composites are interesting because the particles can create a network and therefore provide a pathway for stress propagation leading to improved mechanical properties (Favier et al. 1995, Habibi et al. 2010). The fractured surface of EVA 0 (Fig. 2-1b) and EVA 10 (Fig. 2-1c) shows different appearance. The surface of EVA 10 is rougher than EVA 0. This is probably the result of higher energy dissipation to fracture the nano-composite as cellulosic particles provide different crack paths (Marcovich et al. 2006). At higher resolution, EVA 10 (Fig. 2-1d) shows connected pathways that are most probably created by NCC particles. Although the particles are not clearly distinguishable from the polymer (because the particles and polymer are carbon based and therefore have similar structures under SEM observation), the picture shows a homogenized surface indicating good particle dispersion.

At still higher magnification (Fig. 2-1e), these pathways and the homogeneity of the composite surface are more clearly seen.

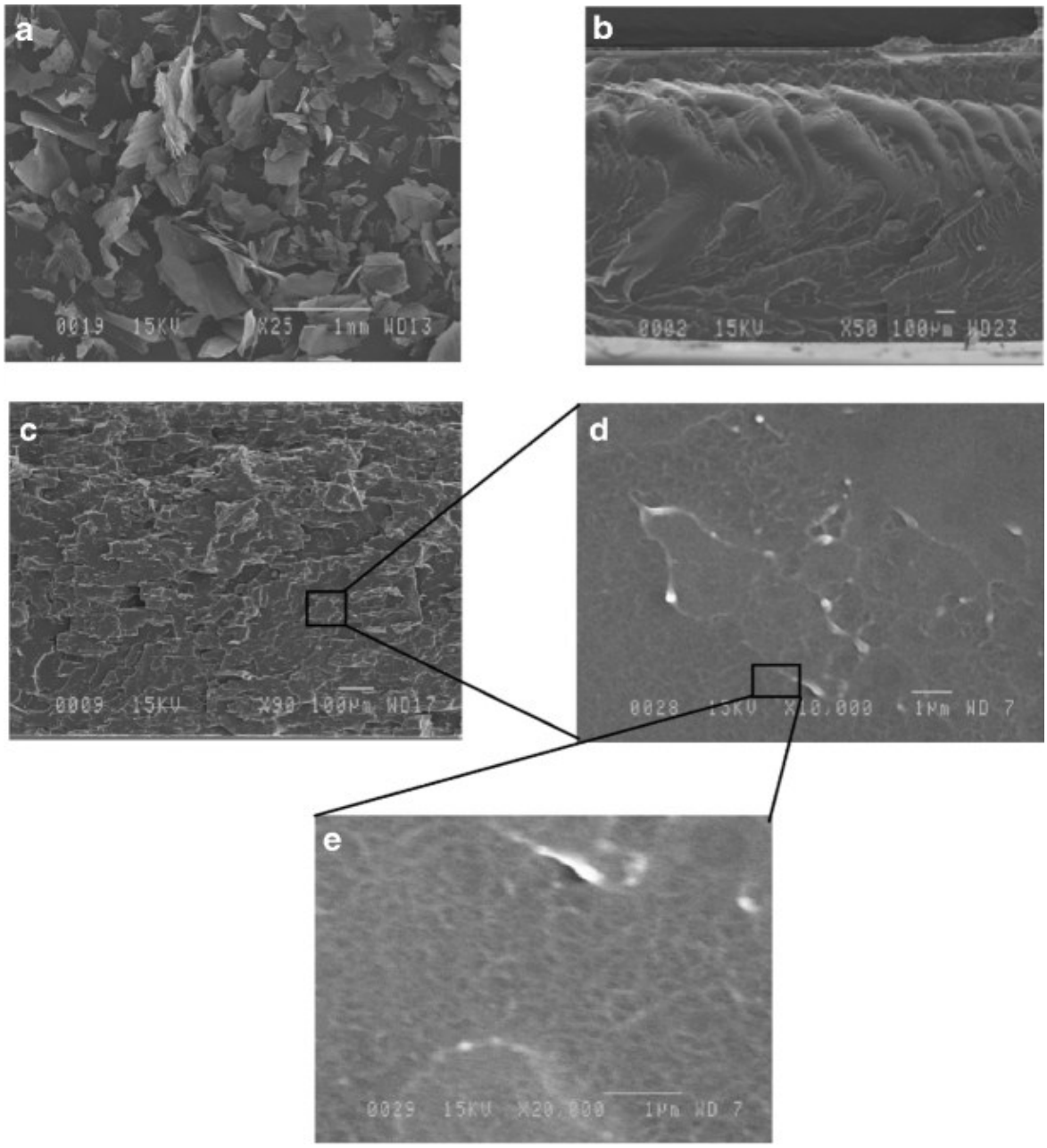

Figure 2-1: SEM images of: a) the original nanocellulose, b) the fractured surface of the neat polymer EVA 0, and c–e) the fractured surface of EVA 10 at different magnification.

2-3-2 Dynamic shear

The rheological behavior of EVA and nano-composites under small amplitude oscillatory shear is presented in Fig. 2-2. At high frequencies, small differences between the polymer matrix and the nano-composites are observed. However, at low frequencies differences are evident, especially as NCC concentration increases. Generally, increased nano-composites modulus can be related to the presence of a rigid filler and to chain strengthening. The latter has been ascribed to polymer-particle interactions (either frictional interactions and/or chemical interactions) and particle-particle interactions. The high frequency region impacts the short-range dynamics of polymeric chains. Considering the nano-scale of the filler, the effect of the particles themselves is not significant at high frequency, which is the range associated to shorter dynamics. At low frequencies, EVA chains can relax and the polymer exhibits typical terminal behaviour for both G' ($\sim\omega^2$) and G" ($\sim\omega^1$). With increasing NCC content, the terminal behavior disappears and the dependence of G' and G" on frequency is weakened. The existence of non-terminal behavior in dynamic shear tests leads to a pseudo solid-like rheological properties.

Two different mechanisms have been proposed for the appearance of solid-like behaviour in nano-composites (Akcora et al. 2010a). One mechanism is based on polymer particle interaction and considers a polymer glassy layer around particles and consequently relates the mechanical improvement to the creation of these confined layers (Merabia et al. 2008, Bogoslovov et al. 2008, Dutta et al. 1994). Since these glassy layers do not relax, a solid-like behavior is observed at low frequencies. Another scenario considers particle-particle interactions. This mechanism states that above a specific concentration called the percolation threshold, nano-particles can create a network structure (Du et al. 2004, Wang et al. 2006). As a result of these networks, particles can create a pathway for stress propagation (Solomon et al. 2001), and therefore cause the nano-composites to show solid-like rheological and mechanical behaviors. These networks are not necessarily physical contacts as it is the case for electrical percolation (Du et al. 2004). For cellulosic nano-composites, it is believed that mechanical improvement is based on the second mechanism which is related to the percolation mechanism (Favier et al. 1995, Habibi et al. 2010). As a result of inter-particle hydrogen bonding particles tend to create such networks especially at high concentrations. Although there is no melt rheological analysis for cellulose nano-composites to compare, mechanical data for these nano-composites can be found and

reduction of particle-particle interactions was shown to decrease the elastic modulus of these nano-composites. For example, results of cellulosic nano-composites based on natural rubber (Nair et al. 2003), acetate butyrate (Grunert and Winter 2002) and polypropylene (Ljungberg et al. 2005) showed that nano-composites have lower modulus by reducing cellulose interactions. Recent simulations (Habibi et al. 2010 and Favier et al. 1997) also revealed that mechanical models based on percolation can well predict the behavior. The percolation threshold was found to depend on various parameters like morphology of the nano-particles, state of dispersion, polymer molecular weight distribution and processing methods. Therefore, different values for percolation thresholds have been reported. For example, Du et al. (2004) reported a percolation of only 0.12% wt for poly(methyl methacrylate)/single wall nano-tubes (SWNT) nano-composites. Akcora et al. (2010b) observed a solid-like behavior in polystyrene/silica nano-composites at 1% wt, while Kim and Macosko (2008) reported 5% wt as the percolating concentration for graphite nano-composites. For cellulosic nano-composites, different percolation concentrations have been also reported: 1% wt by Morin and Dufresne (2002), 1.5% wt by Favier et al. (1995) and 5% wt by Dalmas et al. (2007) using mechanical analysis. Here, the solid-like behaviour is observed only at higher concentrations (7.5 and 10%) indicating a change between 5 and 7.5%. But why the solid behavior is observed at such high concentrations here? This also can be related to the mentioned particle interactions. It seems that when good coupling exists between the particles and the polymer matrix, NCC particles interact with the polymer rather than with each other to interconnect and form the network. In this work, because of the high vinyl acetate content in EVA (25%), good coupling is believed to exist between the polymer matrix and NCC particles. Therefore, less hydrogen bonding is available to participate in NCC-NCC interactions and the behavior is mostly matrix dominant.

The solid-like behavior appears only at high NCC concentrations where hydrogen bonds are more probable. The existence of such network structures can also be seen in Figure 2-1d and 2-1e where NCC appeared to be in an interconnected network. At such a high concentration (10%), in addition to chemical interactions which are resulting from hydrogen bonding, physical contacts also contribute to the creation of a network structure.

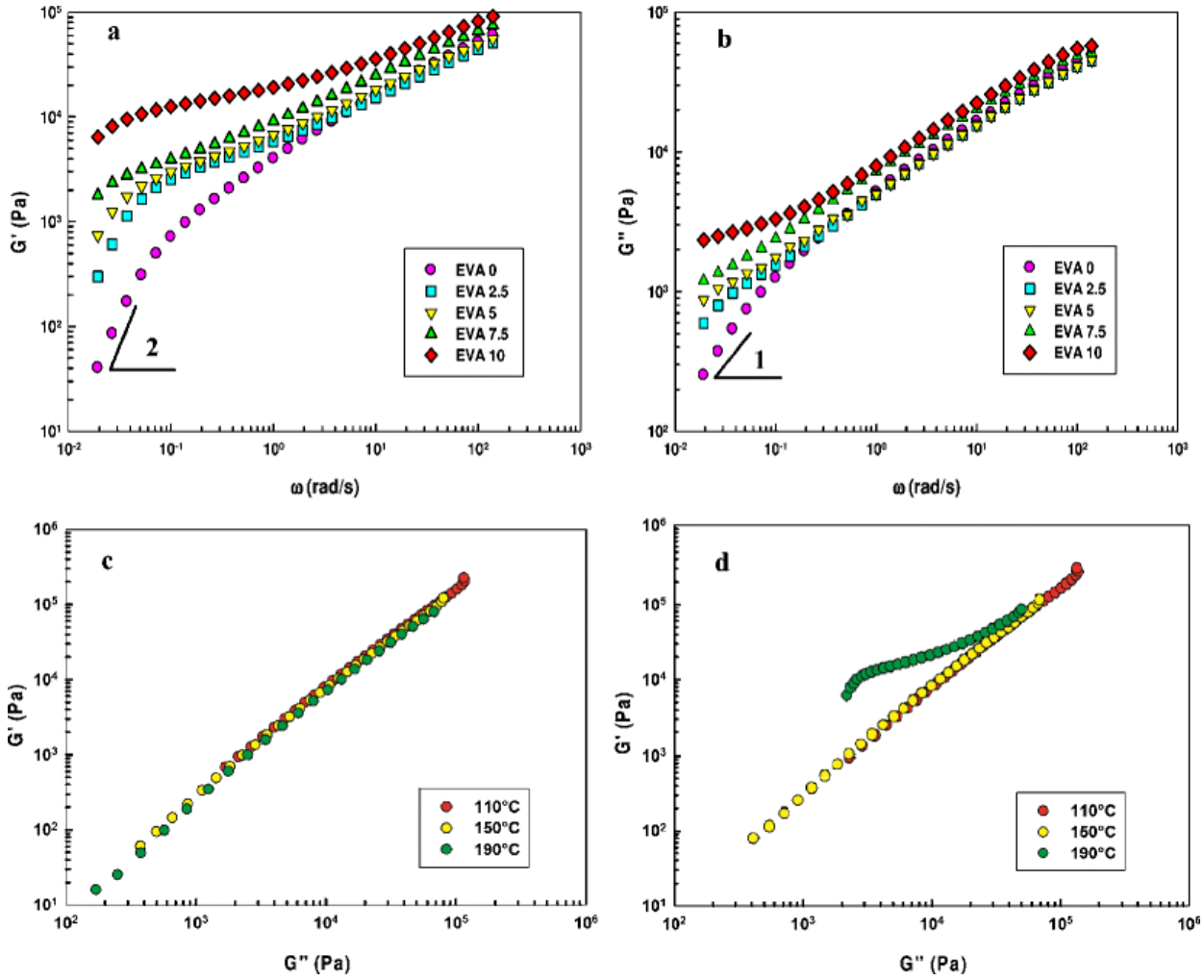

Figure 2-2: Dynamic storage (a) and loss (b) moduli of EVA and the nano-composites at 190°C. Verification of the time–temperature superposition for EVA 0 (c) and EVA 10 (d).

Because of a liquid- to solid-like transition, the nano-composites deviate from the time-temperature superposition. This is shown in Figure 2-2c and 2-2d. It can be seen for EVA that the data at different temperatures are on the same curve, but for EVA 10 the data at high temperature (190°C), which is the range where the solid-like behavior appeared, deviate and shows that the TTS does not apply. For other concentrations also, such deviation was observed but for space limitation, only the data for the highest concentration are presented.

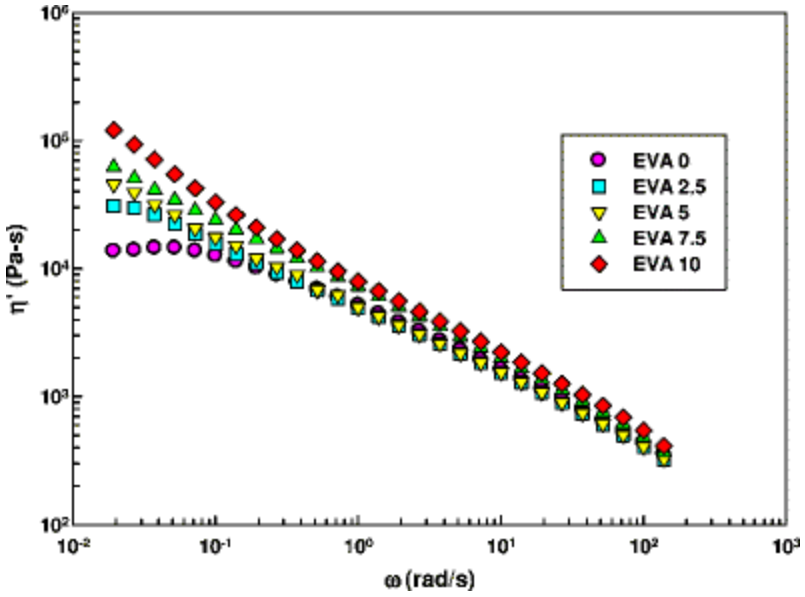

Figure 2-3: Dynamic viscosity of EVA and the nano-composites at 190°C.

The dynamic viscosity (Figure 2-3) of neat EVA and NCC nano-composites also shows a similar trend as G' and G''; i.e. significant differences at low frequencies and small differences at high frequencies. At low NCC content (2.5%), the nano-composites showed higher zero shear viscosity than the neat polymer, while at higher concentrations (5% and above) the nano-composites do not show a measurable zero shear viscosity and present evidence of yield stress. Most of the literature reporting yield phenomenon suggested that this also can be related to the extent of interaction between the filler particles and the formation of a network structure (Hornsby 1999). At low concentration, the amount of hydrogen bonds between the particles is not sufficient to produce a solid-like behavior. As concentration increases, inter-particle distance decreases and more hydrogen bonds can form leading to the presence of an apparent yield stress. The existence of a yield stress is a common characteristic of highly filled polymer melts and for micron size composites, this behaviour was observed (Hornsby 1999, Twite-Kabamba et al. 2009). The difference here is that for nano-composites, the behaviour happens at much lower concentrations than for micro-composites. Another viscosity feature is that nano-composites show a more shear-thinning behaviour than the neat polymer. This can be characterized by using the simple power-law viscosity model as:

$$\eta' = m\,\omega^{n-1} \tag{2-1}$$

where the exponent *n* is related to the slope which represents the degree of shear-thinning behavior and *m* is the consistency index. The data of Figure 2-3 were fitted to Equation (2-1) for the range 0.1-100 rad/s and the values for the parameters are presented in Table 2-2. The results clearly show that *n* decreases and *m* increases with increasing NCC content.

2-3-3 Shear transient

The transient shear viscosity of EVA 0 and EVA 7.5 at different shear rates is shown in Fig 2-4. At low shear rates ($\leq 0.01 s^{-1}$), the viscosity is nearly constant and the behavior is Newtonian. However, a small deviation from Newtonian behaviour is seen for EVA 7.5. At higher shear rates a shear-thinning behaviour is observed: viscosity decreased with increasing shear rate. Another important parameter in transient shear tests which is very informative regarding the nano-composite structure is the presence or not of an overshoot. In a step shear test, the stress can go through a maximum before reaching a steady state. Stress overshoot is known to be related to changes in the morphological structure of the nano-composites (Letwimolnun et al. 2007). Stress-time curves of EVA and nano-composites are depicted in Fig. 2-5. In this figure, it is clear that the value of the maximum stress increases with increasing NCC content. This maximum is believed to be the result of alignment in polymer chains, rearrangement of nano-particles and breakdown of probable NCC networks especially at high concentrations.

Table 2-2. Parameters for the power-law viscosity model of Equation (2-1) for EVA and the nano-composites.

Sample	m ($Pa\text{-}s^n/rad^{n-1}$)	n (-)
EVA 0	4506	0.533
EVA 2.5	4783	0.486
EVA 5	5173	0.457
EVA 7.5	6930	0.443
EVA 10	8671	0.394

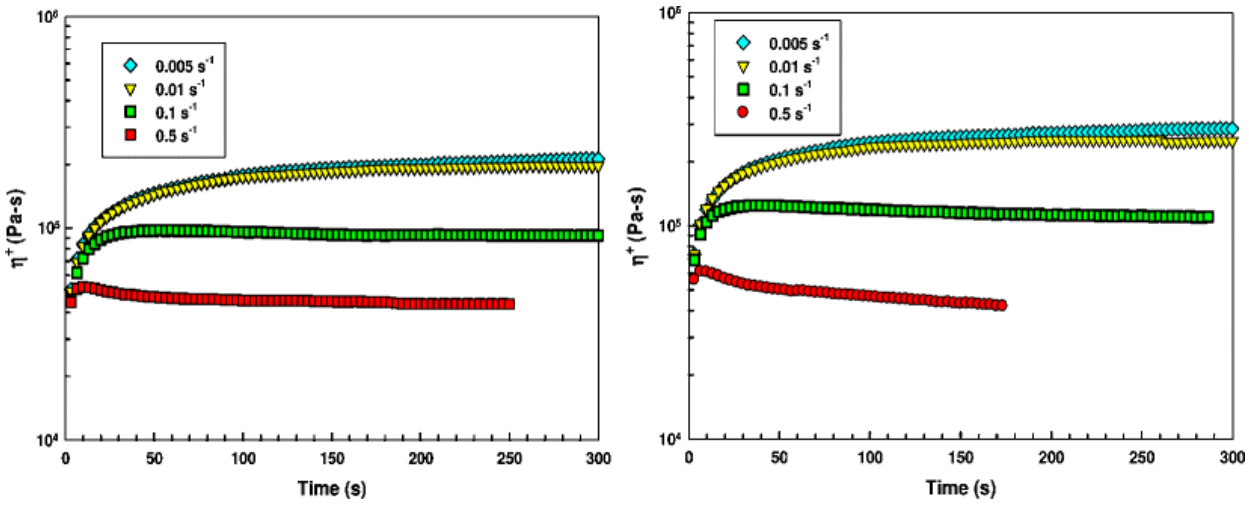

Figure 2-4: Transient shear viscosity of EVA 0 (left) and EVA 7.5 (right) for different shear rates at 110°C.

For the neat polymer, the stress only aligns the chains and therefore stress maximum is not significant. For nano-composites, in addition to polymeric chains, stresses induce nano-particle orientation since the particles are not spherical. Therefore, the level of stress overshoot increases with nano-particle concentration. Furthermore, increasing NCC concentration, as was found from dynamic data, increases the probability to create NCC networks due to hydrogen bonds. Thus, the structural reorganization and breakup of these networks would explain higher stresses levels as NCC content increases and the dissipation of the applied stress before stabilizing at a lower value.

The effect of shear rate on stress overshoot for EVA 10 is also plotted in Fig. 2-5. It can be seen that stress overshoot highly depends on shear rate. Furthermore it can be seen from Figure 2-5 that the time of to reach the maximum is concentration independent (left) and only depends on the applied shear rate (right). Normally, the strain at maximum stress ($\gamma_{at\sigma max}$) is independent of shear rate (Chatterjee and Krishnamoorti 2008, Goel et al. 2006, Kagarise et al. 2010). Here, the strain for maximum stress for each shear rate and concentration was calculated and the same value was obtained for all cases: 4.6±0.2. Considering that $t_{peak} = \gamma_{at\sigma\max} / \dot{\gamma}$ and that $\gamma_{at\sigma max}$ is almost constant, t_{peak} only depends on shear rate and therefore is independent of concentration.

Figure 5 also shows that the behavior in transient flow depends on both shear rate and NCC concentration and each effect must be quantified separately. To this end, dimensionless numbers are useful. Because of the viscoelastic nature of polymeric systems, their behavior cannot be described by a single number. This led to the use of several dimensionless numbers like Deborah (De) or Weissenberg (Wi) to account for viscoelastic effects in a transient deformation. In transient tests when the experimental time scale is long, the flow approaches steady state. For low shear rates, this approach happens gradually while at high shear rates, the time scale for relaxation is too short and a high stress is needed for deformation. Consequently, at high shear rates viscoelastic materials normally show a yield stress or stress overshoot. Therefore, two types of behavior can be obtained: data sets with or without stress overshoots. One criterion to express this transition depends on both characteristic times and testing rate. The influence of both parameters can be addressed by the Weissenberg number which is defined as:

$$Wi = \lambda \dot{\gamma} \tag{2-2}$$

where λ is the relaxation time of the material and $\dot{\gamma}$ is the shear rate applied (Dealy 2010).

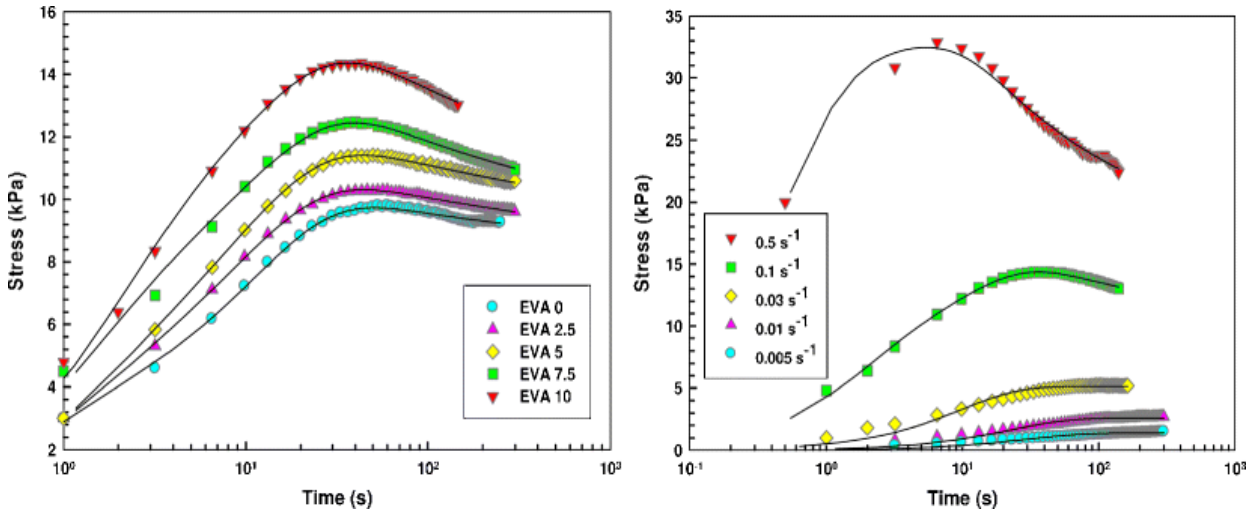

Figure 2-5: Stress overshoot for different nano-composites at a rate 0.1 s^{-1} (left) and for EVA 10 at different shear rates (right) at 110°C. Solid lines are model predictions from Eqs. (2-5) and (2-6) with the parameters of Figs. 2- 6 and 2- 7.

Usually, a Wi number around unity is used as the critical value for the appearance of nonlinear phenomena. Based on our experiments, an overshoot was observed for shear rates of 0.1 s^{-1} and higher. To verify this value, the longest relaxation time (λ) was calculated as:

$$\lambda = \frac{A_G}{\eta} \tag{2-3}$$

where A_G and η are obtained from the low frequency behaviour of the storage and loss moduli, respectively ($G' = A_G\,\omega^2$, $G'' = \eta\,\omega$) (Inoue et al. (2002a)). From these calculations, a value of λ = 10.1 s was obtained to produce a *Wi* number of around one at a shear rate of 0.1 s^{-1}. So the experimental observations are in agreement with this calculation. According to the tube model (Doi and Edwards 1989), in a shear flow two characteristic times are important. One is the orientational relaxation time for a deformed chain. The other one, which is comparatively shorter, is the time for chain equilibration along their contour length. The former is the longest stress relaxation time and the latter is associated with twice of longest Rouse relaxation time (2 τ_R). The origin of nonlinearity is the large difference between these two characteristic times. Recently Inoue et al. (2002a-b) and Osaki et al. (2001), based on the modified tube model proposed by Pearson et al. (1991) and different experimental results, showed the importance of the retraction time of ($2\tau_R$) on the appearance of nonlinear behaviour. They showed that stress overshoot is normally observed at shear rates higher than 1/ 5($2\tau_R$). To examine our results, τ_R was calculated based on the following equation (Osaki et al. 2001):

$$\tau_R = \left(\frac{\alpha M}{1.111 cRT}\right)^2 \tag{2-4}$$

where M is the molecular weight, c is the mass of polymer per unit volume and α is obtained from Rouse expression of storage modulus ($G' = \alpha\,\omega^{1/2}$) (Osaki et al. 2001). By fitting the storage modulus at high frequencies to Rouse mode (α = 18683) and considering $M = 100$ kg/mole (Palermo et al. 2001) and c = 850 kg/mole (Wohlfarth 2001), a value of 0.4s was obtained for τ_R. Based on the work of Inoue et al. (2002a-b), this indicates that at shear rates higher than 0.25 s^{-1} (1/5($2\tau_R$).) overshoot is expected for such material. This is higher than the observed one (0.1 s^{-1}). This discrepancy can be explained in two ways. First is the calculation procedure of τ_R. The proposed method by Osaki et al. (2001) uses the Rouse scaling relationship

for measuring α. Obviously, such scaling is only observed over a limited range of frequencies and this can reduce accuracy. It should be mentioned that other methods for such determination also have some sources of error (Osaki et al. 2001) and sometime the obtained values for τ_R from different methods differ by a factor as large as 8 (Osaki et al. 2001, Roland et al. 2004). The second explanation is regarding the specific value of $1/\ 5(2\,\tau_R)$. The emphasis of the works of Inoue et al. (2002a-b) on this specific value is based on limited experimental results for some polymers and therefore the value can be different for other polymers. The only parameter that is originated from robust rheological models is the retraction time ($2\,\tau_R$) which considers the effect of chain stretching in the Doi and Edwards theory. Generally, at shear rates sufficiently lower than $1/(2\,\tau_R)$ overshoot is not observed. This is a qualitative expression so the exact value for each polymer can be different. Considering these two explanations, the observed stress overshoot at shear rates of 0.1 s^{-1} and higher is conceptually reasonable within experimental uncertainty.

It can be concluded that when $Wi < 0.1$ (1.33 s x 0.08 s^{-1}), there is no overshoot and a simple exponential can be used to fit the stress data as:

$$\sigma(t) = \sigma_\infty \left[1 - \exp\left(-\frac{t}{\tau}\right)\right] \tag{2-5}$$

where σ_∞ is steady stress and τ is a characteristic time related to the material. The values for each parameter at different shear rates and concentrations are reported in Figure 2-6. It can be seen that shear rate has a stronger effect than concentration on the characteristic time τ. This characteristic time was found to follow a power-law relation with roughly the same scaling parameter for all concentrations ($\tau \sim \dot{\gamma}^{-0.45\pm0.03}$). This power-law scaling has been reported for many other viscoelastic materials like layered silicate (Solomon et al. 2001), liquid crystalline polymer solutions and crosslinked polymers (Winter and Chambon 1986). Whittle and Dickinson (1997) related this power-law dependency to the relaxation of the material ($G(t) = a_0\,(t)^{-n}$) and the scaling exponent (n) was found to be close to 0.5 for different systems like flocculated colloidal gels (West et al. 1994) and solid suspensions (Nagase and Okada 1986).

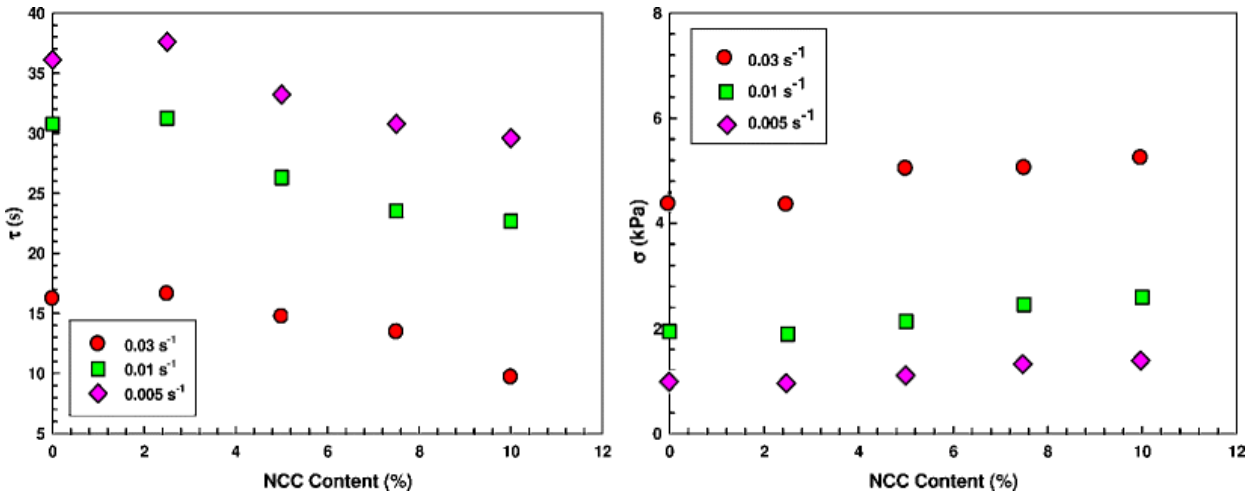

Figure 2-6: Shear rate and concentration dependence of the calculated parameters in Eq. (2-5).

Winter and Chambon (1986) showed that for materials showing a transition between a liquid-like to a solid-like behaviour, the relaxation modulus takes the form of $G(t) = a_0\, t^{-1/2}$. These findings indicate that regardless of particle morphology and reinforcing mechanism, viscoelastic materials showing pseudo solid-like behaviors have similar scaling parameters. In our case, stress relaxation tests gave roughly a similar value for the exponent (0.55). As expected, the steady stress value increases with increasing shear rate and NCC concentration. Since viscosity increases with NCC concentration, more stress is needed for this material to flow.

On the other hand, for Wi > 0.1 the materials presented stress overshoot and the data cannot be expressed by a simple exponential equation as in Eq. (2-5). In this case, Whittle and Dickinson (1997) proposed a semi-empirical model to represent the stress in transient shear tests as:

$$\sigma(t) = \sigma_0 \left[\frac{(t/\tau_1)}{1+(t/\tau_1)^{1+\delta}} \right] + \sigma_\infty \left[1 - \exp(-t/\tau_2)\right] \qquad (2\text{-}6)$$

where, according to the fractal model proposed by Chattejee and Krishnamoorti (2008) for poly-(ethylene oxide) carbon nano-tube composites, τ_1 is the time scale related with the rearrangement of the structure under shear and τ_2 is the time related to the network break-up (or flow), δ is a phenomenological parameter which influences the ratio of elastic response (first part of the equation) to the decay response (second part of the equation). The parameter σ_0 is related to the shear rate dependent elastic modulus and σ_∞ is the steady state shear stress.

Chattejee and Krishnamoorti (2008) used Eq.(2-6) only for concentrations high enough to create connected networks. But at high shear rates, even the neat polymer can show stress overshoots. This is why in this work, Eq.(2-6) was applied for all the concentrations (0-10% NCC). The values for each parameter are presented in Figure 2-7 (a-e).

Although the parameters related to the stress (σ_0 and σ_∞) are both shear rate and concentration dependent, the time scale related to yield stress (τ_2) is nearly concentration independent and only a function of shear rate. This means that while yield stress increases with concentration, associated time with material flow and steady deformation at the same shear rate is similar for all the compositions. On the other hand, τ_1 was found to increases with increasing concentration. This time scale is related to rearrangement of the structure and it seems that by increasing NCC concentration, structure rearrangement happens at higher time scales. The shear rate dependence of related time scales means that the behavior is far from being related to Brownian motion for which time scales should be independent of shear rate (Xu et al. 2009, Wang et al. 2006). This is the case because the viscosity of the matrix is too high to allow Brownian motion to occur. The Peclet number (Pe), which represents the ratio between hydrodynamic and Brownian forces, can be defined in shear flow by (Wang et al. 2006):

$$Pe = \frac{\eta_m \dot{\gamma}}{k_B T (\ln \frac{L}{D} - 0.8)} \tag{2-7}$$

where η_m is the viscosity of polymer melt, $\dot{\gamma}$ is shear rate, L is the NCC length, D is the NCC diameter, k_B is the Boltzmann constant and T is temperature. With the range of shear rates applied (0.005-0.5 s^{-1}), related steady viscosities for each shear rate and using the average dimensions of NCC as 100-1000 nm for L and 10-50 nm for D (Habibi et al. 2010), the associated Pe numbers would be in the range of 2×103 - 4×105. This is much greater than unity and indicates non-Brownian behavior for the particles.

Another feature about time scales is that τ_2 is always higher than τ_1 meaning that before the material flows, structure rearrangement must happen. The parameter δ also increases with shear rate and concentration. However, the concentration dependence is more evident at high shear rate (0.5 s^{-1}). As noted by Chattejee and Krishnamoorti (2008) for intermediate time range, the

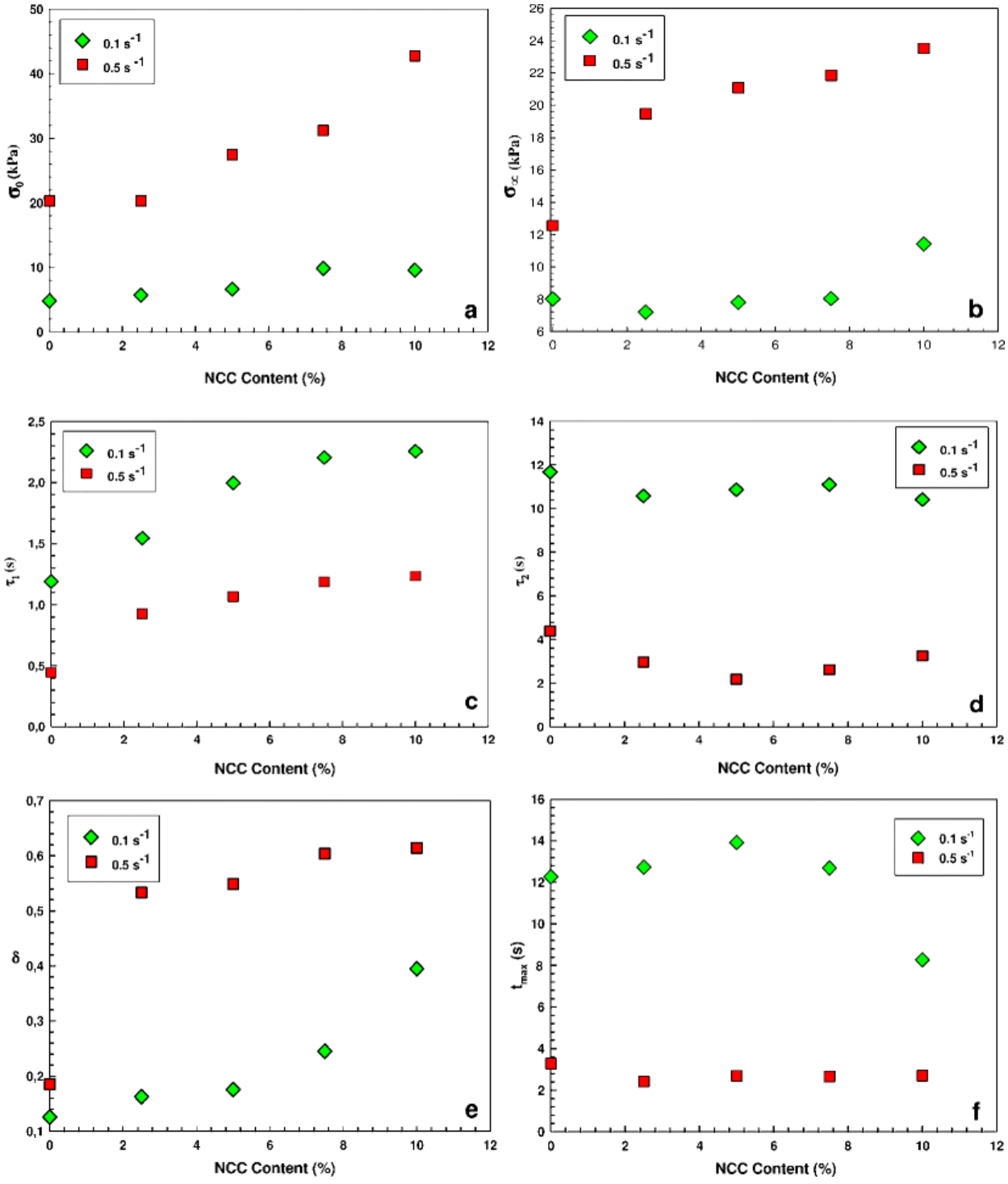

Figure 2-7: Shear rate and concentration dependence of the calculated parameters: a) σ_0, b) σ_∞, c) τ_1, d) τ_2, e) δ for Eq.(2-6), and f) t_{max} according to Eq.(2- 8).

first part of Eq.(2-6) converts to a simple power-law equation ($\sigma = \sigma_0(^{t}/_{\tau_1})^{-\delta}$). So our data indicates that by increasing the shear rate, the decay part becomes more important compared to the elastic response. Whittle and Dickinson (1997) stated that the time to reach maximum stress can be approximated by differentiating the first part of the Eq.(2-6) and set it to zero. By solving the resulting equation for the time, one gets:

$$t_{\max} = \tau_1 \left[\frac{1}{\delta}\right]^{1/(1+\delta)} \tag{2-8}$$

The calculated values for t_{max} at high shear rates (0.1 and 0.5 s^{-1}) are presented in Figure 2-7f and the values are close to τ_2 which is related to network break-up and flow. This was expected since at high shear rates, most of the structure reach full extension and break at time close to the time for maximum stress before the material reach the steady state condition.

In order to better understand the effect of nano-particles orientation in shear flows, transient tests with rest times (as described in the experimental section) were performed. The results for EVA 0 and EVA 10 are plotted in Fig. 2-8 along with a schematic of their representative nano-composite and polymer structure. For EVA 10, the stress overshoot for the second test decreased considerably and in the third test (CCL) decreased even more. In the first test, NCC particles are aligned in the flow direction and possible NCC networks are broken as a result of the applied stress (Fig. 2-8d). Since the behavior is non-Brownian, the structure which is deformed by flow, does not change during the rest time. Therefore, lower stress is needed for the second and third tests. On the other hand, for the neat polymer, the behaviour is partially similar for all the tests. The stress overshoot for unfilled polymer is believed to be related to chain orientation and entanglement/disentanglement transition (Robertson and Roland 2002) (see Fig. 2-8a, c). The rest time (200 s) was longer than the longest stress relaxation time of the polymer (10 s) so during the rest period, polymeric chains relax and return almost completely to their initial equilibrium structure (Fig. 2-8c) therefore the behaviour is similar in subsequent tests. The small difference between the first and subsequent tests is probably related to incomplete or partial re-entanglement of some chains needing considerably longer time than the relaxation time, even some orders of magnitude differences have been reported in the literature (Stratton and Butcher 1971, Dealy and Tsang 1981).

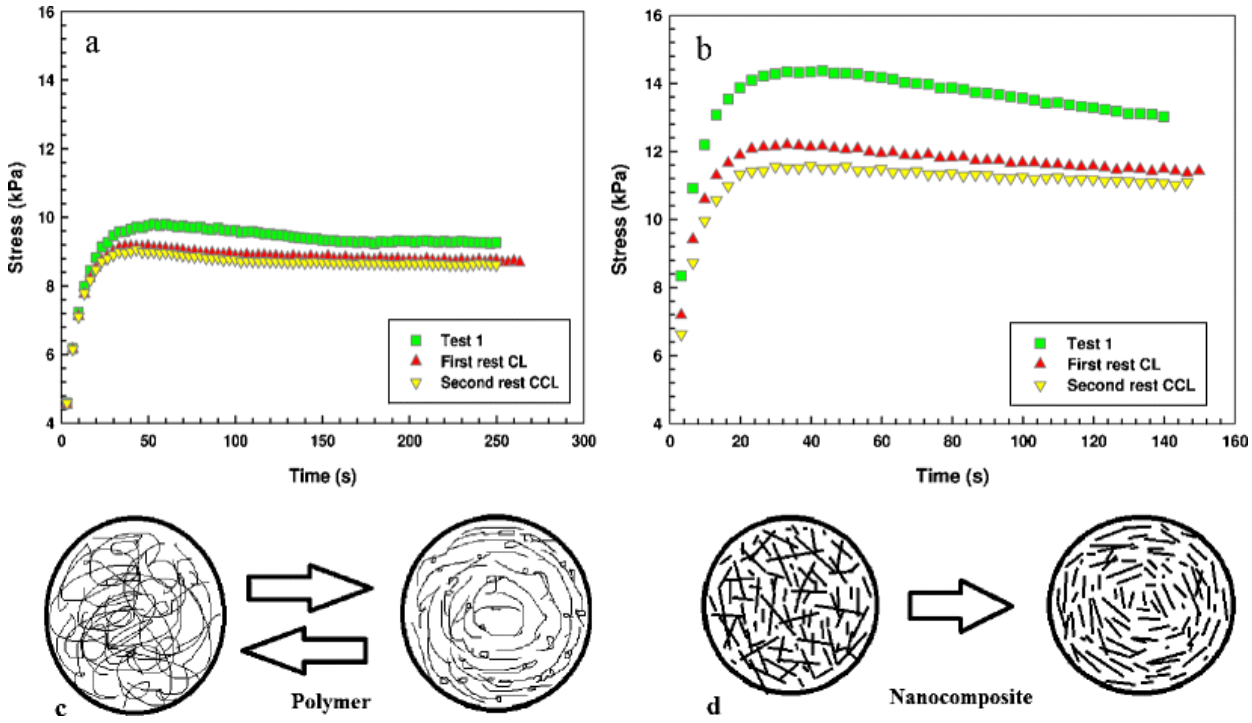

Figure 2-8: Stress–time curve for: a) EVA 0 and b) EVA 10 for shear tests with rest period at a rate 0.1 s^{-1} and 110°C. Schematic representation of the structures of c) EVA 0 and d) EVA 10 before and after shear tests.

Applying Eq. (2-6) for the test with rest times also supports the above mentioned explanation (data are shown in Table 2-3). The stress related parameters (σ_0, σ_∞) show different feature for EVA10 and neat polymer. While for the neat polymer the difference is not significant in different tests, reduction of the parameters values for EVA 10 is considerable. As already stated, these parameters depend on concentration and are related to the structure. When structure changes in the first test, the related parameters also change. This is consistent with the schematic representation proposed in Fig.2- 8. After the first test, the structures are mainly rearranged in the flow direction and therefore lower stress is needed for subsequent tests. Because most of the structure is oriented in the first test, the differences between the second and third tests are not as significant as between the first and second test. On the other hand, for neat EVA, polymeric chains can relax and partially return back to their initial disordered structure during the rest time, thus the differences are not as significant as for EVA 10. The value of δ was found to increase in consecutive tests for both EVA0 and EVA 10. For $t > \tau_1$, the first part of the equation converts to a simple power-law for which δ determines the rate of change. Increasing δ in subsequent

tests means reduction in the characteristic time. Since stress overshoot decreased in each test, the rate of decay also increases and therefore the steady state condition was obtained for shorter times. As noted earlier, the small differences for the neat polymer can be the result of chain scission and higher relaxation time for some chains. Small deviations for the neat polymer in CCL tests are probably related to reversing the deformation direction.

Table 2-3. Calculated parameters of Equation (2-6) for EVA 0 and EVA 10 for different tests at 110°C.

Sample	Test	τ_1 (s)	τ_2 (s)	σ_0 (kPa)	σ_∞ (kPa)	δ(-)
EVA0	0.1 s^{-1}	1.18	11.6	4.79	8.02	0.125
	0.1 s^{-1} after first rest CL*	0.258	9.06	3.87	7.86	0.684
	0.1 s^{-1} after second rest CCL*	0.421	8.64	4.13	7.78	0.906
EVA 10	0.1 s^{-1}	4.14	11.1	11.4	12.1	0.394
	0.1 s^{-1} after first rest CL*	3.92	9.45	8.72	10.8	0.732
	0.1 s^{-1} after second rest CCL*	3.47	8.81	6.95	10.8	0.931

*The test procedure was described in the experimental part.

2-3-4 Extensional rheology

The elongational viscosity growth function $\eta_E^+(t,\dot{\varepsilon})$ is defined by:

$\eta_E^+(t,$ (2-9)

where σ_E is the extensional stress and $\dot{\varepsilon}$ is the strain rate (Dealy and Wissbrun 1990). The extensional viscosity, in the linear viscoelastic regime can also be determined by:

$$\lim_{\dot{\varepsilon}} \eta_E^+(t,\dot{\varepsilon}) = 3\eta^+(t) = 3\int_0^t G(s)\,ds \tag{2-10}$$

where *G(s)* is the relaxation modulus.

The comparison of extensional data with linear properties is useful. First, it provides a practical test of the validity of the non-linear properties. For this reason, a plot of $\eta_E^+(t,\dot{\varepsilon})$ is compared with the value of $3\eta^+(t)$. Furthermore, the deviation from the linear behavior can be assessed and used for non-linear properties description. Extensional properties of the neat polymer and the nano-composites at two different strain rates (0.1 and 0.5 s^{-1}) are shown in Figure 2-9. Also, the $3\eta_0$ curve is shown for comparison. In order to have a better distinction between the results, data for EVA 2.5 and EVA 7.5 were multiplied by 10 and 30, respectively.

At lower times, the extensional viscosities slowly increase with time and this region of the curve represents the linear viscoelastic properties and the data at both rates are similar meaning that the viscosity is only a function of time ($\eta_E^+(t)$). On the other hand, at longer times, the extensional viscosity increases rapidly and the data deviate from the linear behavior. The Trouton ratio (*TR*), which is described here as the ratio of extensional viscosity to the shear viscosity, is higher than 3 at higher times, which is an indication of strain-hardening (*SH*). In this region, viscosity is a function of time and strain rate ($\eta_E^+(t,\dot{\varepsilon})$).

Strain-hardening can also be analyzed by a plot of stress against strain. Strain (ε) and stress (σ) are defined here as:

$$\varepsilon = \dot{\varepsilon} \tag{2-11}$$

$$\sigma = \eta_E^+ \dot{\varepsilon} \tag{2-12}$$

Presenting data in such way is very appropriate since it convert data form a “rheological” to a “mechanical” perspective. The results are also more directly related to processes such as blow

molding and foaming where elasticity and maximum extension are very important parameters to control. The resulting stress-strain curves are presented in Fig. 2-10 where it is clear that stress increases with NCC content. Both EVA and nano-composites show strain-hardening. The observed strain-hardening together with the viscosity increase for the nano-composites indicate a good coupling of NCC with the polymer matrix.

Park et al. (2006), working with polystyrene and polypropylene (PP) clay nano-composites, have reported that for both polymers strain-hardening occurred when proper coupling agents were used, while no strain-hardening was observed without coupling agent. This behavior reveals the effect of compatibilization on strain-hardening. As mentioned earlier, good coupling arises from the polar nature of the polymer and NCC particles. For all the compositions tested, strain-hardening starts at a deformation around one ($\varepsilon = 1$). This is a typical behaviour in many polymers which can also be predicted by famous models like pom-pom (Aguayo et al. 2006, McLeish and Larson 1998) or Giesekus (1982). This means that non-linear data for EVA are separable (Dealy 2010) and this will be discussed in more details in future works.

In order to quantify the data, a strain-hardening ratio (SHR) was defined by Twite-Kabamba and Rodrigue (2008) as:

$$SHR = \frac{\sigma_{\max}}{\sigma_{onset}} \tag{2-13}$$

where σ_{onset} and σ_{max} are the stress at the onset of strain-hardening ($\varepsilon = 1$) and the maximum stress measured, respectively. Data for all composition is presented in Table 2-4. The stress at onset (σ_{onset}), which is related to the stress at low deformations (or linear part), increases with increasing NCC concentration. On the other hand, the non-linear mechanical properties at high strain (σ_{max} and ε_b) decrease with NCC concentrations. This behavior is in direct relation with reduced SHR by increasing NCC concentration. Gupta et al. (2005) using SEM and TEM with extensional rheometry, showed that reorganization of clay particles and creation of clay aggregates during uniaxial extension is a reason for the reduction of strain-hardening in nano-composites. This explanation is believed to be valid in our case.

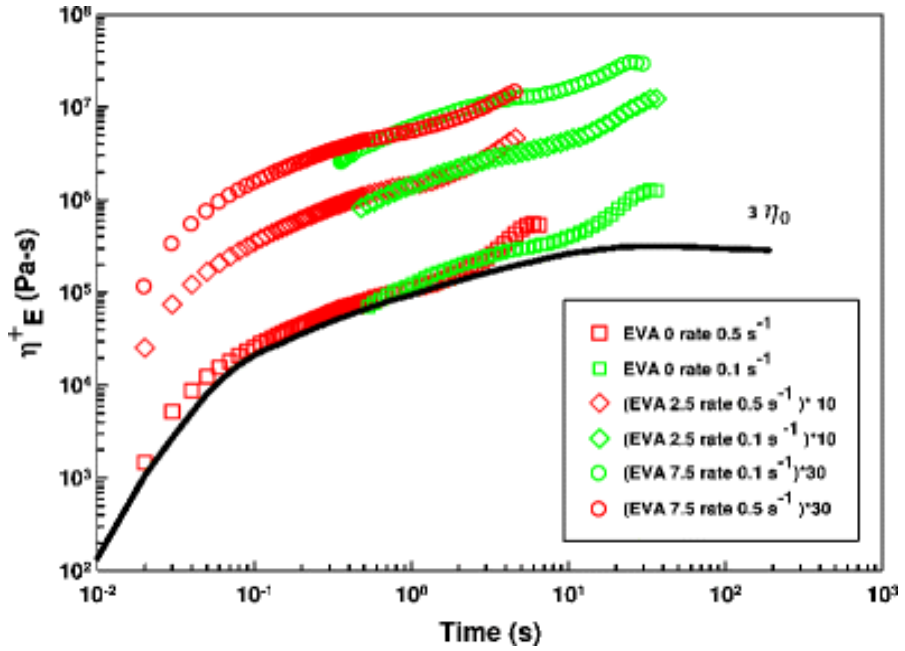

Figure 2-9: Extensional viscosity of EVA and NCC nano-composites for different rates at 110°C.

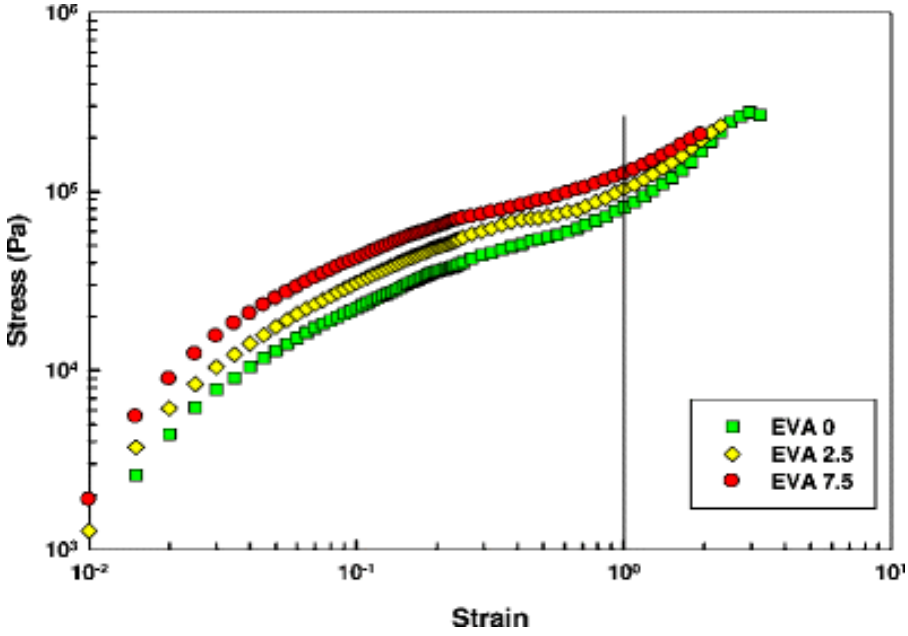

Figure 2-10: Elongational stress-strain curves for EVA and NCC nano-composites at a rate 0.5 s^{-1} and 110°C.

Also anisometric and hard (compared to soft EVA) nature of NCC reduce the extensibility of the materials even more. Nevertheless, in addition to these phenomena another possible explanation is also presented. The amorphous phase in EVA is in the rubbery state because it is above its

glass transition temperature (T_g) and surrounding crystals are melted above the melting temperature (T_m=70-80°C). Considering the elastomeric nature of EVA, it is obvious that at high strains only the polymeric chains contribute in stretching. When the network is stretched, entropic forces come into play, which are related to stresses. Increasing the NCC content leads to lower polymer chains concentration, as well as increased steric hindrance around the particles and therefore fewer chains are available to participate in strain-hardening. This means that the contribution of entropic forces in strain-hardening is reduced by the introduction of nano-particles. Furthermore, at higher concentrations (10%) for which some interconnected networks are created, some of the polymeric chains are probably shielded in between the filler network and do not participate in stretching. The existence of small aggregates can also influence strain-hardening, but to distinguish between these phenomena, more analysis would be needed.

Table 2-4. Stress onset (σ_{onset}), maximum stress (σ_{max}), strain at break (ε_b) and strain-hardening ratio (SHR) for EVA and nano-composites.

Sample	σ_{onset} (kPa)	σ_{max} (kPa)	ε_b (-)	*SHR* (-)
EVA 0	81.6	277	2.96	3.39
EVA 2.5	104	232	2.30	2.23
EVA 5	118	224	2.15	1.90
EVA 7.5	125	207	1.94	1.66
EVA 10	127	200	1.94	1.57

2-4 Conclusion

In this work, a complete study of the linear and non-linear rheological properties of melt blended NCC-EVA nano-composites was presented. In particular, the effect of NCC content was discussed for data in shear and elongation deformation.

For small amplitude oscillatory shear tests, the moduli G' and G'' showed a non-terminal behaviour at low frequencies, while in viscosity appearance of yield stress was observed at higher NCC content. These data indicate a pseudo solid-like rheological behavior related to the formation of nano-particle network as a result of hydrogen bonds between the cellulose particles. Although more analysis is necessary, it seems that particle-particle interactions play a critical role in cellulosic nano-composites.

For transient tests (step rate), the data were also consistent with the idea of nano-network formation. At low shear rates (Weissenberg number), the stress curves did not show any overshoot, while at higher shear rates (*Wi*) the material presented an overshoot before reaching a steady state. The stress overshoot was related to changes in structure orientation under flow, as well as breakdown of NCC networks at high concentrations.

For uniaxial elongational tests, extensional viscosity increased with increasing nanocellulose content. However, strain-hardening decreased with increasing NCC content. This behavior was related to the lowering of entropic forces as result of reducing polymeric chains, as well as increasing the amount of constrain on the polymer chains. In particular, maximum stress increased with NCC content, but elongation at break decreased.

Finally, the rheological analysis was found to be very helpful in understanding structure-property relations of NCC nano-composites. A general scheme of nano-composites structure was depicted, but more work is needed to better understand and quantify the nano-structure. In particular, advanced characterization techniques will be needed to accurately describe and determine the role of particle-particle and particle-polymer interactions on the final properties of these materials.

Acknowledgements

The authors would like to acknowledge the financial support of NSERC (Natural Sciences and Research Council of Canada) and the Quebec Ministry for Economic Development, Innovation and Exportation (MDEIE) for this work.

Chapter 3 Relationships between linear and nonlinear shear response of polymer nanocomposites

H. Mahi and D. Rodrigue, Rheol. Acta, 51, 991-1005 (2012).

Résumé

L'analyse rhéologique a été utilisée pour comprendre les relations structures-propriétés de polymères nanocomposites à base d'éthylène-acétate de vinyle (EVA). Deux nanoparticules géométriquement différentes (sphère de $CaCO_3$ et des plaquettes de montmorillonite) ayant les mêmes différences d'énergie de surface envers le EVA ont été étudiées pour des concentrations entre 2,5 et 15% en poids. Trois phénomènes ont été étudiés: l'apparition d'un comportement de type pseudo-solide dans le domaine viscoélastique linéaire, les limites de la viscoélasticité linéaire et la présence d'un dépassement de contrainte dans des tests de cisaillement transitoire. En particulier, le dépassement de contrainte a été étudié sur la base du concept de tube de chaînes polymères. En outre, les différences liées à la géométrie des nanoparticules (plaquette ou sphérique) ont été étudiées sur la base d'un mécanisme de création d'un réseau de particules. D'une part, en raison d'une probabilité de contact physique plus élevée, les particules en forme de plaquettes peuvent mieux interagir et créer une structure de réseau qui domine la réponse rhéologique. D'autre part, bien que des particules sphériques puissent limiter le mouvement des chaînes polymères sous écoulement, un réseau physique solide n'a pas été formé. Pour les plaquettes, le comportement a été bien décrit par le modèle fractal qui considère l'agrégation directe ce qui n'a pas été observée pour les particules sphériques. Le mécanisme de création de réseau a été validé par analyse d'image.

Abstract

Rheological analysis was used to understand the structure–property relations of polymer nano-composites based on ethylene vinyl acetate. Two geometrically different nano-particles (sphere of $CaCO_3$ and platelet of montmorillonite) having the same energetic attractions with ethylene vinyl acetate were studied for concentrations between 2.5 and 15 wt%. Three phenomena were studied: the appearance of a solid-like behavior in the linear viscoelastic domain, the limits of linear viscoelasticity, and the presence of stress overshoot in step shear tests. In particular, stress overshoot was investigated based on the tube concept of polymeric chains. Also, differences related to nano-particle geometry (platelet vs. spherical) were investigated based on a filler-network mechanism. Due to higher physical contacting probability, platelet particles can better interact and create a network structure, which dominates the rheological response. On the other hand, although spherical particles can limit the motion of polymeric chains under flow, a strong physical network was not formed. For platelets, scaling behavior was well described by fractal model which considers direct aggregation, and such scaling was not observed for spherical particles. The filler-network mechanism was validated by image analysis.

3-1 Introduction

It is well known that the addition of only small amounts of nano-particles to polymers can result in significant improvement in various properties. This behavior is associated with the specific size of these materials, i.e., their high surface to volume ratio (Jancar et al. 2010). However, to design tailor-made nano-composites, relations between structural variables and final properties need to be understood. To understand such relations, different techniques and methods like thermal (Bogoslovov et al. 2008; Zheng and Xu 2010), mechanical (Ci et al. 2008; Lin et al. 2008), and rheological (Krishnamoorti and Giannelis 1997; Du et al. 2004) analyses have been used.

Because of the possibility to achieve thermodynamic equilibrium conditions, it is well accepted that rheological analysis is a reliable method to understand the effect of nano-composite structure on both linear and nonlinear viscoelastic properties. Therefore, an important amount of works has been published on the use of rheological analysis for structural analysis (Krishnamoorti and Giannelis 1997; Du et al. 2004; Anderson and Zukoski 2009, 2010; Utracki et al. 2010). Despite the large volume of literature, there are still several parameters that are not well elucidated yet. One of the most common observed and discussed phenomena is the appearance of a solid-like behavior at low frequency (dynamic rheology) which results in a non-terminal relaxation behavior. This behavior has been ascribed to different mechanisms like polymer–particle coupling (Lee and Han 2003; Manitiu et al. 2009), frictional forces between polymer and particles (Mansoutre et al. 1999; Galgali et al. 2001), particle network (Akcora et al. 2009, 2010b; Chen et al. 2010), bridging effect of chains around particles (Zhu et al. 2005; Song and Zheng 2010), immobilized polymer layers (Kalfus and Jancar 2007; Sarvestani 2008), and fractal structures (Jouault et al. 2009; Chevigny et al. 2010).

Another important property, which has been less discussed in the literature, is the so-called stress overshoot observed in shear transient tests (step shear). So far, experiments on nano-composites having platelet (Solomon et al. 2001; Ren and Krishnamoorti 2003), tubular (Chatterjee and Krishnamoorti 2008), and spherical (Goel et al. 2006) particles show that, regardless of the reinforcing mechanism, the stress response to a constant shear rate (much shorter than the polymer relaxation time) produces an overshoot before reaching a steady state. But the origin of such overshoot in nano-composites is not well understood yet.

An important challenge for describing both phenomena (solid-like behavior and stress overshoot) is to determine whether this behavior can be explained on a polymeric (polymer–particle interactions) or a particle (particle–particle interactions) point of view. The first scenario implies polymer–particle interactions (either frictional interactions or chemical/physical interactions) resulting in a more confined state for the macromolecular chains. In the second scenario, however, it is supposed that the behavior is controlled by the nano-particles instead of the polymeric chains. Although many experimental evidences points towards the particle-based scenario (Chatterjee and Krishnamoorti 2008; Akcora et al. 2009, 2010b; Chen et al. 2010; Chevigny et al. 2010), some important evidences for the first scenario has been reported (Litvinov and Spiess 1991; Robertson and Roland 2008; Sarvestani 2008). There is currently no consensus because of some inconsistencies in the reported results and the difficulty to distinguish between both phenomena.

While most of the literature reporting on these two phenomena (solid-like and overshoot) treated them separately, the main objective of this work is to investigate the relation between both phenomena with a special attention given to particle–particle and polymer–particle interactions. In this context, some important questions are treated here: to what extent these two phenomena are related? To what extent the tube theory can consider some aspects related to stress overshoot? Do mechanisms explaining the solid-like behavior under SAOS can be applied to describe the stress overshoot, and to what extent polymer–particle interactions and particle–particle interactions are important in both responses?

Since the linear properties of nano-composites have been extensively discussed, a focus is made here on nonlinear properties like stress overshoot. Nevertheless, linear data will also be presented and discussed for comparison. The stress overshoot in nano-composites has been mainly discussed based on particle network models (Krishnamoorti and Giannelis 1997; Whittle and Dickinson 1997; Solomon et al. 2001; Letwimolnun et al. 2007). The novelty of this work is that the stress overshoot for nano-composite will be discussed based on the tube concept (Doi and Edwards 1989) of polymeric chains with an attempt to distinguish (at least qualitatively) the effect of particle–particle and polymer–particle interactions on linear and nonlinear data. As a first step, two geometrically different nano-particles (sphere of $CaCO_3$ and platelet of montmorillonite) having the same energetic attractions with the polymer matrix are used. This

choice was based on the fact that the physical contact probability of particles in a fixed volume is highly geometry dependent (Chen et al. 2010). Obviously, platelet particles are more effective than spherical ones in this context: while two spherical particles only have one point of contact (tangent point), two platelets have different contact probabilities from fully overlapping to single point. Therefore, shape difference would result in different ability of each particle to form a contact-aggregated structure.

3-2 Experimental section

3-2-1 Materials and sample preparation

Ethylene vinyl acetate was used as the matrix: ELVAX 360 from DuPont which contains 25 % of vinyl acetate. This polymer has a melt index of 2 dg/min, a density of 948 kg/m^3, and a melting point of 78 °C. In order to have similar energetic interactions between the polymer and each particle, surface-modified particles were chosen: modified nano-clay (montmorillonite) particles (Cloisite 20A) were obtained from Southern Clay Products and nano-particles of calcium carbonate (Ultra-flex) were obtained from Specialty Minerals Co. Before processing and before each test, all the materials and samples were dried at 60 °C for 4 h. To prepare the nano-composites, ethylene vinyl acetate (EVA) was melt-blended with different concentrations of nano-particles as described in Table 3-1. Blending was performed in a batch mixer (Rheocord 40 from Haake Büchler) for a total time of 15 min at a speed of 70 rpm and a temperature of 130 °C. At first, the polymer was introduced to get a homogeneous melt. When the torque became stable (normally after 2 min), the selected amount of nano-particles was added slowly to the mixer. In order to have similar processing history, the neat polymer was also processed under the same conditions to impose a similar thermo-mechanical history for the matrix. The compounds were then compression-molded at 150 °C under 2,300 kg (5,000 lb) of force in a rectangular mold having dimensions of 100 × 100 × 1.8 mm^3 for 3 min. Finally, the samples for rheological testing were directly cut in the molded plates.

Table 3-1. Compositions of the nano-composites produced.

Sample	EVA (% wt.)	Clay (%wt.)	Sample	EVA (% wt.)	$CaCO_3$ (% wt.)
EVA 0	100	0	-	-	-
Clay 2.5	97.5	2.5	Ca 2.5	97.5	2.5
Clay 5	95.0	5.0	Ca 5	95.0	5.0
Clay 7.5	92.5	7.5	Ca 7.5	92.5	7.5
Clay 10	90.0	10	Ca 10	90.0	10
Clay 15	85.0	15	Ca 15	85.0	15

3-2-2 Morphological characterization

A scanning electron microscope (SEM) JEOL JSM 840A from JEOL USA, Inc. was used for morphological investigations. The samples were first frozen in liquid nitrogen before being fractured to expose the structure which was then coated with Pd/Au prior to observation. In order to complete the morphological characterizations, transmission electron microscopy (TEM) images were obtained using a JEOL JEM-1230 electron microscope operated at 80 kV. Samples were embedded in epoxy, and by using an ultramicrotome Ultracut E from Reichert-Jung, sections of 80 nm thick were prepared. Micrographs were taken in various regions of each sample at different magnifications.

3-3-3 Contact angle and surface tension measurements

An optical contact angle analyzer (OCA 15 EC Plus, Dataphysics) was used to measure the surface tension of the polymer and the nano-particles. The system is composed of a high-resolution camera and a specific software developed to capture and analyze the contact angle on very small and curved surfaces. To ensure the reproducibility, measurements were performed on five different samples and at three different positions. The test was performed using two liquids: deionized water and ethylene glycol. For precise measurements, small drops of 0.15 µl were dispensed via an ultrathin needle with an internal diameter of 0.18 mm. For contact angle measurement of nano-particles, highly compacted pills of particles were formed by compression. SEM images verified the highly smooth surface of the pills to ensure that the effect of porosity and roughness on the measurement was minimized.

3-3-4 Dynamic shear tests

All the shear rheological tests were performed on a strain-controlled TA Instruments rheometer (ARES) with a torque transducer (0.02–2000 g-cm) and a normal force transducer (2–2000 g) under a nitrogen (N_2) atmosphere. All measurements were done using a 25 mm diameter parallel plate geometry with gaps between 1.5 and 2 mm. The no gap-effect condition for such gap range was recently presented elsewhere (Mahi and Rodrigue 2012a). At first, to determine the linear viscoelastic range of each sample, strain sweep tests were performed at a frequency of 1 rad/s. A deformation of 2 % was then chosen to perform frequency sweeps in the range 0.01–300 rad/s in an ascending manner. It is well known that property of clay nano-composites is loading/time dependant (Krishnamoorti and Giannelis 1997; Ren and Krishnamoorti 2003; Letwimolnun et al. 2007; Vermant et al. 2007). To control such history effect, samples were annealed for 10 min after loading at the set temperature for each test. Time sweep tests showed a continuous modulus evolution within the experimental time (4,500 s). However, after the initial time (5–10 min), the rate of increase was very small (see Appendix B) Also, it was found that when EVA is placed at high temperature for a long time (>2 h), the material shows an increased modulus due to gelation and degradation. The annealing time of 10 min was chosen to make a compromise between these two phenomena. To prevent the effect of orientation on rheological measurements, new samples were used for each test. To determine the effect of temperature, tests were performed at 110, 150, and 190 °C.

3-3-5 Strain sweep tests

To study the strain dependence of the viscoelastic properties, a strain range of 0–200 % and frequency of 1 rad/s was used for strain sweep tests. The tests were performed at different temperatures: 110, 150, and 190 °C.

3-3-6 Transient shear tests

The shear viscosity growth function η^+ was obtained with the same geometry as for the dynamic tests (25-mm parallel plates). The shear rates used were 0.005, 0.01, 0.03, 0.05, 0.1, 0.5, and 1 s^{-1}. Each composition was sheared at 110 °C for a time of 1,000 s in order to achieve fully steady shear response. For each applied shear rate, a new sample was used.

3-4 Results and discussion

3-4-1 Morphology

The morphological structures of the nano-particles and different nano-composites are shown in Fig. 3-1. First, SEM pictures of the nano-particles as they were received are shown in Fig. 3-1a, b which reflects the spherical and platelet geometry of $CaCO_3$ and clay, respectively. Transmission electron micrographs of the nano-composites show that despite the presence of some aggregates (more apparent for spherical ones), the particles are well distributed. For spherical particles, the size of the original particles was around 70 nm. But, as concentration increases, separated local fractals are formed for which at the highest concentration (15 %), some of these local flocs are interconnected. It is well established that interconnection between spherical aggregates will result in important alteration of properties (Chevigny et al. 2010). For clay particles, however, a continuous network at concentrations higher than 5 % is observed. The geometric and size differences between particles led to a higher contacting probability for platelet particles, and therefore physical percolation for clay particles occurs at much lower concentration (roughly 5 %) than for $CaCO_3$ (not observed even at 15 %). Based on the contact angle measurement, the measured surface energies (γ ± 1 mN/m) were 28.1, 25.1, and 30.8 mN/m for EVA, $CaCO_3$, and clay, respectively. This means that the absolute value of surface energy differences between the particles and the polymer ($|\Delta\gamma_{np}|$) is 2.7 mN/m for clay and 3.0 mN/m for $CaCO_3$ which are relatively similar. Naturally, these two particles have a highly hydrophilic nature. However, the hydrophilicity of the grades used was modified by using calcium stearate for $CaCO_3$ and ammonium compounds for clay (Koo 2006). Although even after surface modification, the surface properties of the particles are not exactly the same, their difference compared with the polymer is negligible. Beside particle shapes, although the same energetic attraction was obtained for both particles, other parameters should be considered for each system: (1) state of dispersion, (2) the higher chain uptake for platelet particles than spheres (Ren et al. 2000; Krishnamoorti and Yurekli 2001; Chen and Evans 2006; Harton et al. 2010), and (3) particle size characteristics. To better discuss the state of dispersion, the number of clay layers per tactoid (n_{per}) was calculated as (Ren et al. 2000; Krishnamoorti and Yurekli 2001)

$$n_{per} = \frac{4}{3\varphi_{per}}\left[\frac{w_{per}\rho_{org}}{w_{per}\rho_{org} + (1-w_{per})\rho_{clay}}\right]\frac{R_h}{h_{clay}} \qquad (3\text{-}1)$$

where R_h is the platelet radius, h_{clay} is the thickness of particle layers which is approximately 1 nm (Paul and Robeson 2008), and ρ_{org} (0.948 g/cm^3) and ρ_{clay} (1.77 g/cm^3) are the densities of the polymer and clay, respectively. φ_{per} is the percolation volume fraction for spherical particle which is 0.30 (Isichenko 1992), and w_{per} is the percolation threshold obtained for clay particles. Considering the average reported values for clay diameter ($2R_h$) as 100–300 nm (Paul and Robeson 2008) (the same sizes can be seen in TEM images here) and considering a percolation threshold of 5 % which was revealed in rheological data, the average tactoid size is found to be around 7–20 layers. Looking at TEM images, it can also be seen that the thickness of the black lines representing the number of layer is different. The obtained values show that the average aspect ratio is around 15 which is the same as reported elsewhere (Krishnamoorti and Yurekli 2001; Vermant et al. 2007). This shows that clay particles are not completely delaminated (a single plate has a thickness of 1 nm and an aspect ratio in the range of 100–300). Although the particles are not fully separated, the situation is relatively the same for spherical particles, i.e., dispersion quality is considered to be similar. TEM images also show the presence of some local aggregates in both cases (as dense black plates for clay and aggregates for spheres). The structure however in both cases is adequately distributed.

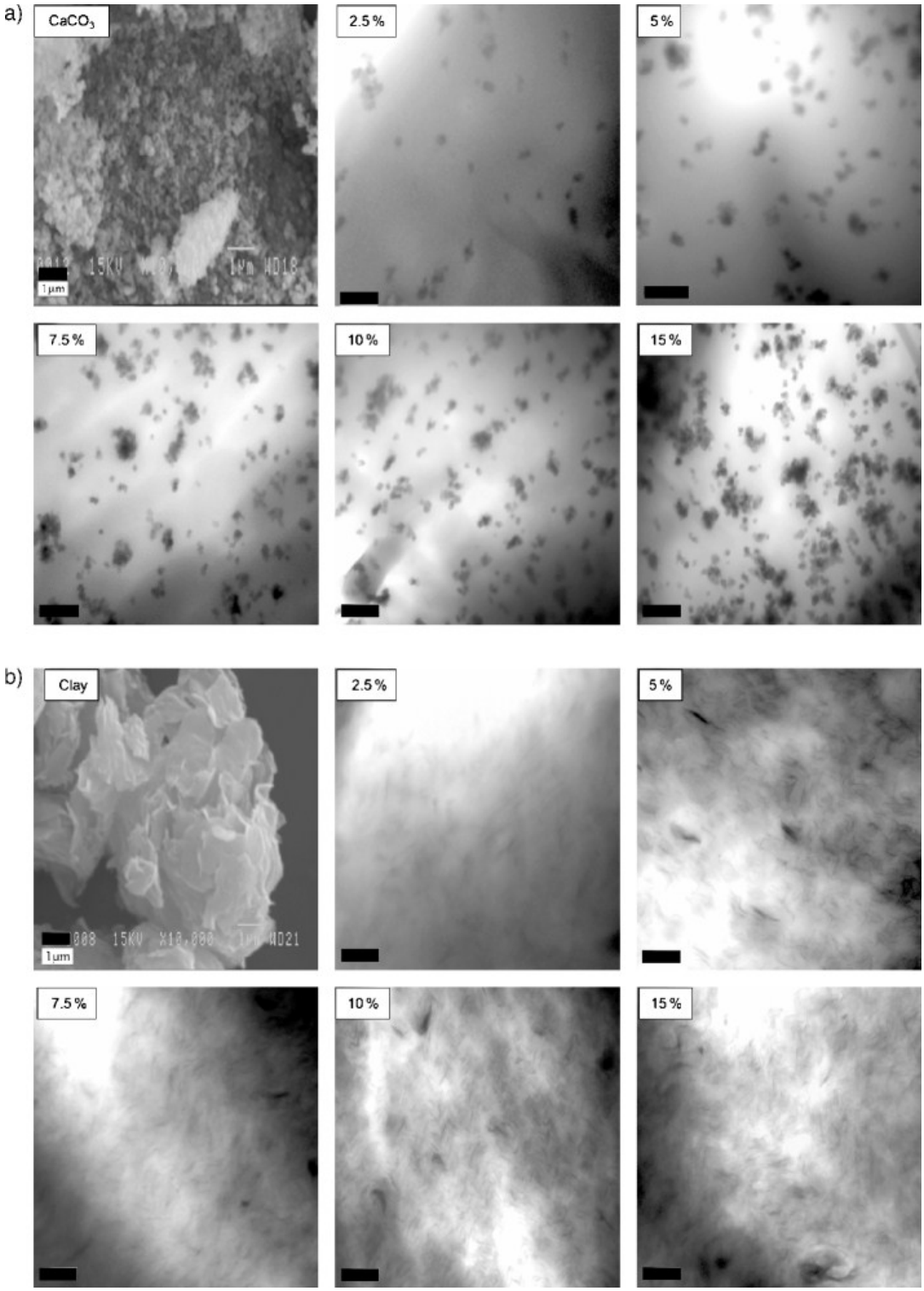

Figure 3-1: Morphological images of a) SEM of $CaCO_3$ and TEM images of its nano-composites and b) SEM of clay and TEM images of its nano-composites. The scale bar is 500 nm for TEM and 1 μm for SEM.

Another important parameter is the higher chain uptake by platelet particles than spheres. It has been shown (Krishnamoorti and Yurekli 2001; Chen and Evans 2006; Harton et al. 2010) that even at similar concentration, chain confinement is stronger for flat particles compared to spherical ones. This can be due to higher surface area of platelet particles, as well as the effect of surface curvature for spherical ones (Harton et al. 2010). The latter one becomes important when the particle size is too short compared to the polymer's radius of gyration (R_g) in which chain can entangle around particles (Mu and Winey 2007). Considering the large particle size used here (75 nm for $CaCO_3$ and 100–300 nm for clay), this effect is not significant in this case. So, in addition to the different contacting probability (particle–particle interactions), different surface area and consequently different chain confinement (polymer–particle interactions) is also resulting from shape differences. As a final remark on morphological analysis, the size effect should also be mentioned. Considering the particles used here (spheres with d = 70 nm and platelet with d = 100–300 and thickness of 1 nm), even for the same weight concentration, the number of platelet particles would be higher than for spherical ones, and this would result in higher particle–particle and higher polymer–particle interactions for clay. So, in addition to increased interactions resulting from shape differences, size differences would also lead to higher interactions for platelet particles. Therefore, even for a relatively similar state of dispersion, the number of contact points would be higher for platelet particles. The increased particle number coupled with shape differences (higher aspect ratio) will help platelet particles to better form a network inside the polymer and consequently, although the particle distribution is similar, the particle microstructure inside the matrix is different for both systems due to size and shape differences. In the following sections, the modality of the response of these different structures under linear and nonlinear shear will be discussed.

3-4-2 Shear transient

The time-dependent stress response obtained during shear transient test for different samples is shown in Fig. 3-2. The results show that stress increases with filler concentration, with a stronger effect for clay particles.

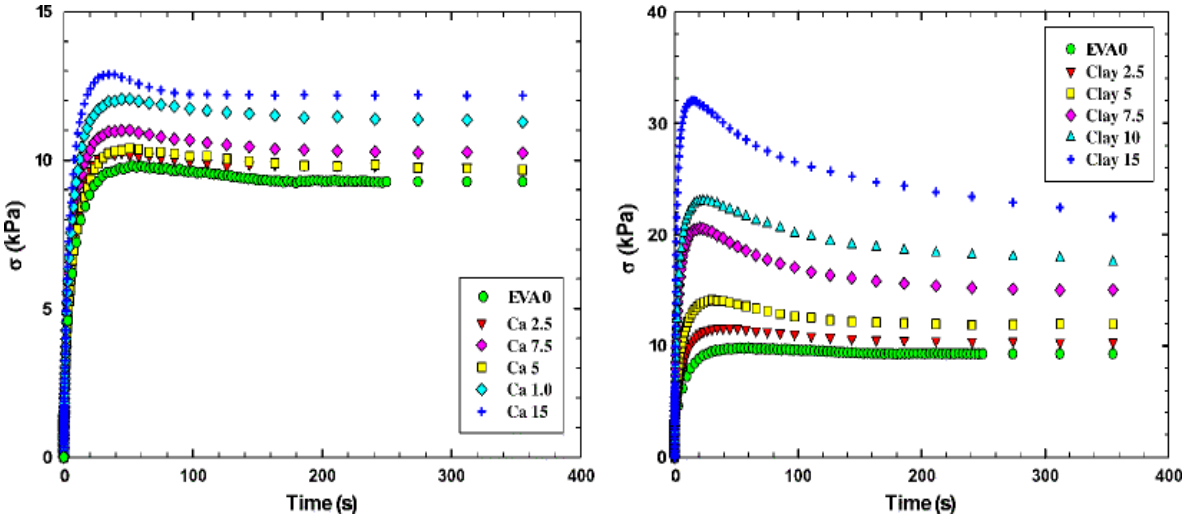

Figure 3-2: Stress as a function time for $CaCO_3$ (left) and clay (right) nano-composites at a rate of 0.1 s^{-1} and 110 °C.

The transient shear curves can be decomposed into three different domains: (1) At short observation times and regardless of shear rate, the response is purely elastic and stress increases monotonically ($\sigma=G(\gamma,\dot{\gamma})\gamma$), (2) for sufficiently long times, the stress reaches a steady-state condition (except for very high shear rates for which no steady state was achieved within the time frame of the experiment), and (3) at intermediate time (transition region between 1 and 2) where, depending on the applied shear rate and material structure, stress would go through a maximum (overshoot) or not. The data at both extremities (short and long times) represent the linear and steady-state behavior, respectively. A qualitative comparison shows that both modulus and steady-state stress increase with increasing nano-particle concentration with a much stronger effect for clay particles. However, the focus of this work is to discuss more on the transition region which can be very useful with respect to the material structure.

As mentioned earlier, the appearance or not of an overshoot depends on the applied shear rate and material structure. This overshoot is predicted to occur when the product of the shear rate and relaxation time of the polymer exceeds unity (Pearson et al. 1991). For EVA and all $CaCO_3$ compositions, the overshoot was observed for $\dot{\gamma} \geq 0.1\, s^{-1}$, while for all the clay nano-composites, it was found to occur at $\dot{\gamma} \geq 0.05\, s^{-1}$. The first observation is that relaxation times are most probably altered by the presence of clay platelets. This can be verified by using linear data (Fig. 3-3) where the longest stress relaxation time (τ_d) can be calculated as (Inoue et al. 2002a)

$$\tau_d = \frac{A_G}{\eta} \tag{3-2}$$

where A_G and η are obtained from the low-frequency behavior of the storage and loss moduli, respectively ($G' = A_G \omega^2$, $G'' = \eta \omega$ as $\omega \to 0$) (Inoue et al. 2002a). Based on dynamic data, a value of τ_d = 10.1 s was obtained for EVA and $CaCO_3$ nano-composites. So $\tau_d \times \dot{\gamma}$ for EVA and $CaCO_3$ nano-composites is unity for shear rates around 0.099 s^{-1} which is in agreement with the experimental observations. For clay, however, because of the observed non-terminal behavior (see Fig. 3-3), the relaxation time cannot be calculated by Eq. (3-2). In this case, by considering the presence of an overshoot for rates higher than 0.05 s^{-1}, a value of $\frac{1}{\dot{\gamma}_{cr}} = 20\ s$ is obtained leading to $\tau_d \approx 20$ s, which reflects a shift towards longer relaxation times. Although such a shift in relaxation time is conceptually reasonable, it is discussed further here. According to the tube model (Doi and Edwards 1989), in a shear flow two characteristic times are important. The first one, which is related to the longest stress relaxation time (τ_d), is the orientational relaxation time for a stretched chain. The other one, which is comparatively shorter, is the time for chain equilibration along their contour length (τ_e). The latter is associated with twice the longest Rouse relaxation time ($2(\tau_R)$). Recently, Inoue et al. (2002a and 2002b) and Osaki et al. (2001), based on the modified tube model proposed by Pearson et al. (1991) and different experimental results, showed that the origin of non-linearity is associated with large differences between τ_d and $2(\tau_R)$. τ_R can be calculated by the Rouse expression of storage modulus ($G' = \alpha \omega^{1/2}$) (Rouse 1953). Such measurement for EVA has been done in our previous work and a value of 0.4 s was obtained for τ_R (Mahi and Rodrigue 2012a). This clearly demonstrates the large differences between τ_d (10.1 s) and τ_R (0.4 s) for the polymer matrix and the $CaCO_3$ nano-composites. Increased non-linearity (reduced $\dot{\gamma}$) for clay nano-composites means that the difference between these two times increased even more by the introduction of clay. This can be the result of the changes in τ_d and/or τ_R, but we believe that this is mainly due to longer stress relaxation time (τ_d), and τ_R has much lower contribution. τ_R, which is calculated from the high frequency region (Rouse regime), is a very short time scale therefore τ_R is not altered significantly by nano-scale particles. This can be verified by using linear data.

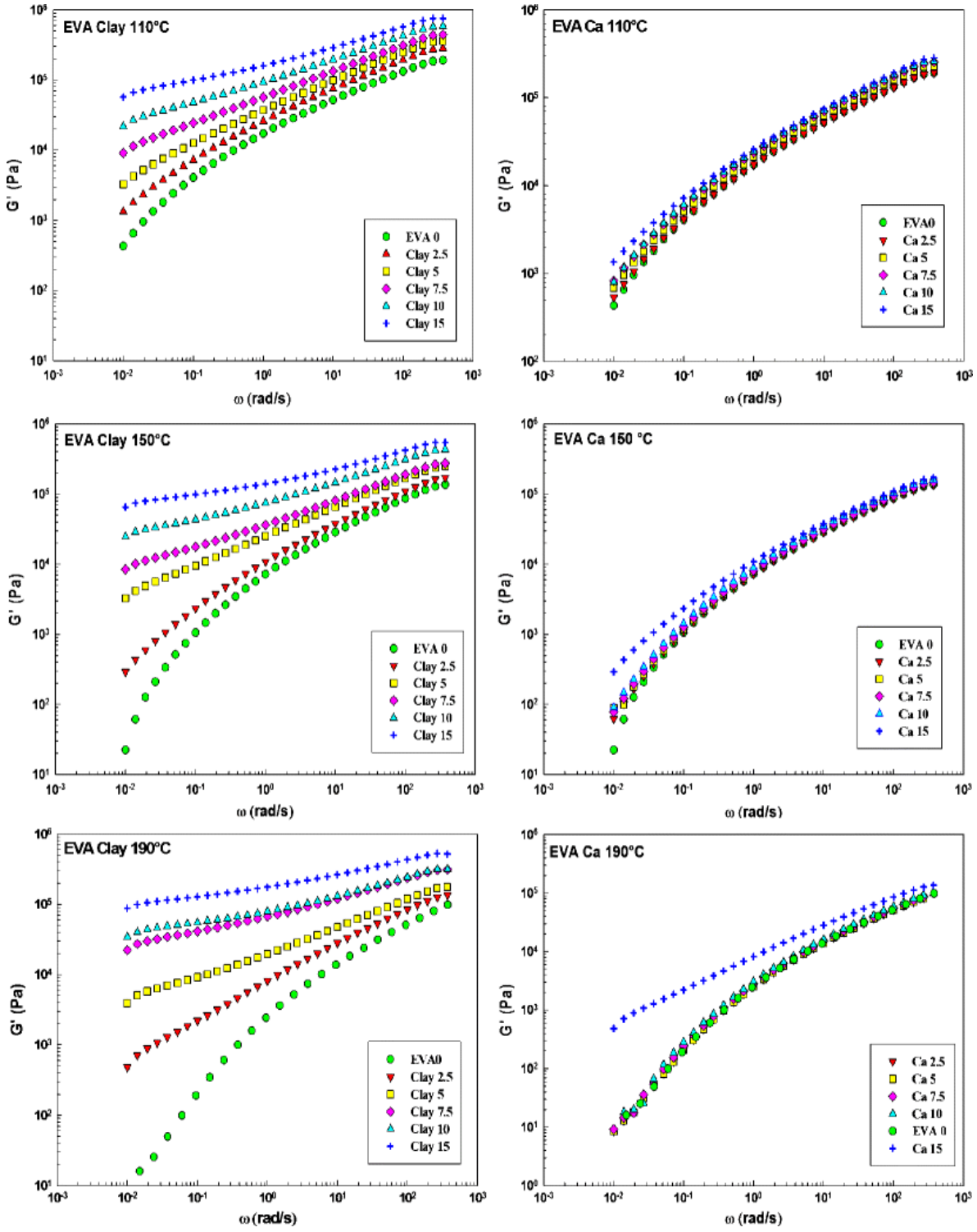

Figure 3-3: Elastic shear modulus (G′) of clay (left) and $CaCO_3$ (right) nano-composites at different temperatures.

The linear data at different temperatures are presented in Fig. 3-3. At high frequencies (Rouse regime), the experimental time is very short. Therefore, only very short dynamics are included (Kalfus and Jancar 2008). Considering the nano-size of the particles, these relaxations are not considerably affected by the introduction of particles (see data at 110 °C). However, even in this region, platelet particles are more effective than spherical ones, especially at concentrations higher than 5 % where structural analysis revealed a physically interconnected network. Although size scales comparable to the particle size are not involved in this region of the test, the network structure is able to affect even short dynamics as some of these vibrations are confined by clay networks. On the other hand, at low frequencies, a much more differentiated behavior is observed. The neat polymer exhibits a common terminal behavior of $G' \sim \omega^2$ (see data at 190 °C) which is associated with long relaxations and liquid-like behavior of polymers. The introduction of nano-particles leads to significant variation of polymer dynamics in this range. Low-frequency region involves nano-scale dynamics; hence, the difference between both systems is clearly manifested in this region where anisometric particles have much stronger effect on the terminal relaxation time than spherical ones for all the temperatures studied. These data justify the shift in the stress relaxation time (at least qualitatively) which was already predicted from transient data for clay particles. The increased relaxation time by clay particle confirms that even for similar energetic attraction, chains are more confined by platelet particles than spherical ones, a phenomena which was explained in the morphological part and discussed more in depth in Krishnamoorti and Yurekli (2001), Chen and Evans (2006), and Harton et al. (2010). Interestingly, such higher chain uptake was clear at least qualitatively in shear transient tests.

While transient data for clay reflected a measurable shift in relaxation time (twice the polymer relaxation), linear data show a solid-like behavior which does not relax within the experimental time domain. This can be explained based on the particle–particle interaction mechanism. The obtained shift in relaxation time from transient data can be referred to the slowing of chain relaxation due to polymer–particle interactions (e.g., frictional forces or chain confinement). The solid-like behavior in linear data however is the result of the combination of polymer–particle interactions and particle–particle interactions. At high platelet concentrations (5 % and higher), the nature of the nano-network dominates the linear response. Rheological response controlled by a filler network cannot be predicted by the tube theory which is purely based on chain dynamics. Although size and shape are different, chain confinement is higher for platelet and the

appearance of a solid-like behavior which does not relax within the experimental time can be better explained by particle–particle interactions (Ren et al. 2000; Galgali et al. 2001; Akcora et al. 2009; Nusser et al. 2011) Due to their size characteristic which was explained in the morphological section, even for a similar concentration, the number of platelet particles is higher than spherical ones. This increased particle number in addition to their shape characteristic would result in a higher contacting probability for platelet particles. Structural analysis showed that platelet particles are easily interconnected even at low concentration, while spherical particles do not have this ability. For 7.5 % clay and higher, a continuous network is formed which dominates the behavior (plateau region) and the behavior in this region is controlled by nano-particles rather than polymeric chains. The only $CaCO_3$ concentration showing such non-terminal behavior is the highest (15 %). Although, even for Ca 15, the reinforcement is not comparable to clay, the appearance of a pseudo solid-like response reflects structural variations. TEM image of Ca 15 (see Fig. 3-1a) showed that at such a high concentration and due to the increased number of spheres, some of the local fractals are interconnected. This is in accordance with data reported by Jancar et al. (2010) and Cassagnau (2003, 2008). They reported that by improving the dispersion quality of fumed silica (spherical particles), the modulus decreased whereas it increased for organoclays. Although from a dispersion point of view this reflects a paradox, from a particle–particle interactions or filler-network point of view, both cases represent the same phenomena. For spherical particles, when the dispersion quality improves, the probability of particle–particle interactions and consequently the probability of creating connected pathways would decrease. For hard spheres, aggregation and network structures need the same surface contact area (tangent point). For platelet particles, however, increasing the dispersion quality means increasing the number of plates. For platelet particles, aggregation can be referred to a wide range of morphologies from complete overlap to those having only one point of contact (the ideal situation for a network). Improving dispersion quality in this case would separate overlapped plates, and therefore the number of particles for network formation would increase accordingly.

The appeared fractal structure for clay led to significant property changes. The terminal storage modulus G′ exhibits a power-law scaling with respect to concentration as $G' \sim \varphi^{3.02}$ (see Fig. 4) which is in agreement with the models based on particle-aggregated structure (Shih et al. 1990). From Figs. 3-3 and 3-4, it can be seen that EVA modulus decreased by more than an order of

magnitude with increasing temperature from 110 to 190 °C. Although the same trend is observed for clay 2.5, for higher clay concentrations, a relatively temperature independency is observed. The slight increase in modulus with temperature for clay 7.5 and higher concentrations is most probably due to the modulus evolution with time (Ren and Krishnamoorti 2003; Vermant et al. 2007) which was also mentioned in the experimental part. The variation in temperature dependency at 5 % indicates this concentration as the percolation threshold where the response is mainly controlled by the networks instead of chains. Obviously, this behavior resulted in invalidity of the time temperature superposition (TTS) for nano-composites (results are not shown here). The TTS was recently shown to be applicable only for neat EVA (Mahi and Rodrigue 2012a). The appropriate fractal model will be discussed later when strain sweep data will be presented. Such scaling behavior is not observed for $CaCO_3$ in the range of concentration studied. For spherical particles, numerical simulations indicate a percolation threshold of 0.3 for randomly packed spheres and 0.7 for closely packed spheres (Isichenko 1992). Thus, it is believed that by increasing concentration, such fractal property would be observed even for spherical particle, but the subject is outside the scope of the current study.

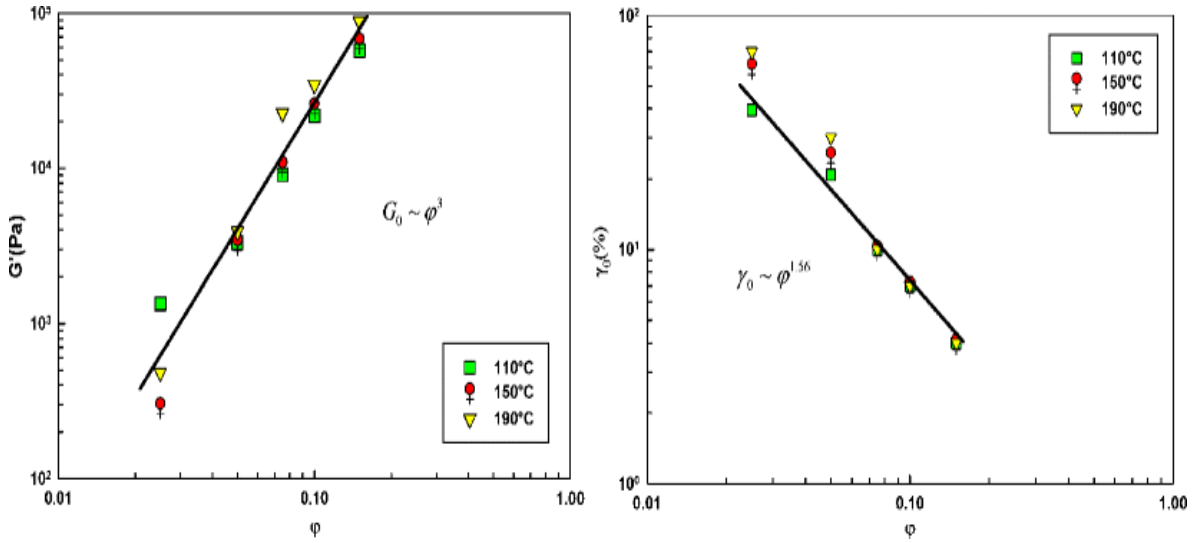

Figure 3-4: Concentration dependency of plateau modulus G_0 (left) and limit of linearity γ_0 (right) for clay nano-composites at different temperatures.

3-4-3 Scaling properties of stress overshoot

The value of the maximum stress (σ_{max}) can then be explained by characteristic relaxation times. It is generally accepted that the maximum stress for nonlinear viscoelastic materials exhibits a

power-law scaling behavior with shear rate ($\sigma_{max} \sim \dot{\gamma}$. This scaling property would appear to be related to the scaling property of the relaxation modulus *G (t)* (Whittle and Dickinson 1997), and the power-law exponent would be the same as for the relaxation behavior:

$$G(t) = a(t)^{-n} \tag{3-3}$$

where *a* is the material stiffness and *n* is the power-law exponent.

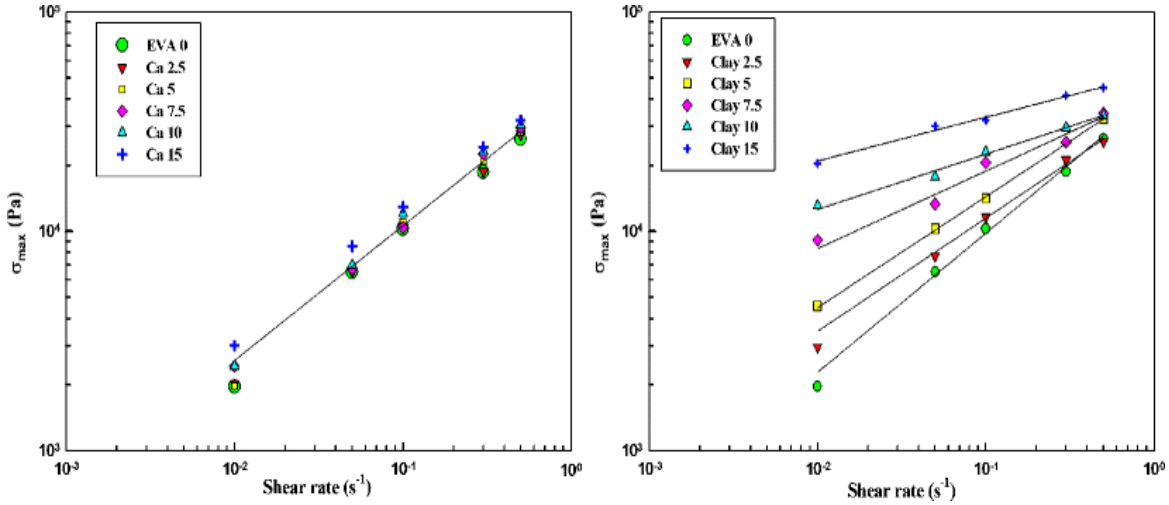

Figure 3-5: Shear rate dependency of σ_{max} for $CaCO_3$ (left) and clay (right) nano-composites at 110 °C. The solid lines are power law fittings with the parameters reported in Table 3-2.

For EVA, the scaling behavior was found to be $\sigma_{max} \sim \dot{\gamma}$, which did not change significantly by adding spherical nano-particles ($CaCO_3$). On the other hand, the scaling for clay is different. The power-law exponent was found to decrease with increasing clay concentration (see Fig. 3-5 and Table 3-2). Considering the relevancy between relaxation time and stress overshoot, no change in the exponent for $CaCO_3$ particles implies no significant effect on relaxation time. This was already confirmed by our linear data and discussion regarding the appearance of an overshoot. Strong change in *n* for platelet particles (clay) again reflects a significant effect on relaxation time. This was also revealed by linear data but was more closely investigated here. Considering the relaxation modulus of the system as in Eq. (3-3), the following equations are obtained for dynamic data (Whittle and Dickinson 1997):

$$G'(\omega) = \omega \int_0^\infty G(t)\sin(\omega t)\,dt = a_0 \frac{\pi\,\omega^n \csc(n\pi/2)}{2\Gamma(n)} \tag{3-4}$$

$$G''(\omega) = \omega \int_0^\infty G(t)\cos(\omega t)\,dt = a_0 \frac{\pi\,\omega^n \sec(n\pi/2)}{2\Gamma(n)} \qquad (3\text{-}5)$$

where $\Gamma(n)$ is the gamma function.

The exponent (n) values from linear data and from ($\sigma_{max} \sim$; are presented in Table 3-2 for comparison where good agreement between the independently obtained values is observed.

Table 3-2 Comparison of the obtained values for n and $tan\delta$ from linear and transient data at 110 °C.

Sample	n from ($\sigma_{max} \sim$;	n from ($G' \sim \omega^n$)	Predicted $tan\delta$ from transient data (Eqs.(3-4,3-5)	Obtained $tan\delta$ from linear data
EVA 0 and Ca 2.5-10	0.64	0.68	1.53	1.81
Ca 15	0.62	0.55	1.49	0.99
Clay 2.5	0.55	0.54	1.33	0.98
Clay 5	0.50	0.44	1.00	0.74
Clay 7.5	0.33	0.31	0.57	0.53
Clay 10	0.24	0.25	0.40	0.44
Clay 15	0.20	0.21	0.32	0.33

Lower n values with increasing clay concentration would impose a lower frequency dependency for G′ and G'' (see right side of Eqs. (3-4) and (3-5) as $n \rightarrow 0$). Such behavior was observed in oscillatory data where the terminal slope decreased with increasing clay concentration. The power-law exponent for clay 2.5 and clay 5 is close to 0.5. Numerically speaking, a value of 0.5 for n means that $G' = G'' \sim \omega^{1/2}$. Two separate points should be discussed here: the exponent value of 1/2 and the equality of the loss and storage modulus.

The scaling of 1/2 is predicted by the Rouse mode of the polymer chains (Prince and Rouse 1953). It is well understood that Rouse mode does not cover all the frequency range and, for

polymers, is only valid in the high-frequency region (low-frequency region is characterized by slopes of 2 and 1 for G' and G'', respectively). But, as observed in the linear data, the terminal slope decreased significantly with increasing clay concentration as to produce a scaling behavior close to $G' \sim \omega^{1/2}$. Winter and Chambon (1986) showed that the exponent 0.5 is an indication of the transition from a liquid-like to a solid-like behavior which can also happen for other viscoelastic materials like cross-linked polymers (Winter and Chambon 1986; Groot and Agterof 1995), percolated suspensions (Nagase and Okada 1986), and nano-composites (Goel et al. 2006). The linear data also indicated that clay 2.5 and clay 5 are transition concentrations. It seems that the dominating mechanism for systems showing liquid to solid-like transition is via Rouse relaxation (Whittle and Dickinson 1997). Furthermore, the values of G' and G'' are roughly close. The average value of G''/G' $(= tan\delta)$ for the frequency range studied is 0.98 and 0.72 for clay 2.5 and clay 5, respectively, which reveals a relatively good consistency with transient data. At concentrations higher than 5 %, $n \rightarrow 0$ reflecting a frequency independent modulus. This is also consistent with the observed non-terminal behavior (plateau modulus) in oscillatory measurement.

For concentrations in which fractal networks are completely formed, the amount of stress overshoot increases very significantly and shows a low shear rate dependency ($n \rightarrow 0$). This is due to the contribution of the fractals in material flow where structural reorganization and breakdown of such networks are necessary and produce a high stress overshoot. At the same time, due to breakdown and orientation of the structure, a more shear-thinning character is obtained. The importance of such orientation distribution has been extensively discussed for percolated systems formed by spherical (Whittle and Dickinson 1997; Mohraz and Solomon 2005), plate-like (Letwimolnun et al. 2007; Dykes et al. 2012), and tubular (Pujari et al. 2009) particles. As the impact of orientation is more important for anisometric particles (Pujari et al. 2009; Dykes et al. 2012), especially for concentrations higher than percolation, stress overshoot is lower for spherical particles here since no continuous network was formed within the concentration range studied.

3-4-4 Strain sweep and fractal structure

The strain dependence of the nano-composites modulus is depicted in Fig. 3-6. All the materials show a strain-softening behavior which is the so-called Payne effect, a common behavior in viscoelastic materials especially for filled elastomers. The most accepted explanation for such effect is based on interparticle interactions (Heinrich and Klüppel 2002). As a result of interaction disruptions at high strains, strain softening is observed. Obviously, introduction of hard fillers reduced the range for the linear viscoelastic regime, again the effect being more severe for clay. While the limit of linearity γ_0 follows a clear concentration dependency for clay particles, such scaling is missing for $CaCO_3$. Clay exhibits a power-law scaling variation with respect to concentration (φ) as $\gamma_0 \sim \varphi^{-1.56}$ (see Fig. 3-4), while for $CaCO_3$ although the introduction of filler reduced the linear domain, γ_0 was almost constant ($\gamma_0 \sim 60$ %) for all the concentrations tested. This power-law scaling has been reported for percolated-type materials like silica (Yziquel et al. 1999; Sternstein and Zhu 2002) and clay (Durmus et al. 2007; Mobuchon et al. 2007; Vermant et al. 2007). However, depending on particle interactions (Rueb and Zukoski 1997) and surface modification (Yziquel et al. 1999), the exponent is different. Such scaling behavior has been well explained theoretically and numerically by models based on interparticle interactions (Shih et al. 1990). Shih et al. (1990) used a fractal model and showed that the scaling properties for both the limit of linearity in strain sweep and solid-like behavior in oscillatory measurement are caused by particle interactions and can be correlated as

$$\gamma_0 \sim \varphi^{-(1+x)/(3-d_f)} \tag{3-6}$$

$$G_0 \sim \varphi^{(3+x)/(3-d_f)} \tag{3-7}$$

where d_f is the fractal dimension and x is an exponent related to the number of particles per aggregate. By simply solving these equations based on the experimentally observed scaling parameters, the obtained values for d_f and x are 1.62 and 1.16, respectively. By a general comparison with other studies (Yziquel et al. 1999; Cassagnau 2008), it can be qualitatively concluded that the value of d_f here represents a well-exfoliated structure and x indicates the existence of connected fractals. As a specific case compared to the recent work of Vermant et al. (2007) which used the same nano-clay, a lower value for d_f (1.6 compared to 2.2-2.4) shows a

more open fractal structure here. On the other hand, the concentration power-law dependency of γ_0 (1.6) and G_0 (3.02) obtained here is lower than for the mentioned work (1.8-1.9 and 4.6-6 for γ_0 and G_0, respectively) indicating the weaker effect of the fractal structure in this work. Different parameters like degree of exfoliation, particle–particle interaction, and even different matrix used can be the origin of the observed differences, but due to the complexity of the structure, making a more direct link between these values and real structure should be avoided.

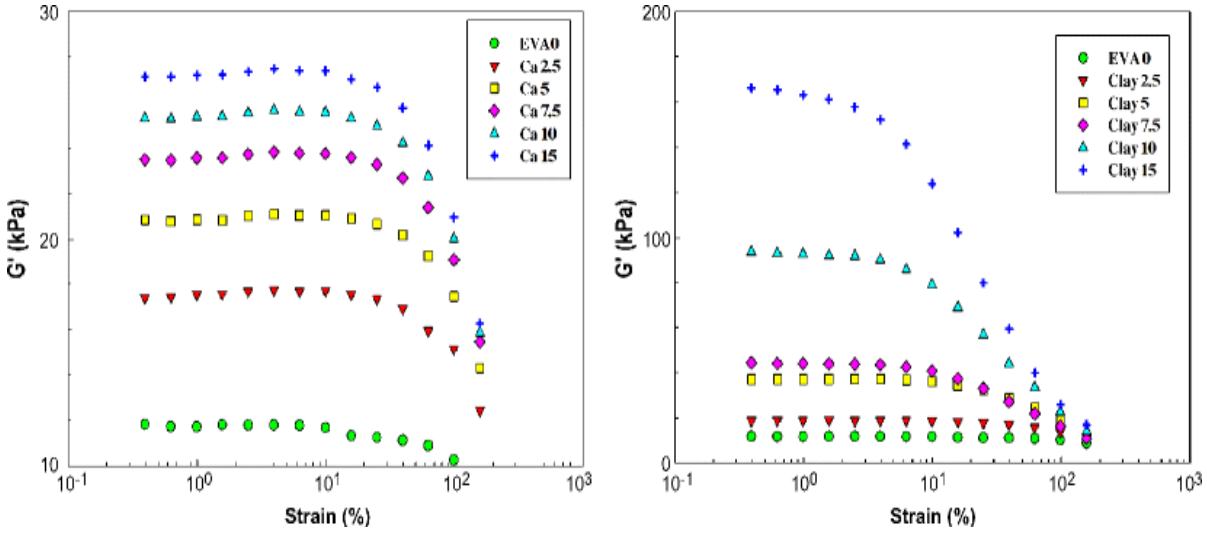

Figure 3-6: Strain dependence of the elastic modulus (G') for clay (right) and $CaCO_3$ (left) nano-composites at 110 °C and ω = 1 rad/s.

Regardless of what is the real explanation for these values, the agreement with this power-law scaling indicates the reliability of the particle-network mechanism. It is noteworthy to say that this dependency is not observed for $CaCO_3$. Referring to the literature even for spherical particles, this power-law dependency has been reported (Cassagnau 2008). Therefore, without looking at TEM images, a discontinuous structure for $CaCO_3$ could be guessed based on rheological data. As mentioned previously, a percolation threshold of 0.3 % was predicted for randomly packed spheres via numerical simulations (Isichenko 1992; Zhang and Archer 2002). However, much lower percolation thresholds have been reported experimentally (Zhang and Archer 2002; Cassagnau 2003). This is because under low to medium deformations, even systems having discontinuous local fractals can sometimes act like percolated structures (Chevigny et al. 2010), the same behavior which was observed for Ca 15.

Another evidence for the presence of a particle-based mechanism is that although for EVA, at all $CaCO_3$ concentrations and low concentrations of clay (2.5 and 5 %), the limit of linearity is temperature dependent, at higher clay concentrations (7.5 % and higher), the appearance of a nonlinear region is relatively temperature independent (see Table 3-3). Such a temperature independence is also observed in the linear data for the same range of concentration (7.5 % and higher) (see Fig.3-4). This temperature independency indicates that the behavior is controlled by a fractal network rather than by temperature-dependent viscoelastic chains. The main conclusion from these data is that 7.5 % is a critical concentration from a physical percolation point of view. Generally speaking, experimental studies show that the percolation threshold for clay is between 0.5 and 2 wt% (Cassagnau 2008). So what does this high (7.5 %) concentration mean? The reported percolations in the literature are mainly based on the appearance of a non-terminal behavior in linear rheology. Non-terminal behavior in rheological properties is not necessarily associated with a situation for which all the particles are interconnected. Usually, the rheological threshold is lower than that for other properties like electrical conductivity (Du et al. 2004). In this work, a non-terminal behavior was observed even for clay 2.5. But the critical concentration of 7.5 % is associated with a situation where all the particles are interconnected. This result indicates that special care must be taken while determining criteria for percolation.

The observed scaling behavior in shear transient can also be investigated based on a fractal structure. As reported by Muthukumar (1989), the exponent n ($\sigma_{\max} \sim \dot{\gamma}^{n}$) can be related to the fractal structure as:

$$n = {3 - d_f}/{2} \tag{3-8}$$

As Eq. (3-8) was originally proposed for neat polymer systems, it can be modified based on Eq. (3-7) for nano-composites to give:

$$n = {3 - d_f}/{3 + x} \tag{3-9}$$

Table 3-3 Limit of linear elasticity (γ_0) for the nano-composites at different temperatures (ω = 1 rad/s).

	γ_0 (%) for clay			γ_0 (%) for $CaCO_3$		
Filler (%)	110°C	150°C	190°C	110°C	150°C	190°C
0	70	80	100	70	80	100
2.5	40	60	70	40	62	70
5	20	25	30	40	62	70
7.5	10	10	10	40	62	70
10	7	7	7	40	62	70
15	4	4	4	40	50	62

Using the parameters from the linear data (d_f = 1.62 and x = 1.16), a value of 0.33 is obtained for *n*. Surprisingly, this value is close to the mean value obtained independently from transient data (see Table 3-2). It should be mentioned that in Eq. (3-9), the fractal dimension is related to shear stress. Based on the fractal model, even though the fractal size is considered to be constant, the number of fractal increases with particle concentration (Shih et al. 1990; Chatterjee and Krishnamoorti 2008), and therefore the stress-related parameter *n* is concentration dependent. The similarity of the obtained *n* value in Eq. (3-9) with that of clay 7.5 (average concentration) reflects the fact that it is reasonable to calculate the fractal dimension via linear data. This validates our interpretation regarding filler-network mechanism since it confirms that the observed exponents in shear flow are resulting from fractal structures.

3-5 Conclusions

The question of whether nano-strengthening is originating from polymer–particle interactions or particle–particle interactions is not completely answered yet. To improve our understanding of the situation, two nano-particles having the same energetic attractions with a polymer matrix (EVA), but of different shape: sphere ($CaCO_3$) vs. platelet (clay) were used. For this specific system, the effect of nano-particle concentration on the viscoelastic properties of polymeric chains was determined. This shape difference combined with their size difference resulted in a lower percolation threshold and higher chain uptake for platelet particles. For clay, TEM analysis revealed the existence of connected network at concentrations higher than 5 %, while for spherical particles, despite the formation of some local fractals, a continuous network was not

observed within the studied concentration range (2.5-15%). Some of the local fractal was interconnected only at 15% of $CaCO_3$. These different structures produced very different responses in rheological tests.

Our results clearly showed that particle–particle interaction (here physical contacting) has a fundamental impact on the linear and nonlinear viscoelastic properties. When a continuous nano-network is formed, the behavior is dominated by the nature of this interstructure rather than the polymeric chains and, therefore, the rheological property changed significantly so that theories based on chain dynamics can no longer predict the response.

For spherical particles, both linear and nonlinear data showed no significant change in the relaxation behavior of polymer chains meaning that the polymer chains are dominating the behavior. For clay on the other hand, although chain confinement was higher than spherical ones, it was not enough to explain all the differences in properties, and therefore significant changes in the rheological behavior were mainly described by a fractal model. The consistency of scaling properties of the system in the linear behavior ($G_0 \sim \varphi^n$), limit of linearity ($\gamma_0 \sim \varphi^n$), and under shear flow ($\sigma_{max} \sim \dot{\gamma}^n$) validated our interpretation regarding the filler-network mechanism.

Another important observation was the modification of the relaxation behavior of viscoelastic materials which can be well predicted by shear transient data. The concentration dependence of the exponent n from $\sigma_{max} \sim \dot{\gamma}^n$ is an indicator for the relaxation behavior. As long as the relaxation time is not altered, the power-law exponent does not change. On the other hand, when stress relaxation times increased by the presence of nano-particles, the exponent n in shear transient tests decreased accordingly.

Finally, the rheological methods used here were found to be very reliable tools to understand the structure–property relationships of nano-composites, especially when coupled with other structural analysis like SEM and TEM.

Acknowledgements

The authors acknowledge the financial support of Natural Sciences and Research Council of Canada and the Quebec Ministry for Economic Development, Innovation and Exportation for

this work. Financial support from the ArboraNano Center of Excellence is also acknowledged. Special thanks go to Specialty Minerals, Inc. for the $CaCO_3$ and Southern Clay Products, Inc. for the nano-clay samples. Finally, Prof. Maria Cornelia Iliuta and Mrs. Sanaz Mosagedh Sedghi are acknowledged for the contact angle measurements.

Chapter 4 Effect of nano-particles on flow and recovery of polymer nanocomposites in the melt state

H. Mahi and D. Rodrigue, Int. Polym. Proc., 28, 151-158 (2013).

Résumé

L'effet de la géométrie de nanoparticules sur l'écoulement et la recouvrance de polymères fondus à base d'éthylène-acétate de vinyle (EVA) a été étudié. Deux nanoparticules, le carbonate de calcium ($CaCO_3$) et la nano-argile (montmorillonite), ont été utilisées avec des concentrations comprises entre 2,5 et 15% en poids. Tout d'abord, à l'aide d'oscillation à faible amplitude de cisaillement et d'essais de cisaillement transitoire, la réponse linéaire et non-linéaire des nano-composites a été étudiée. Ensuite, pour examiner la recouvrance de structure, le même comportement a été étudié sur des échantillons pré-cisaillés. Les données linéaires et non-linéaires ont révélé que l'effet des nanoparticules sur l'écoulement de matière est plus important pour les particules anisotropes ce qui peut être attribué à leur capacité de former une structure fractale contrôlant les propriétés rhéologiques; tandis que les particules sphériques sont incapables de former de tels réseaux. Des expériences de recouvrance ont révélé que, bien que les nano-composites contenant des particules sphériques aient des réponses relativement similaires lors d'essais ultérieurs, les propriétés rhéologiques ont nettement diminué pour les particules d'argile. Les résultats de recouvrance ont également été interprétés par un mécanisme de création de réseau et de la réduction de l'effet de nanoparticules anisométriques liée à l'effondrement du réseau de particules. Ces observations ont été validées par des études morphologiques.

Abstract

The effect of nano-particle geometry on flow and recovery of polymer melts based on ethylene vinyl acetate (EVA) was investigated. Two nano-particles, calcium carbonate ($CaCO_3$) and montmorillonite clay, were used with concentrations between 2.5 and 15% by weight. First, by using small amplitude oscillatory shear and transient step shear tests, the linear and non-linear response of the nano-composites was studied. Then, to examine the structure recovery, the same behavior was studied on pre-sheared samples. The linear and non-linear data revealed that the effect of nano-particles in material flow is more important for anisometric particles which can be attributed to their ability to form a fractal structure controlling the rheological properties while spherical particles are not able to form such networks. Recovery experiments revealed that while nano-composites containing spherical particles have relatively similar response in subsequent tests, the rheological properties decreased significantly for platelet particles. The recovery results were also interpreted based on a filler-network mechanism and the reduction of the nano effect for anisometric particles was related to the breakdown of the filler network. These observations were validated by morphological investigations.

4-1 Introduction

To design tailor-made nano-composites, relations between structural variables and final properties need to be understood. Because rheological analysis can achieve thermodynamic equilibrium conditions and considering the easiness of applying these methods, rheological measurements are known to be very reliable to understand such relations (Nagase and Okada 1986, Cassagnau 2008, Utracki et al. 2010, Krishnamoorti and Chatterjee 2011). Despite the large volume of literature on the rheological analysis of nano-composites, there are still several parameters that are not well elucidated yet. For example, increases in rheological properties like $G^*(\omega)$, $\eta^*(\omega)$, as well as the appearance of a solid-like behaviour even at very low particle content, have been commonly observed in nano-composites (Krishnamoorti and Giannelis 1997, Solomon et al. 2001, Sarvestani 2008, Song and Zheng 2010), the exact origin of such nano-strengthening is still unclear. These phenomena are generally ascribed to different mechanisms (Akcora et al. 2010a, Song and Zheng 2010), but the actual body of knowledge can be summarized by two primary mechanisms: those emphasizing on particle-particle interactions (Chatterjee and Krishnamoorti 2008, Akcora et al. 2010a, Chen et al. 2010) and those based on polymer-particle interactions (Robertson and Roland 2008, Sarvestani 2008, Zheng and Xu 2010). Nevertheless, the important question of which parameter has the main contribution in nano-strengthening is not completely answered yet.

To simplify the situation in our recent work (Mahi and Rodrigue 2012b), one variable was fixed (polymer-particle interactions) to examine the effect of the other (particle-particle interactions). This was done by using two geometrically different nano-particles having the same energetic attractions with the polymer matrix (EVA). The geometric differences resulted in different contacting capability for each filler. It was found that anisometric (platelets) particles are more effective than spherical ones in influencing both linear and non-linear properties of polymer melts. Since polymer-particle interactions were similar, differences in rheological behavior were discussed based on different particle-particle interactions (filler networking mechanism). Here, to validate our discussion regarding the filler networking mechanism, their recovery behavior will be studied on pre-sheared materials. This is especially important because recovery highly depends on structural variables and it is well known that polymers have a reversible character (Cassagnau 2003). Therefore, if the behavior is dominated by polymer chains, then most of the

property is expected to be recovered. On the other hand, if the filler network dictates the response, it is expected that, as a result of the disruption of filler networks under flow, the properties would not completely recover. Also, since the focus of the former work was on stress overshoot and dynamic relaxation, flow behavior was not discussed. In addition to structural analysis, flow properties are very important for processing issues and must be understood to determine how the melt flow properties (especially shear-thinning behavior) are influence by the presence of nano-particles. Hence before discussing the recovery behavior, the effect of nano-particles on the shear flow behavior will be presented.

4-2 Experiments

4-2-1 Materials and samples preparation

Ethylene vinyl acetate (EVA) was used as the matrix: ELVAX 360 from DuPont which contains 25% of vinyl acetate (MI = 2 dg/min, ρ = 948 kg/m^3, Tm = 78°C). Modified clay particles (Cloisite 20A) were obtained from Southern Clay Products, while surface modified nano-particles of calcium carbonate (Ultra-flex) were obtained from Specially Minerals Co. Sample preparation and more details on characterization can be found elsewhere (Mahi and Rodrigue 2012b).

4-2-2 Morphological characterization

A scanning electron microscope (SEM) JEOL JSM 840A from JEOL USA Inc. was used for morphological investigations. The samples were first frozen in liquid nitrogen before being fractured to expose the structure which was then coated with Pd/Au prior to observation.

4-2-3 Rheological analysis

All the rheological tests were performed on a strain controlled TA Instruments rheometer (ARES) with a torque transducer (0.02-2000 g-cm) and a normal force transducer (2-2000 g) under a N_2 atmosphere. All measurements were done using a 25 mm diameter parallel plate geometry with gaps between 1.5 and 2 mm. Strain sweep tests were performed in a strain range of 0-200% with a frequency of 1 rad/s at 110°C. To examine the recovery capability of the samples, the same strain sweep tests were performed on pre-sheared samples after a rest time of 500 s. Shear transient tests were done for selected shear rates of: 0.005, 0.01, 0.05, 0.1, and 0.5 s^{-1}. To study shear induced alignment, the samples were first sheared during a preset time (1000 s)

and the test was stopped allowing the sample to rest for a time period (500 s). Next, the test was started again at the same shear rate in the same (CL) or opposite direction (CCL).

4-3 Results and Discussion

4-3-1 Morphological characterization

Since the rheological behavior of the nano-composites will be related to their structure, their morphologies are presented first. Although TEM images have been discussed elsewhere (Mahi and Rodrigue 2012b), SEM images are presented here for discussion in Figure 4-1. These micrographs show that, although some aggregates are formed in both compositions (more apparent for spherical particles), the particles are well distributed. For spherical particles, as the concentration increases, the number of aggregates increases and at the highest concentration (15%) some of these local flocs are interconnected. On the other hand for clay particles, although some single particles can be seen at 2.5 and 5%, at higher concentration (>5%) the fractured surface show a very homogenous structure indicating that clay particles created a connected network which highly affects the surface fracture. These networks were more clearly observed in TEM analysis (Mahi and Rodrigue 2012b). The geometric differences between both types of particles resulted in a much lower percolation concentration (around 7.5%) for platelet particles than spherical ones (not observed even at 15%). It should be mentioned that the same energetic attraction between the polymer matrix and each particle was previously measured (Mahi and Rodrigue 2012b). Therefore, in the following sections, the “nano” effect on viscoelastic properties will be discussed specifically based on these morphological differences.

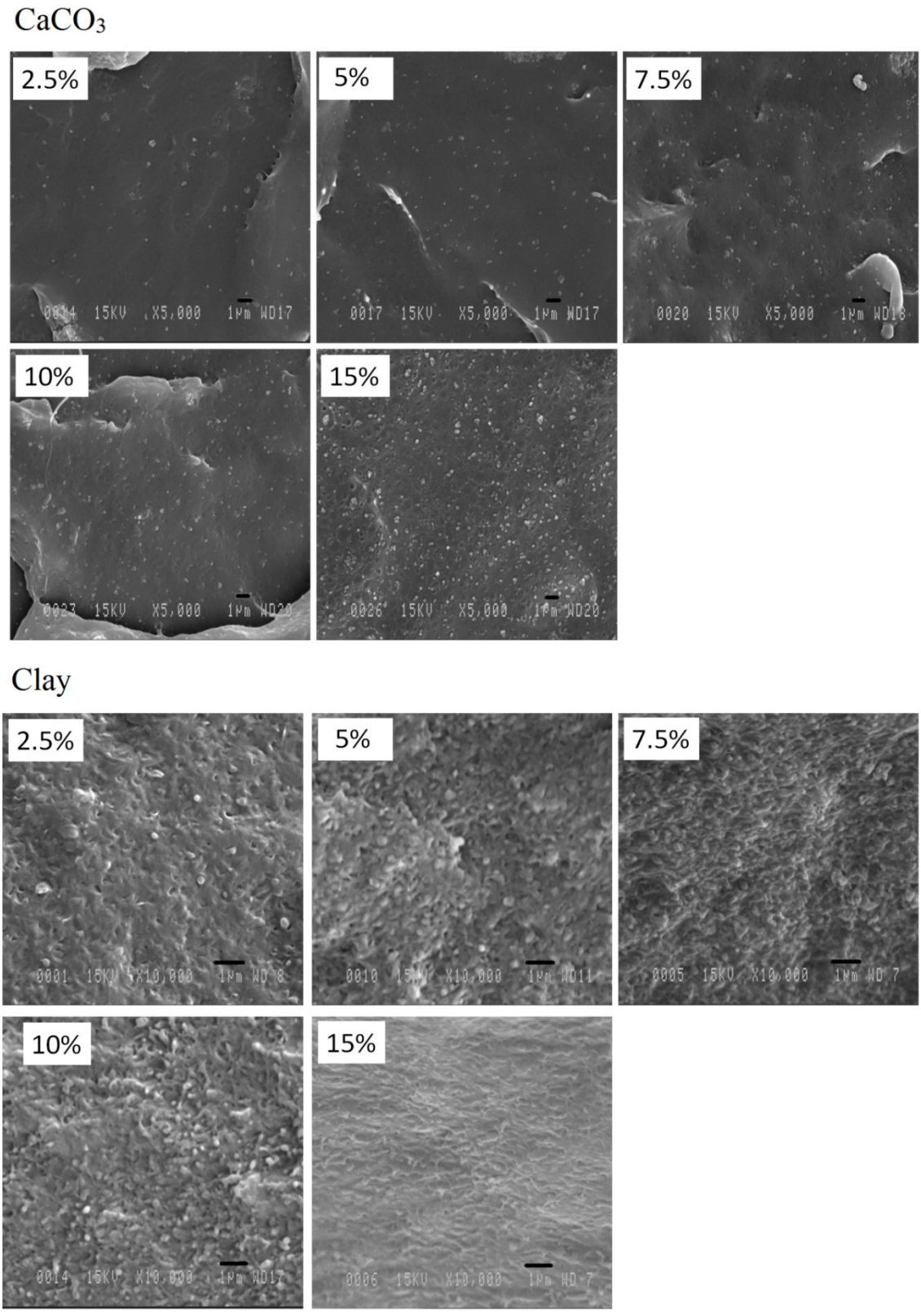

Figure 4-1: SEM images of $CaCO_3$ (top) and clay (bottom) nano-composites. The scale bar shown for all images is 1 μm.

4-3-2 Dynamic data

Recently, linear rheological data of these two systems have been extensively discussed (Mahi and Rodrigue 2012b), but the focus was mainly on dynamic modulus. Here, the effect of nano-particles on complex viscosity will be discussed. The complex viscosity of EVA and nano-composites is shown in Figure 4-2. The complex viscosity increases with nano-particle concentration with a more apparent increase for platelet particles especially at low frequency. The differences between the nano-effect at low and high frequency region arises from the fact that each region include special dynamics of polymeric chains. At high frequency, very short dynamics are included therefore the effect of nano-scale particles is not significant in this region (Kalfus and Jancar 2008). On the other hand at low frequency, nano-scale dynamics are included and consequently the effect of nano-particle is more important in this region. The neat polymer shows a typical behavior for the viscosity curve: a Newtonian plateau at low shear rates (η_0) followed by a shear-thinning region. By increasing spherical particles concentration, viscosity increased accordingly and all Ca compositions have a Newtonian plateau at low frequency. On the other hand, clay nano-composites behave very differently from spherical particles. First, the viscosity increase is more significant compared to $CaCO_3$. Second, at concentrations higher than 2.5%, the materials do not show a Newtonian plateau with evidences of yield phenomena indicating that the response for is more solid-like. In order to better discuss the viscosity curves, a modified Carreau-Yasuda model (Naderi et al. 2007) was used to fit the experimental data via:

$$\eta(\omega) = \frac{\sigma_0}{\omega} + \eta_0 \left[1 + (\lambda\omega)^a\right]^{(n-1)/a} \tag{4-1}$$

where σ_o is the yield stress, η_o is the zero shear viscosity, λ is a time constant, a is the Yasuda parameter and n is the power-law index. While the first two parameters represent the low frequency response, the last three parameters characterize how the material behaves in the non-Newtonian region (shear-thinning zone). The values of the model parameters for EVA and the nano-composites are presented in Table 4-1. For EVA and all Ca, there is no apparent yield stress as these compositions have a zero shear viscosity. However, the zero shear viscosity increases with concentration from 9.9 kPa-s for neat EVA to 38.7 kPa-s for Ca 15 which shows that polymer chain mobility is limited even by spherical particles. The reduced mobility can be the result of frictional forces as well as polymer particle interaction. It should be mentioned that

recently (Mahi and Rodrigue 2012) contact angle measurement revealed a good attraction between particles and polymer. Such attraction can limit the motion of polymer chain. Clay 2.5 also showed no yield stress, however the viscosity increase significantly higher compared to Ca particles. The zero shear viscosity of clay 2.5 (75.7 kPa-s) is already higher than the highest Ca concentration (38.7 kPa-s for Ca 15) tested. Also, η_0 shows a more important concentration (ϕ) dependence for platelet particles (scaling of $\eta_0 \sim \phi^{2.4}$) than spherical ones (scaling of $\eta_0 \sim \phi^{0.6}$) which reflects a much stronger effect of platelet particles than spherical ones on limiting chain mobility, a similar finding has been recently reported elsewhere (Harton et al. 2010). For other clay compositions (> 2.5%) a yield stress is observed which increases with concentration. Although different mechanisms have been proposed for this yield response, it is believed that the dominant mechanism for such yield phenomenon is the filler networking mechanism (Shih et al. 1990, Krishnamoorti and Giannelis 1997, Akcora et al. 2009, Akcora et al. 2010a). Platelet particles have higher contacting capability than spherical ones. As a result of physical contacting between the particles a network structure is formed which dominates the response, an ability that spherical particles do not have within the studied concentrations. The mentioned network mechanism has been extensively discussed in our recent work (Mahi and Rodrigue 2012b). TEM images also showed that at concentrations higher than 2.5%, clay particles were interconnected and a continuous network was formed. The time parameter λ is around 2.5 s/rad for EVA and does not change significantly with $CaCO_3$ addition. This time scale can be related to a relaxation time associated with the onset of shear-thinning. The data of Figure 4-2 also show that shear-thinning starts around the same frequency for spherical articles. λ values for clay composites are much higher (over an order of magnitude) and increase with concentration. Because of the appeared yield phenomena in clay nano-composites the onset of shear-thinning as predicted by the model occurs at very low frequencies. The shear-thinning exponent (n) shows a more uniform trend compared to other parameters. By increasing nano-particle concentration n decreases, again with a stronger effect for clay particles (from 0.53 for EVA0 to 0.18 for clay 15) than for $CaCO_3$ (from 0.53 for EVA0 to 0.41 for Ca 15). This implies that nano-particles increased the shear-thinning characteristics of the polymer matrix which is typical for filled polymer melts (Hornsby 1999, Wagener and Reisinger 2003, Kagarise et al. 2010).

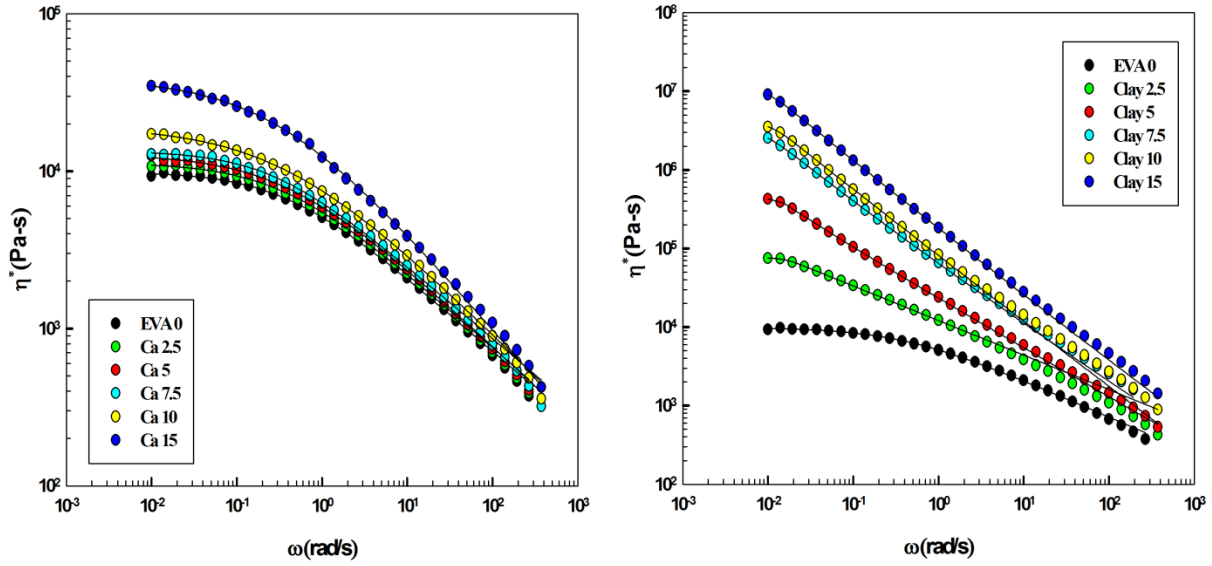

Figure 4-2: Complex viscosity of Ca (left) and clay (right) nano-composites at 190°C. Solid lines are curve fitting to Equation (4-1).

Table 4-1 Modified Carreau-Yasuda model parameters for EVA and the nano-composites at 190°C.

Sample	σ_0 (kPa)	η_0 (kPa-s)	λ (s/rad)	a (-)	n (-)
EVA 0	0	9.90	2.62	0.821	0.531
Ca 2.5	0	11.3	2.28	0.688	0.529
Ca 5	0	12.9	2.50	0.691	0.495
Ca 7.5	0	13.5	2.75	0.690	0.485
Ca 10	0	19.2	2.85	0.585	0.460
Ca 15	0	38.7	3.32	0.535	0.371
Clay 2.5	0	75.7	63.9	5.77	0.501
Clay 5	1.35	260	67.8	5.89	0.411
Clay 7.5	1.48	1082	75.8	6.24	0.293
Clay 10	10.9	2521	76.9	6.25	0.211
Clay 15	48.7	4274	77.1	6.45	0.186

4-3-3 Shear transient response

The response of viscoelastic materials to a constant shear rate includes three regions (see Figure 4-3): an elastic response at short times, a steady response at long times, and a transition region in between (Mahi and Rodrigue 2012a). The focus of our recent work was on the transition region where depending on material structure and applied shear rate, the materials can present an overshoot. The importance of such overshoot and its relation with structural variables were extensively discussed in that work. Here, to better discus the different behavior of both nano-composites in shear transient tests, the following equation was used to predict the transient stress response of nano-composites (Whittle and Dickinson 1997):

$$\sigma(t) = \sigma_0 \left[\frac{(t/\tau_1)}{1+(t/\tau_1)^{1+\delta}} \right] + \sigma_\infty \left[1 - \exp(-t/\tau_2)\right] \tag{4-2}$$

where, according to the fractal model (Chatterjee and Krishnamoorti 2008), τ_1 is the time related with the rearrangement of the structure, τ_2 is the time related to the network break-up (or flow), δ is a phenomenological parameter, σ_0 is related to the shear rate dependent elastic modulus and σ_∞ is related to the steady state shear stress. The values for the model parameters are shown in Table 4-2. The main difference between the particles is reflected in stress related parameters (σ_0 and σ_∞) and more especially in the elastic stress σ_0. As mentioned, σ_0 and σ_∞ represent the elastic and steady response respectively. Higher values for clay particles again reflect the stronger effect of platelet particles on both steady and elastic response. The larger difference between σ_0 and σ_∞ for clay particles validates the explanation regarding the domination of linear response by clay networks. Since σ_0 is related to the linear response and since for clay, particle networks are formed, σ_0 presents much higher differences than σ_∞ which is related to material equilibrium flow. Time scales parameters (τ_1, τ_2) did not however change significantly in both cases. In transient tests, it was found that while the amount of stress overshoot increased with nano-filler concentration, the characteristic time related to this stress was relatively constant (Mahi and Rodrigue 2012a). This is because the strain at the maximum stress ($\gamma_{at\ \sigma max}$) is independent of shear rate (Goel et al. 2006, Letwimolnun et al. 2007, Kagarise et al. 2010). In this work also, the strain at maximum for each shear rate and concentration was the same (~4.6). Considering that

$t_{peak} = \gamma_{at\sigma\max} / \dot{\gamma}$ and the fact that since $\gamma_{at\sigma max}$ is constant, t_{peak} will only depend on shear rate and since τ_1 and τ_2 are time scales related to t_{peak}, they did not change significantly.

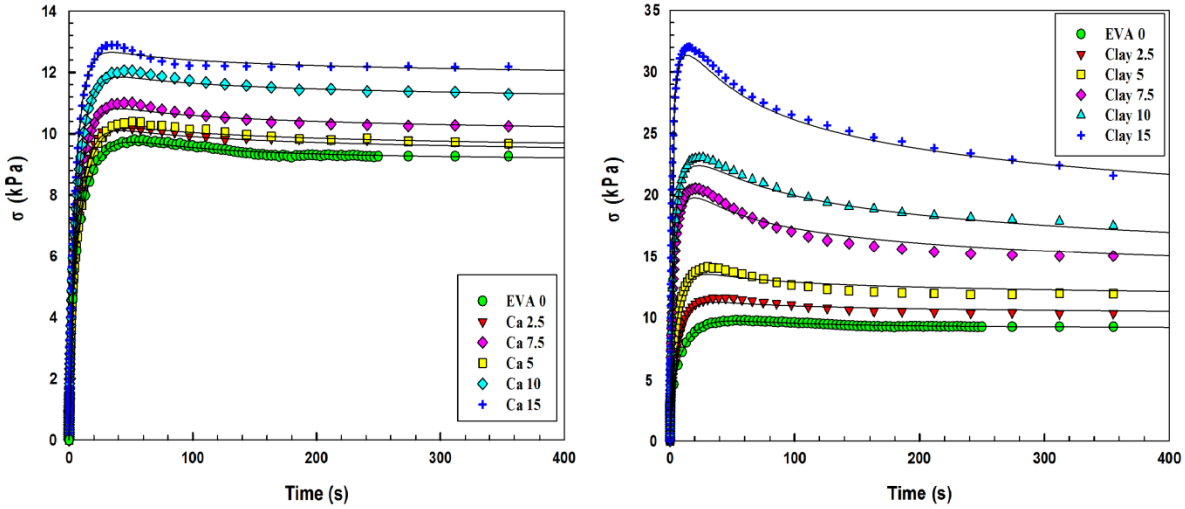

Figure 4-3: Time dependant shear stress of Ca (left) and Clay (right) nano-composites at 110°C. The solid lines are curve fitting to Equation (4-2).

Table 4-2. Parameters of Equation (4-2) for EVA and the nano-composites based on the data shown in Figure 4-3.

		Clay						$CaCO_3$				
	EVA 0	2.5	5	7.5	10	15		2.5	5	7.5	10	15
σ_0 (kPa)	4.71	5.22	7.46	19.7	21.0	37.8		4.65	4.78	4.95	4.82	5.11
τ_1 (s)	1.21	1.38	1.31	2.04	1.81	1.62		0.614	0.821	0.932	0.633	0.781
δ (-)	0.128	0.202	0.231	0.242	0.222	0.213		0.161	0.184	0.195	0.171	0.114
σ_∞ (kPa)	8.02	9.04	9.81	10.1	11.8	11.2		8.48	8.97	8.53	10.1	10.6
τ_2 (s)	11.6	8.08	7.47	7.41	7.87	7.40		8.23	8.27	9.21	7.94	7.85

4-3-4 Recovery properties under flow

In the last section, different effects of platelet and spherical particles on linear and transient viscosity were investigated with an emphasis on inter-particle interaction. Recently, it was shown (Mahi and Rodrigue 2012b) that non-linear behaviors like strain-softening (Payne effect) and stress overshoot are affected by the introduction of nano-particles with a stronger effect for

anisometric particle (platelets). It was also shown that the scaling behavior of nano-composites is well described by fractal models which consider direct contact mechanisms. To better discuss the importance of particle-particle interaction on rheological properties, the recovery behavior of the polymer and nano-composites is discussed here. The recoverability is examined on pre-sheared samples which have rested a determined amount of time after shearing. In order to eliminate the polymer contribution in recovery tests, the rest time (500 s) was taken to be much longer than the longest relaxation times reported earlier for shear flows τ_d = 10.1 s. Hence, the differences observed can be directly attributed to the particles. It is generally agreed that for anisometric particles, the applied shear would impose an orientation and therefore the structure and the properties will be altered, while for spherical particles this effect is not expected.

The variation of the storage modulus in the plateau region of strain sweep tests and σ_{max} (in transient test) in successive tests for all the samples are shown in Table 4-3. While significant reduction in the second test is observed for clay samples, the properties are relatively constant for $CaCO_3$. To explain these data, the Payne effect can be used. Payne effect for polymers is a reversible process (Cassagnau and Mélis 2003, Zhu and Sternstein 2003, Cassagnau 2008) and it is expected that as long as the behavior is dominated by the polymer structure, the material would retain its original equilibrium structure by a relaxation process. For all $CaCO_3$ concentrations and clay 2.5, the moduli did not change significantly. This means that for these concentrations the response is still controlled by the viscoelastic chains. This was confirmed by linear data (Mahi and Rodrigue 2012b) in which for these concentrations, the relaxation spectrum did not change significantly. Referring to morphological images, SEM here and TEM images (Mahi and Rodrigue 2012b), for such concentrations, a connected network was not created. However, for clay contents between 5 to 15%, the moduli decreased considerably in the second test and only part of the structure is recovered. Considering the reversible nature of the polymer, the only explanation for such reduction is based on a filler network mechanism. As a result of the applied flow, some of the clay networks are disrupted and since the Peclet number is high (Pe >>1) (Mahi and Rodrigue 2012a), these networks are not rebuilt during the rest time, thus significantly lower moduli are observed in subsequent tests. For the transient behaviour, it is believed that stress overshoot of polymers can be well predicted from their characteristic relaxation behaviour and vice versa (Whittle and Dickinson 1997, Mahi and Rodrigue 2012b).

Hence, the change or not of transient properties in consecutive tests can be explained based on those findings. For EVA 0, all $CaCO_3$ nano-composites and clay 2.5, the relaxation behaviour is dominated by polymeric chains, so the stress is recovered in the second tests. For clay 5-15% where the connected network dictates the response, part of the overshoot is not recovered.

In order to better discuss the differences between spherical and platelet particles in shear transient test, Equation (2) was applied on the stress response of Ca 10 and clay 10 in the first and subsequent tests. The choice for this concentration (10%) was to ensure that the networks of platelet particles are formed while for spherical ones are not. Typical responses are shown in Figure 4-4 where the related parameters values are presented in Table 4-4. The only parameters showing significant changes within the sequential tests are σ_{max} and σ_∞ for Clay 10, while the time scales parameters (τ_1, τ_2) and δ did not change significantly in both cases. As mentioned earlier, the characteristic time scales in shear transient tests are highly shear rate dependent and since the shear rate is the same in subsequent tests time scales are also relatively constant in each test. The parameter δ determines the importance of the elastic response (first part of Equation (4-2)) to the decay part (second part of Equation (4-2)). Although stress is highly sensitive to particle shape and shear history, no changes in δ indicates greater properties reduction for clay and indicates that filler network creation is a dominant phenomenon controlling the behavior while polymer-particle interactions is a secondary contribution. It is obvious that the latter did not change (at least significantly) by the shear rates imposed that the ratio between the elastic and decay parts did not change in successive tests. Figure 4-4 also confirms that the trend of stress response in repeated tests is similar for both particles. The effect of particle shape differences is clearly observed on the values of σ_0 and σ_∞. The most important difference is reflected in the elastic response where clay shows much higher σ_0 values. At very short times, the response is linear and dynamic data also showed that anisometric particles are more effective than spherical ones in controlling the linear behaviour. The shape difference is also reflected in the recovery behaviour of stress related parameters (σ_0 and σ_∞); while for Ca 10 the values are similar in subsequent tests, the reduction is significant for clay. As the applied shear would impose orientation of clay particles, the number of inter-platelet contacts is reduced, thus the stress decreased significantly for the second test. For spherical particles, there is no orientation effect; a random structure is substituted by another random structure, so the parameters are unchanged.

Table 4-3. Property reduction (storage modulus in the plateau region of strain sweep tests and stress overshoot in transient tests) of pre-sheared sample relative to the unsheared samples.

	G' reduction (%)		σ_{max} reduction (%)	
EVA 0	1		2	
Filler content (%)	Clay	$CaCO_3$	Clay	$CaCO_3$
2.5	5	1	6	5
5	20	1	21	5
7.5	38	1	36	5
10	54	2	49	5
15	60	5	65	5

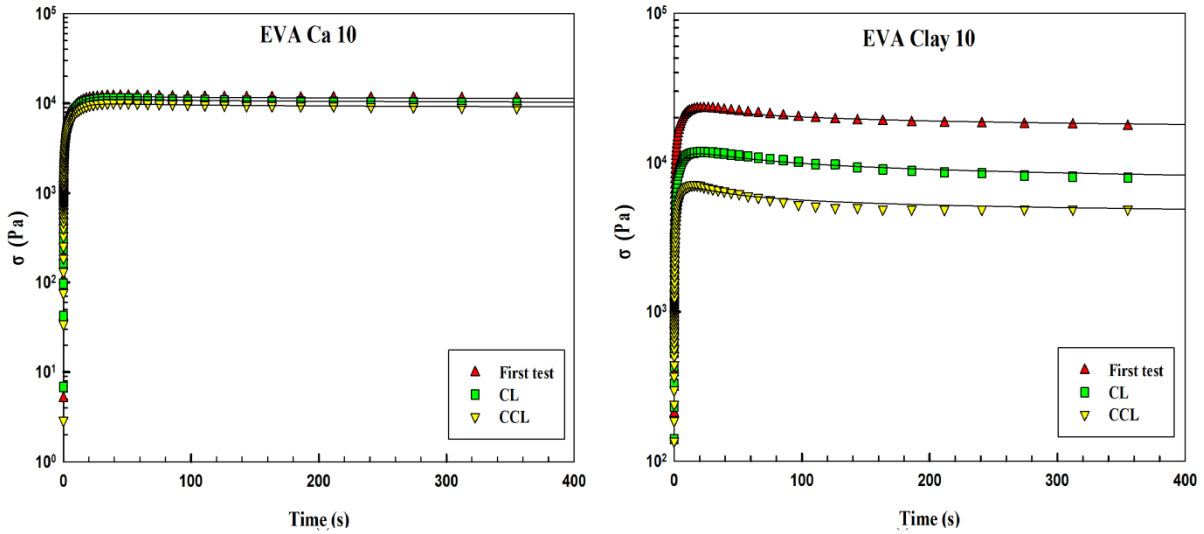

Figure 4-4: Stress-time curves for Ca 10 (left) and clay 10 (right) at a shear rate of 0.1 s^{-1} in first test and subsequent tests in clockwise (CL) direction and counter-clockwise (CCL) direction. The solid lines are curve fitting to Equation (4-2).

Table 4-4. Parameters of Equation (4-2) for Ca 10 and clay 10 at 110°C in subsequent tests (data are shown in Figure 4-4).

Sample	Test	τ_1 (s)	τ_2 (s)	σ_0 (kPa)	σ_∞ (kPa)	δ (-)
Ca 10	0.1 s^{-1}	0.631	7.94	3.80	10.1	0.172
	0.1 s^{-1} after first rest CL*	1.12	8.84	4.84	8.86	0.202
	0.1 s^{-1} after second rest CCL*	1.08	8.61	4.31	7.88	0.204
Clay 10	0.1 s^{-1}	1.82	7.89	20.9	11.9	0.221
	0.1 s^{-1} after first rest CL*	2.67	8.85	14.5	3.59	0.223
	0.1 s^{-1} after second rest CCL*	1.97	6.68	7.09	3.45	0.308

4-4 Conclusions

To determine the effect of particle contact ability of nano-fillers on rheological properties of nano-composites, two geometrically different nano-particles were used. As special cases, $CaCO_3$ and clay nano-particles were dispersed in EVA to study their flow and recovery behavior in the melt state. Particle shape differences resulted in a lower percolation threshold for platelet particles (clay) in which a connected network was formed at concentrations higher than 5%, while for spherical particles ($CaCO_3$) it was not observed within the studied concentration range (2.5-15%).

These two structures responded very differently under both dynamic and transient shear. Linear data showed that while viscosity increased by both nano-particles, its increase was more significant for clay particles than spherical ones and even the lowest clay concentration (2.5%) showed a higher zero shear viscosity (75 kPa-s) than the highest Ca concentration (36 kPa-s for Ca15). At higher clay concentration (> 2.5%) a yield phenomenon was observed which indicated a solid response for these nano-particles. Also by using a modified Carreau-Yasuda model it was found that viscosity related parameter (η_0 in model) showed more concentration dependency for platelet particles (scaling of $\eta_0 \sim \phi^{2.4}$) than spherical ones (scaling of $\eta_0 \sim \phi^{0.6}$). The appeared solid response together with higher concentration dependency for clay particle was related to the formation of particle network and it was concluded that when a continuous nano-network is

formed (which is the case for clays) the linear behavior is dominated by the nature of this structure rather than by the polymeric chains.

Shear transient data also showed a same trend as linear data; the response of polymer under large deformation was affected much more strongly by clay particles than $CaCO_3$. By using a fractal model it was found that the related parameter to the dynamic stress increases monotonically for platelet particle (from 4.7 kPa for EVA to 38 kPa for Clay 15). On the other hand the differences were not that significant for $CaCO_3$ where the value for the highest concentration was 5.11 kPa. These differences indicate that in addition to the stronger effect of platelet particles on linear respond their contribution in material flow is also much more apparent than for spherical particles.

Recovery experiments also showed that clay nano-composites have an irreversible character and the properties decrease significantly in consecutive tests. On the other hand, when particles are not physically interconnected (spherical particles) the polymeric chains dictate the response and the nano-composite can recover almost all of their properties. It can be concluded that particle-particle interactions (here physical contacting) have a fundamental impact on the linear and non-linear viscoelastic properties of polymer melts and it can be considered as the main reinforcement mechanism.

Chapter 5 Validity of the modified molecular stress function theory to predict the rheological properties of polymer nanocomposites

H. Mahi, M. Abbasi, M. Wilhelm, D. Rodrigue, J. Rheol., 57, 881-899 (2013).

Résumé

Le cisaillement transitoire et les propriétés extensionnelles de nano-composites à base d'éthylène-acétate de vinyle contenant deux nanoparticules géométriquement différentes (sphères de $CaCO_3$ et plaquettes d'argile) ont été étudiés expérimentalement et les données ont été comparées aux prédictions rhéologiques de la théorie de la fonction de contrainte moléculaire modifiée (MSF) telle que proposée récemment par Abbasi et al. [Rheol. Acta, 51, 163-177 (2012)]. Alors qu'une concordance a été obtenue pour les particules sphériques, des écarts ont été observés pour les plaquettes à des concentrations supérieures à 2,5% en poids. La limitation de la théorie MSF pour de telles compositions est liée à la domination de la réponse rhéologique linéaire par la présence d'un réseau de particules sur la contribution des chaînes polymériques. Il a été observé que cette contribution de réseau augmente la non-linéarité sous de grandes déformations, un phénomène qui a été quantifié par la rhéologie de transformée de Fourier des données obtenues sous des tests de cisaillement oscillatoire de grande amplitude.

Abstract

The transient shear and extensional properties of ethylene vinyl acetate nano-composites containing two geometrically different nano-particles (spheres of $CaCO_3$ and platelet of clay) were investigated experimentally and the data were compared to the rheological predictions of the modified molecular stress function (MSF) theory as recently proposed by Abbasi et al. [Rheol. Acta, 51, 163-177 (2012)]. While good agreement was obtained for spherical particles, deviations were observed for platelet particles at concentrations higher than 2.5 wt.%. The limitation of MSF theory for such compositions was related to the domination of the linear rheological response by the presence of particle nano-networks over polymeric chains contribution. This particle network contribution was also found to increase nonlinearity under large deformation, a phenomenon which was quantified via Fourier transformed rheology on data obtained under large amplitude oscillatory shear.

5-1 Introduction

Nano-strengthening, a term used for describing the substantial effect of nano-particles on polymeric systems properties can be observed on several macroscopic properties (Sinha Ray and Okamoto 2003, Paul and Robeson 2008, Kim et al. 2010). Today, an important amount of literature can be found on the effect of nano-particles on mechanical (Crosby and Lee 2007, Ci et al. 2008, Paul and Robeson 2008, Jancar et al. 2010), thermal (Moniruzzaman and Winey 2006, Han and Fina 2011), dielectric (Ma et al. 2009, Yoonessi and Gaier 2010, Zhou et al. 2011) and rheological (Krishnamoorti and Giannelis 1997, Krishnamoorti and Yurekli 2001, Knauert et al. 2007, Anderson and Zukoski 2009, Hobbie 2010, Utracki et al. 2010, Via et al. 2011) properties to call for some.

However, consistent models enabling to link these macroscopic properties to the nano-structure are scarce and not developed yet. This is mainly because the field of nano-composite is still in an early stage and also due to diversity of particle sizes and shapes leading to data scatter as reported in the literature (Sinha Ray and Okamoto 2003, Jancar et al. 2010, Nusser et al. 2010). In polymer science the situation for neat polymer is less ambiguous. Despite the complexity of polymer molecules, and even though some complex features of polymers (especially for polydisperse and highly branched systems) are not well elucidated presently (Dealy and Larson 2006), the dynamics of polymeric chains are fairly well described by advanced rheological models which are mainly based on the tube concept proposed by Doi and Edward (DE) (1989). Nevertheless, more detailed analysis has been achieved by using various modified models based on DE theory for characterization of polymeric melts. Some of these common models can be found in the literature (Marrucci and Grizzuti 1988, Pearson et al. 1989, Pearson et al. 1991, McLeish and Larson 1998, Mead et al. 1998, Wagner et al. 2000, Wagner et al. 2004a, Wagner et al. 2004b, Wagner et al. 2005a).

For polymer nano-composites however, a limited amount of work has been undertaken to develop advanced predictive models (Letwimolnun et al. 2007, Rajabian et al. 2010, Kairn et al. 2005, Kagarise et al. 2008, Schneider et al. 2011, Li et al. 2012). An important challenge for the modeling of nano-composite properties is to determine whether the behavior is discussed mainly based on a polymer or a particle scenario. In the first case, the emphasis is mainly on polymer-particle interactions (Sternstein and Zhu 2002, Picu and Rakshit 2007, Robertson and Roland

2008, Sarvestani 2008, Zhou et al. 2011, Li et al. 2012) and therfore the effect of nano-particles on the viscoelastic properties is considered as an additional factor controlling some of the terms related to chain dynamics. In the latter one however, it is supposed that the behavior is controlled mainly by nano-fillers (filler-filler interactions) instead of polymeric chains (Akcora et al. 2009, Akcora et al. 2010b, Chatterjee and Krishnamoorti 2008, Dykes et al. 2012). This scenario is especially important when the particle concentration is high enough to create physical contacts between particles (connected or percolated network). For this situation, prediction of the viscoelastic behavior is complex and still represents a challenge even for sophisticated models used for polymeric melts.

Recently, Mahi and Rodrigue (2012b) studied experimentally the effect of two geometrically different nano-particles (spheres of $CaCO_3$ and platelet of clay) on the linear and non-linear properties of nano-composites based on ethylene vinyl acetate (EVA). The aim of that work was to determine the effect of particle geometry and therefore their contact ability on rheological properties especially under shear deformations. It was found that the effect of anisotropic particles (clay) on viscoelastic properties was much stronger than spherical ones. For example, modulus improvement for platelet particles was much higher than predicted by classical models like Guth-Gold (Guth and Gold 1938). Differences in behavior were discussed based on a fractal model considering direct contact (percolation) as a main parameter controlling the rheological response.

Considering the wide applicability of models based on DE theory to predict the viscoelasticity of polymer melts, it is the main objective of this work to verify to what extent a model based on the tube concept can predict our previous rheological data (Mahi and Rodrigue 2012b) via simulations. Furthermore, while the recent work considered only shear deformation, extensional properties will also be discussed in this work and the experimental data will be compared to the extensional properties predicted by a model based on the tube theory. For these purposes, a modified version of DE theory based on MSF concept (Wagner and Schaeffer 1993) which has been recently proposed by Abbasi et al. (2012) is applied on the rheological data. To our knowledge, this is the first time that a model based on the tube concept, more particularly a MSF model, is used to predict the rheological properties of nano-composites. In this context, the validity and limits of such model for predicting nonlinear rheological properties of nano-

composites will be investigated. In order to better address the limitation of the MSF model, quantification of LAOS data by FT-rheology will be accompanied with model prediction which help to address the nonlinearity resulting from a nano-particle network. The structure of the paper is as follow: first, the MSF model will be briefly discussed in the next section and a detailed description can be found elsewhere (Wagner et al. 2000, Wagner et al. 2001, Wagner et al. 2004a, Abbasi et al. 2012). Then, the temperature effect for neat polymer will be discussed since such effect has not been yet discussed for the MSF model. Finally, the MSF predictions for the nanocomposites will be presented. In order to quantify the nonlinearity produced by the presence of nano-particles, LAOS data are presented and discussed via FT-rheology analysis.

5-2 Modeling

The constitutive equation used here is based on the MSF model (Wagner et al. 2001). This integral model is based on the original Doi-Edwards theory, (Doi and Edwards 1989) and allows chain stretching by deformation. Marrucci and Grizzuti (1988) introduced the concept of chain stretching in the model by considering a variable tube diameter. Wagner and Schaeffer (1993) used the concept of chain stretching to develop the MSF theory based on the DE theory where the extra stress tensor is given by:

$$\boldsymbol{\sigma}(t) = \int_{-\infty}^{t} m(t-t')\, f^2(t,t')\, \boldsymbol{S}_{DE}^{IA}(t,t')\, dt' \tag{5-1}$$

where $m(t\text{-}t') = \partial G(t\text{-}t')/\partial t'$ is the memory function and can be calculated from linear viscoelastic data (Dealy and Larson 2006). Initially, Wagner and Schaeffer (1993) proposed that deformation lead to a decrease in tube diameter and introduced this effect in the DE theory by the molecular stress function f which is defined as the ratio of tube diameter at equilibrium (a_0) to its value at time t ($a(t,t')$) as:

$$f(t,t') = \frac{a_0}{a(t,t')} \tag{5-2}$$

The value is unity when the tube diameter is constant (e.g. when deformation is linear) and increases as deformation increases. The rate of increase however, depends on polymer

characteristics like molecular weight, molecular weight distribution and branching (Wagner et al. 2000, Rolón-Garrido and Wagner 2007).

In equation (5-1), $\boldsymbol{S}_{DE}^{IA}(t,t')$ represents the strain measure of the DE model with independent alignment assumption (Watanabe 1999):

$$\boldsymbol{S}_{\boldsymbol{DE}}^{\boldsymbol{IA}}(t,t') = 5\left\langle \frac{(\boldsymbol{F}_{t,t'}^{-1}.\boldsymbol{u}(t'))(\boldsymbol{F}_{t,t'}^{-1}.\boldsymbol{u}(t'))}{\left|\boldsymbol{F}_{t,t'}^{-1}.\boldsymbol{u}(t')\right|^2}\right\rangle = 5\,\boldsymbol{S}(t,t') \tag{5-3}$$

where $\boldsymbol{u}$ is the tube segment orientation vector at time t' and $\boldsymbol{F}_{t,t'}^{-1}$ is the displacement gradient tensor between t and t'. $\boldsymbol{S}$ is the orientation tensor and <···> denotes an ensemble average over the surface of a unit sphere. The orientation tensor $\boldsymbol{S}$ can be approximated using Currie's formula as (Pattamaprom et al. 2000):

$$\boldsymbol{S} = \left(\frac{1}{J-1}\right)\boldsymbol{B} - \left(\frac{1}{(J-1)\left(I_2+\frac{13}{4}\right)^{0.5}}\right)\boldsymbol{C} \tag{5-4}$$

$$J = I_1 + 2\left(I_2 + 13/4\right)^{0.5} \tag{5-5}$$

where $\boldsymbol{C}$ and $\boldsymbol{B}$ are respectively Cauchy and Finger tensors, while I_1 and I_2 are the trace of $\boldsymbol{B}$ and $\boldsymbol{C}$, respectively. Eq. (5-1) is an integral constitutive equation (MSF model), but another equation is required for the molecular stress function f. Different types of empirical and theoretical equations have been proposed for such purpose (Wagner et al. 2001, Wagner et al. 2003). Recently, Abbasi et al. (2012), by assuming side chain stretching along with backbone stretching, proposed a pair of evolution equations for f as:

$$\frac{\partial f_s}{\partial t} = f_s\left((\boldsymbol{\kappa}:\boldsymbol{S}) - \frac{f_s(f_s^{\,3}-1)}{\tau_a}\right) \tag{5-6a}$$

$$\frac{\partial f^{\,2}}{\partial t} = \beta f^{\,2}\left((\boldsymbol{\kappa}:\boldsymbol{S}) - \frac{CR}{f^{\,2}-1}\right) - (\beta-1)\frac{\partial f_s^{\,2}}{\partial t} \tag{5-6b}$$

where f and f_s represent backbone stretching and side chain stretching, respectively. The parameter f_{max} is related to the maximum stretch that the polymer chain can be subjected to in flow before chains slip past one another without further stretch (Rolón-Garrido et al. 2009), and governs the steady state value of viscosity in extensional flows. The value for f_{max} depends on the molecular topology and increases with increasing number of branching (Rolón-Garrido and Wagner 2007, Abbasi et al. 2012). It also depends on the ratio of the radius of gyration ($<Rg^2>$) of a branched polymer to the linear one with the same molar mass; the smaller the ratio the higher the value for f_{max} (Rolón-Garrido and Wagner 2007). The relaxation time τ_a is a relaxation time defined as the time needed for the surrounding chains to allow for the side chain tube to return to its equilibrium (Wagner and Rolón-Garrido 2010, Abbasi et al. 2012). In this model β represents the ratio of molar mass of the branched polymer to the molar mass of the backbone and determines the slope of strain-hardening in transient extensional flows and therefore its value is unity for linear polymers (linear PS) and higher than 1 for long chain branched polymers (LDPE, LCB-PP, Comb-PS) (Wagner et al. 2006, Abbasi et al. 2012). The parameter CR is a constraint release due to the motion of neighbor chains and is defined by:

$$CR = \frac{(f^2-1)^2}{f_{\max}^2-1}\sqrt{\boldsymbol{D}^2:\boldsymbol{S}} + a_2(f^2-1)^2\sqrt{|\boldsymbol{W}\boldsymbol{D}:\boldsymbol{S}|} \tag{5-7}$$

κ, D and W are the velocity gradient, rate of deformation and rate of rotation tensors, respectively.

In uniaxial extensional flows when $\dot{\varepsilon}$, ($\dot{\varepsilon}$ being the extensional rate), it is possible to neglect the effect of side chain stretching to get (see Appendix C):

$$\frac{\partial f^2}{\partial t} = \beta\dot{\varepsilon}\left(\cdot S_{33} - \frac{f^2-1}{f_{\max}^2-1}\sqrt{S_{11}+\frac{1}{2}S_{33}}\right) \tag{5-8}$$

For transient shear deformation when $\dot{\gamma}$ ($\dot{\gamma}$ being the applied shear rate), by neglecting the effect of side chain stretching one gets (see Appendix C):

$$\frac{\partial f^2}{\partial t} = \beta \dot{\gamma} \left(\frac{f^2 - 1}{2\left(f_{max}^2 - 1\right)} \sqrt{S_{11} + S_{22}} - \frac{a_2}{2}\left(f^2 - 1\right)\sqrt{\left|S_{11} - S_{22}\right|} \right) \tag{5-9}$$

where a_2 is related to the overshoot degree in transient shear viscosity measurements. Finally, Equations (5-8 and 5-9) in combination with Eq. (5-1) are used as integral constitutive equations for the MSF model.

5-3 Experimental section

5-3-1 Materials and samples preparation

The polymer used was an ethylene vinyl acetate (EVA) copolymer from DuPont: ELVAX 360 which contains 25% of vinyl acetate (MI = 2 g/min, ρ = 948 kg/m^3, T_m = 78°C). The two nano-particles used are modified clay particles (Cloisite 20A) from Southern Clay Products with an average diameter of 100-300 nm, verified recently by TEM (Mahi and Rodrigue 2012b), and modified calcium carbonate (Ultra-flex) spheres with diameters of around 70 nm from Specially Minerals Co. EVA was melt blended with different concentrations of nano-particles as described in Table 5-1 in a batch mixer (Rheocord 40 from Haake Büchler) for a total time of 15 min at a speed of 70 rpm and a temperature of 130°C. More details on sample preparation and characterization can be found elsewhere (Mahi and Rodrigue 2012b).

Table 5-1. Compositions of the nano-composites produced.

Sample nomenclature	EVA (wt. %)	Clay (wt. %)	Sample nomenclature	EVA (wt. %)	$CaCO_3$ (wt. %)
EVA 0	100	0	EVA 0	100	0
Clay 2.5	97.5	2.5	Ca 2.5	97.5	2.5
Clay 5	95.0	5.0	Ca 5	95.0	5.0
Clay 7.5	92.5	7.5	Ca 7.5	92.5	7.5
Clay 10	90.0	10	Ca 10	90.0	10

5-3-2 Transient shear tests

All the shear transient rheological tests were performed on a strain controlled TA Instruments rheometer (ARES) with a torque rebalance transducer (0.02-2000 g-cm) and a normal force transducer (2-2000 g) under a nitrogen atmosphere. All measurements were done using a 25 mm diameter parallel plate geometry with gaps between 1 and 1.5 mm. Before testing, the lack of gap effects for such gap range was verified by using different gaps between the plates (Mahi and Rodrigue 2012a). Loading history effect is a well know phenomenon in clay nano-composites (Ren and Krishnamoorti 2003, Letwimolnun et al. 2007, Mobuchon et al. 2007, Vermant et al. 2007). To verify and to control such effect on the data, time sweep tests were performed on the samples. For clay nano-composites a continuous modulus evolution with time was observed. However, after 5 minute the modulus evolution was very small. Therefore, to remove the effect of history on the results, each sample was annealed for 10 min after loading at the selected temperature before starting each test. The shear viscosity growth function $\eta^{+}(t,\dot{\gamma}$ was obtained at 110 °C with different shear rates: 0.005, 0.01, 0.03, 0.05, 0.1, 0.5 and 1 s^{-1}.

5-3-3 Transient elongational tests

Uniaxial elongation tests were performed using the SER HV-A01 model of the SER universal testing platform from Xpansion instrument (Sentmanat 2004). Rectangular samples with dimensions of 17 x 10 mm^2 and thicknesses between 0.8 and 1.0 mm were used. The tests were performed at three different temperatures (110, 150, 190 °C) and six extensional rates (0.05, 0.1, 0.3, 0.5, 1, and 5 s^{-1}). In order to determine sample dimensions at the testing temperature, PVT data for EVA were used (Wohlfarth 2001).

5-3-4 Small amplitude oscillatory shear (SAOS) data and model parameters

The data obtained from SAOS experiments with the experimental procedure was reported elsewhere (Mahi and Rodrigue 2012b). The linear data of that work is used here for the MSF theory prediction. Discrete relaxation spectra with partial moduli (g_i) and relaxation times (λ_i), was calculated by fitting SAOS data to the generalized Maxwell model (7 modes) using the RepTate software version V1.0.0.0 and the obtained parameters for all the compositions tested are presented in Table 5-2 where data fitting at T = 110 °C is shown in Figure 5-1.

5-3-5 Large amplitude oscillatory shear (LAOS)

LAOS measurements were undertaken on Scarabaeus SISV50 (Scarabaeus GmbH, Wetzlar, Germany), in grooved closed cone-cone geometry with diameter of 40 mm at 110 °C. The grooved geometry postpones the slippage at high strain amplitudes. The excitation frequency was carried out at 0.05 Hz. The raw torque data is externally digitized using a 16-bit analog-to-digital converter (ADC) card (PCI-MIO-16XE, National Instruments, Austin, TX) operating at sampling rates up to 100 kHz for one channel, or 50 kHz for two channels. Two channels enable the measurement and oversampling of shear strain and torque to further increase sensitivity. FT-rheology analysis was carried out via custom LabVIEW routines (LabVIEW 5.1, National Instruments, Austin, TX) and all measurements were taken after a periodic-steady state has been reached. A total of 10 cycles were recorded for each measurement. The setup and more detail on testing methods can be found in Wilhelm et al. (1999), van Dusschoten and Wilhelm (2001), and Wilhelm (2002).

5-3-6 Morphological characterisation

Transmission electron microscopy (TEM) images of the samples were obtained using a JEOL JEM-1230 electron microscope operated at 80 kV. All the samples were embedded in epoxy, and sections 80 nm thick were prepared by using an ultramicrotome Ultracut E from Reichert-Jung. For the analyses, micrographs were taken in various regions of each sample under different magnifications.

Table 5-2. Relaxation spectra for all the composition using a 7 mode Maxwell model with partial moduli (g_i) and relaxation times (λ_i) obtained from SAOS data of Mahi and Rodrigue (2012b).

EVA (T=190 °C)		**EVA (T=110 °C)**		**Ca 2.5 (T=110 °C)**		**Ca 5 (T=110 °C)**		**Ca 7.5 (T=110 °C)**		**Ca 10 (T=110 °C)**	
g_i (Pa)	λ_i (s)	g_i (Pa)	λ_i (s)	g_i (Pa)	λ_i (s)	g_i (Pa)	λ_i (s)	g_i (Pa)	λ_i (s)	g_i (Pa)	λ_i (s)
1.04×10^{5}	3.72×10^{-3}	2.06×10^{5}	3.79×10^{-3}	1.48×10^{5}	1.56×10^{-3}	1.47×10^{6}	9.00×10^{-5}	1.86×10^{5}	1.96×10^{-3}	1.88×10^{5}	1.77×10^{-3}
1.84×10^{4}	1.77×10^{-2}	7.37×10^{4}	2.11×10^{-2}	1.03×10^{5}	9.78×10^{-3}	1.05×10^{4}	8.24×10^{-4}	1.28×10^{5}	1.17×10^{-2}	1.36×10^{5}	1.11×10^{-2}
1.54×10^{4}	8.41×10^{-2}	4.33×10^{4}	1.17×10^{-1}	4.47×10^{4}	6.13×10^{-2}	1.62×10^{5}	7.54×10^{-3}	5.39×10^{4}	7.00×10^{-2}	5.64×10^{4}	6.98×10^{-2}
6.22×10^{3}	4.00×10^{-1}	2.18×10^{4}	6.52×10^{-1}	2.42×10^{4}	3.84×10^{-1}	6.41×10^{4}	6.90×10^{-2}	3.14×10^{4}	4.19×10^{-1}	3.24×10^{4}	4.38×10^{-1}
1.84×10^{3}	1.90×10^{0}	9.95×10^{3}	3.63×10^{0}	1.08×10^{4}	2.41×10^{0}	2.88×10^{4}	6.32×10^{-1}	1.38×10^{4}	2.50×10^{0}	1.39×10^{4}	2.75×10^{0}
1.05×10^{3}	9.05×10^{0}	3.42×10^{3}	2.02×10^{1}	3.70×10^{3}	1.51×10^{1}	9.90×10^{3}	5.79×10^{0}	5.12×10^{3}	1.50×10^{1}	5.10×10^{3}	1.72×10^{1}
7.86×10^{0}	4.30×10^{1}	9.42×10^{2}	1.12×10^{2}	9.70×10^{2}	9.44×10^{1}	2.43×10^{3}	5.30×10^{1}	1.53×10^{3}	8.96×10^{1}	1.23×10^{3}	1.08×10^{2}

EVA (T=150 °C)		**Clay 2.5 (T=110 °C)**		**Clay 5 (T=110 °C)**		**Clay 7.5 (T=110 °C)**		**Clay 10 (T=110 °C)**	
g_i (Pa)	λ_i (s)	g_i (Pa)	λ_i (s)	g_i (Pa)	λ_i (s)	g_i (Pa)	λ_i (s)	g_i (Pa)	λ_i (s)
1.51×10^{5}	3.17×10^{-3}	2.30×10^{5}	1.22×10^{-3}	3.08×10^{5}	1.21×10^{-3}	4.24×10^{5}	2.29×10^{-3}	4.53×10^{5}	3.44×10^{-4}
4.50×10^{4}	1.73×10^{-2}	1.69×10^{4}	8.53×10^{-3}	2.16×10^{5}	9.47×10^{-3}	2.43×10^{5}	1.75×10^{-2}	1.71×10^{5}	8.42×10^{-3}
2.55×10^{4}	9.48×10^{-2}	7.04×10^{4}	5.97×10^{-2}	8.72×10^{4}	7.43×10^{-2}	1.00×10^{5}	1.33×10^{-1}	8.96×10^{4}	5.90×10^{-2}
1.07×10^{4}	5.18×10^{-1}	3.45×10^{4}	4.18×10^{-1}	3.97×10^{4}	5.84×10^{-1}	4.89×10^{4}	1.02×10^{0}	4.42×10^{4}	2.44×10^{-1}
3.90×10^{3}	2.83×10^{0}	1.47×10^{3}	2.92×10^{0}	1.74×10^{4}	4.58×10^{0}	2.39×10^{4}	7.76×10^{0}	2.58×10^{4}	1.01×10^{0}
9.28×10^{2}	1.55×10^{1}	5.13×10^{3}	2.04×10^{1}	6.17×10^{3}	3.60×10^{1}	9.12×10^{3}	5.92×10^{1}	9.10×10^{3}	4.06×10^{0}
7.54×10^{1}	8.46×10^{1}	1.78×10^{3}	1.43×10^{2}	3.06×10^{3}	2.82×10^{2}	1.17×10^{4}	4.51×10^{2}	2.25×10^{4}	1.60×10^{1}

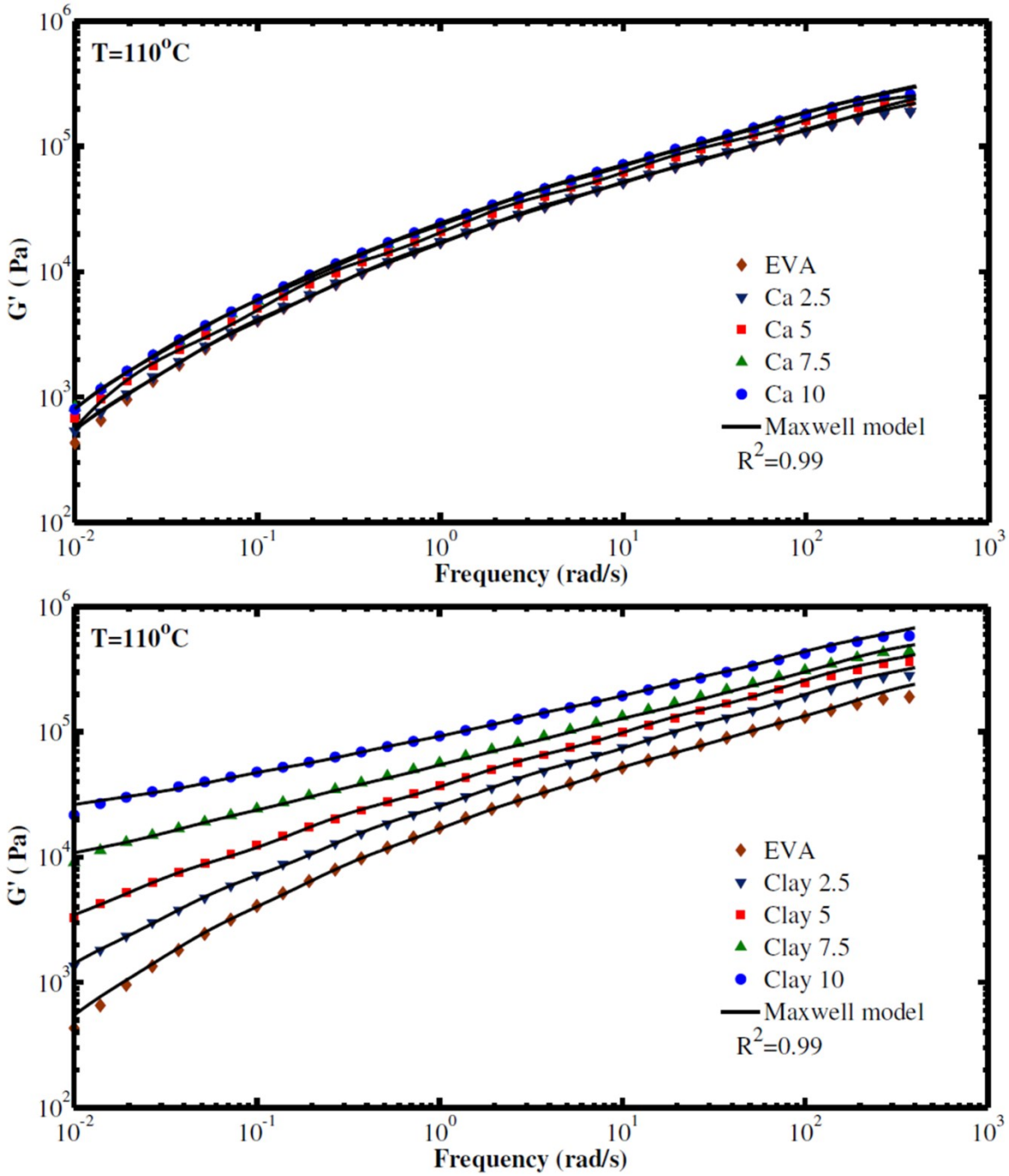

Figure 5-1: Dynamic modulus (G′) of Clay (top) and Ca (bottom) nano-composites at 110°C. Solid lines are fits to the generalized Maxwell model (seven modes) with the parameters given in Table 5-2.

5-4 Result and discussion

5-4-1 Temperature dependence of the model parameters

The relations of MSF parameters with molecular structure have been extensively discussed elsewhere (Wagner et al. 2004b, Wagner et al. 2005b, Rolón-Garrido and Wagner 2007, Rolón-Garrido et al. 2009). However, the variation of model parameters with temperature has not been studied yet. Therefore, before investigating the nano-composites, the extensional viscosities of the neat polymer at different temperatures (110, 150, and 190 °C) is discussed (see Fig.5- 2). Although some experimental scatter is observed at very short time, the model prediction for extensional viscosities is in agreement with experimentally obtained viscosities. It can be seen that while the parameter β (slope of the strain-hardening region) did not change with temperature, f^2_{max} (the amount of strain-hardening) increased with temperature (from 9 at 110 °C to 25 at 190 °C). No change in β, which is an indicator of hardening dynamic, indicates that β depends on molecular structure (Rolón-Garrido and Wagner 2007). Referring to the model description, β was introduced as the ratio of molar mass of the branched polymer to the molar mass of the backbone; obviously such parameter is not expected to change with temperature. On the other hand, f^2_{max} not only depends on molecular structure, but also on temperature. In the MSF model, f^2_{max} depends on molecular parameters like molecular weight distribution, molecular topology (linear and branching), number of branches, length of branches, and chain flexibility, (Wagner et al. 2000, Wagner et al. 2004b, Rolón-Garrido and Wagner 2007). Among these parameters, the only possible parameter that may change with temperature is chain flexibility. Considering that f^2_{max} is related to the maximum chain stretching without sliding, increasing temperature has two different effects on viscosity curves. On the one hand, by increasing temperature chain flexibility increases and polymeric coils are more open giving the chain a possibility to be more stretched. Therefore, the maximum chain stretch or the maximum energy that can be stored in a chain under deformation increases. This increased stored energy is directly related to the value of f^2_{max} (Wagner et al. 2005b) and therefore f^2_{max} also increases with temperature. On the other hand, increasing temperature would increase the viscous contribution as the system show a more liquid-like characteristics at higher

temperature. This effect can be seen in the viscosity curve where even with increased strain-hardening at higher temperatures, the amount of viscosity at any time is lower at higher temperatures. Therefore, due to the reduced viscosity at higher temperature, lower stress is needed for deformation. Because of increased flexibility, the chains can be stretched more and store more energy at higher temperatures and accordingly show higher f^2_{max}. More details on the relations between MSF model parameters and the molecular structure of polymers has been extensively discussed elsewhere (Rolón-Garrido and Wagner 2007, Rolón-Garrido et al. 2009, Wagner et al. 2005b). In the next section, the variation of such parameters with the addition of nano-particles is investigated in more details.

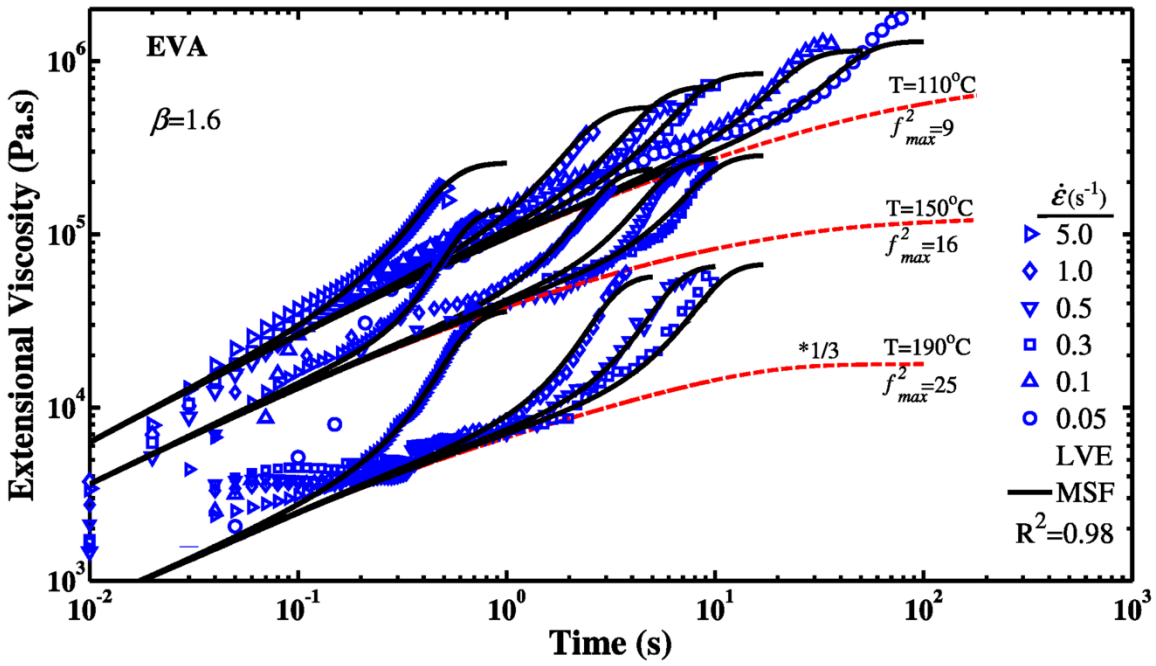

Figure 5-2: Extensional results for EVA at different temperatures. Full lines are MSF predictions and dashed lines are obtained from linear viscoelastic data. Experimental and modeling results at T=190°C are vertically multiplied by a factor 1/3 and displayed.

5-4-2 Model prediction for nano-composites

The measured and predicted extensional viscosities for different nano-composites are presented in Figure 5-3 and the values for the model parameters are presented in Table 5-3.

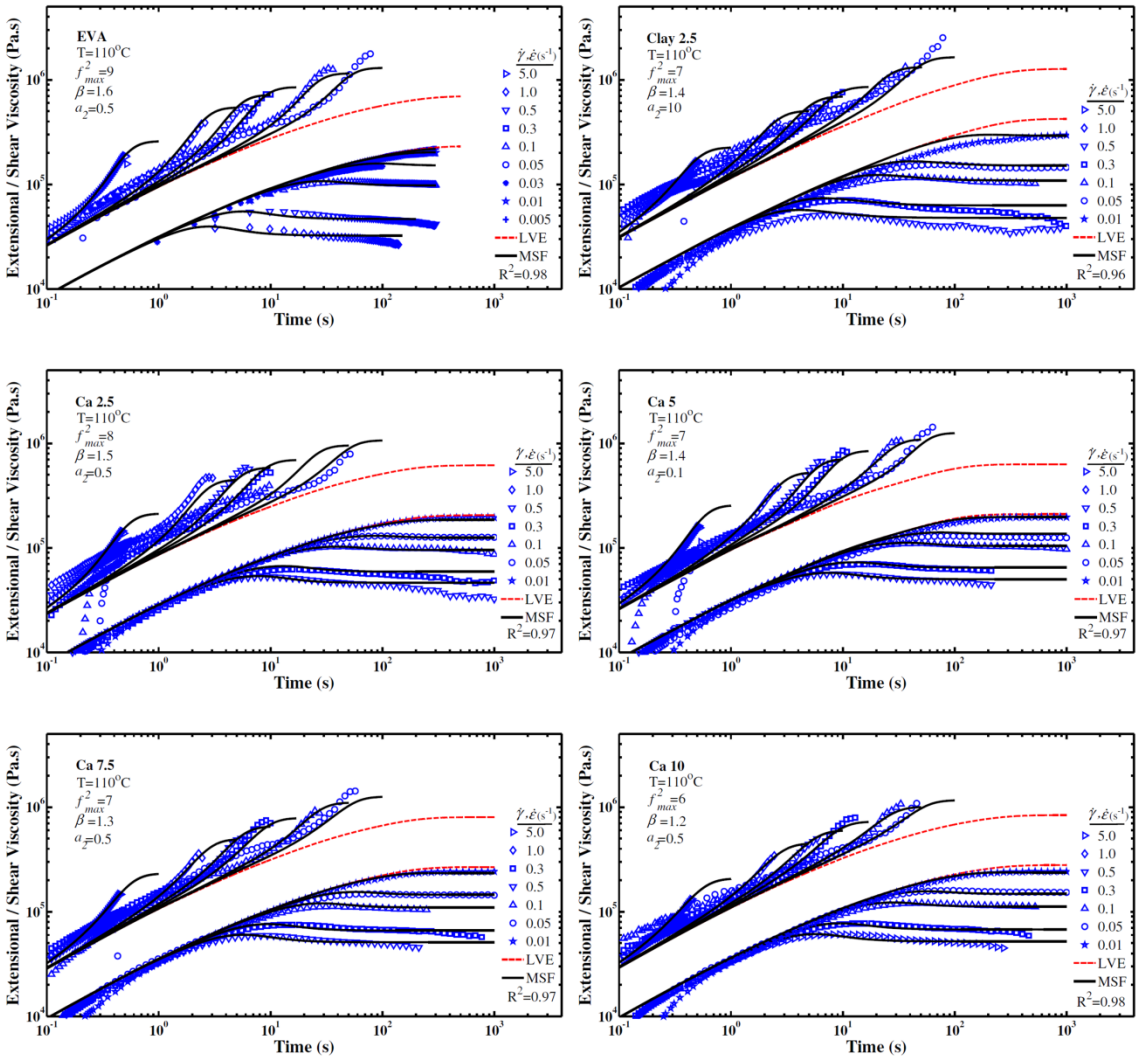

Figure 5-3: Shear and extensional viscosities of EVA, clay 2.5 and all Ca compositions at 110°C. Full lines are viscosity prediction by the MSF model. Dashed lines are obtained from linear viscoelastic data.

It should be mentioned that for clay at concentration higher than 2.5 wt. %, it was not possible to predict the extensional response from SAOS data. However, the results for these compositions are shown separately in Figure 5-4 and discussed later. The nano-particle effect on model parameters can be observed by two main features. First, the extensional parameters (f_{max} and β) decrease with increasing concentration. Second, while the shear transient parameter (overshoot related parameter a_2) did not change notably for spherical particles, it increased significantly for clay even at the lowest concentration (a_2 = 0.5 for EVA and a_2 = 10 for clay 2.5). For higher clay concentrations (> 2.5 wt. %) although due to the discrepancy between model predictions and experimental result the stress overshoot in shear transient test is not quantified here, the increased overshoot has been recently discussed elsewhere (Mahi and Rodrigue 2012b). Because of the different nature of the deformation in extension and shear, these two features are discussed separately.

Table 5-3. Values of the model parameters for EVA 0, all Ca compositions and Clay 2.5 at 110 °C.

Sample	a_2	f^2_{max}	β
EVA 0	0.5	1.6	9
Ca 2.5	0.5	1.5	8
Ca 5	0.1	1.4	7
Ca 7.5	0.5	1.3	7
Ca 10	0.5	1.2	6
Clay 2.5	10	1.4	7

The extensional response can be partly explained by polymer-particle and partly by filler-filler interactions: due to filler-polymer interaction (enthalpic), the extensibility of chains

attached to the particles surface is reduced, and also because of the contribution of the fillers (rigid particles), nano-composites show lower extensibility (lower f_{max}).

The existence of some small aggregates can also reduce the extensibility even more. Although good particle distribution was achieved in these two nano-composites, the formation of such aggregates can be seen in Figure 5-5. Despite the fact that the parameter β is expected to be constant, its decreasing value with nano-particle concentration can be related to polymer-particle interactions. It seems that due to these interactions, side chains are more confined than backbone chains by the presence of nano-particles and resulted in lower β values for the nano-composites.

To interpret the second feature regarding the stress overshoot parameter a_2 (very strong effect for clay particles and no significant effect for spherical ones), the data of a recent work was reconsidered (Mahi and Rodrigue 2012b). Based on the tube theory the stress overshoot in polymeric systems is related to large differences between twice the Rouse relaxation time ($2\tau_r$) and the longest stress relaxation time (τ_d) (Doi 1987, Inoue et al. 2002a). The first time ($2\tau_r$) is related to chain equilibrium along their contour length and the latter (τ_d) is related to orientational relaxation for stretched chains. Although the original tube theory fails to predict some non-linear phenomena like the plateau after stress overshoot and strain-hardening in extensional tests, it properly indicates the importance of these two time scales on chain dynamics. Even though recent versions of the tube theory like Doi-Edwards-Marrucci-Grizzuti (DEMG) (Marrucci and Grizzuti 1988), Mead-Larson-Doi (MLD) (Mead et al. 1998), Likhtman-Milner-McLeish (Likhtman et al. 2000) and MSF (Wagner et al. 2001) consider other relaxation mechanisms like chain stretching, primitive path fluctuations and different mechanisms for constraint release (CR), in all these models reptation (τ_d) and retraction ($2\tau_r$) are very important relaxation types. Therefore, for the sake of simplicity, a focus is made only on these two main relaxation phenomena.

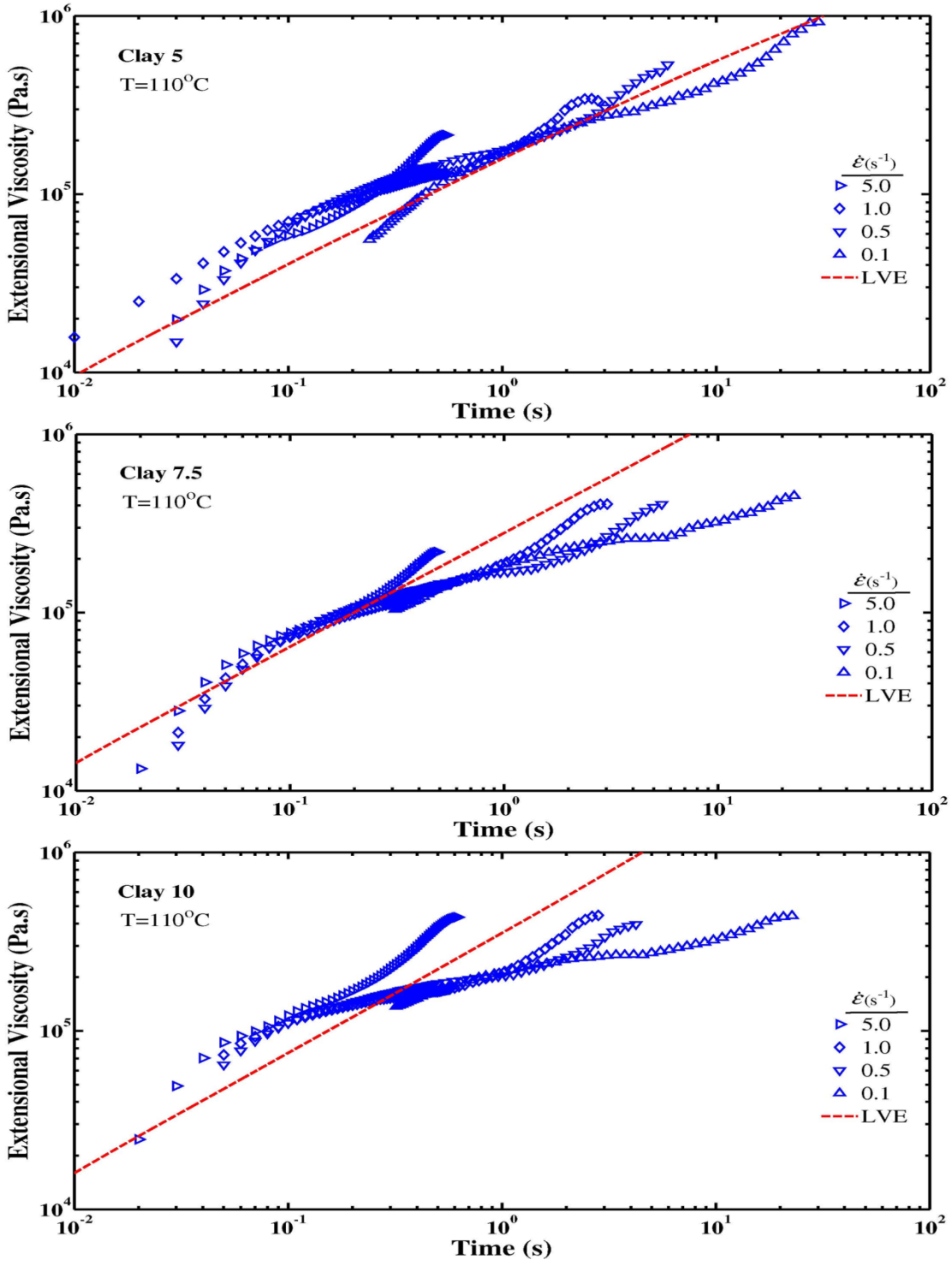

Figure 5-4: Extensional viscosity of clay nano-composites at 110°C. Dashed lines are obtained from linear viscoelastic data. For these clay concentrations (5, 7.5, and 10 wt.%), the viscosity predictions by LVE go beyond the experimentally obtained viscosities.

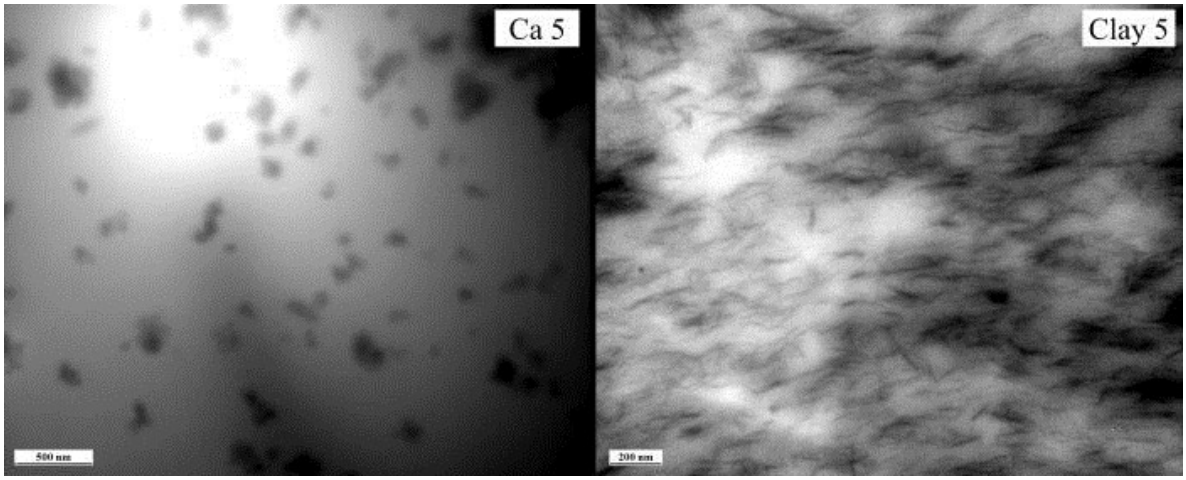

Figure 5-5: TEM images for Ca (left) and clay (right) nano-composites at 5 wt.%.

Referring to the obtained time scales for EVA (τ_d = 10.1s and τ_r = 0.4 s) (Mahi and Rodrigue 2012a, Mahi and Rodrigue 2012b), a stress overshoot in transient shear test occurs for neat EVA at shear rates $\dot{\gamma} \geq 0.1 \sim (1/\tau d)$. No significant change in the value of the overshoot parameter a_2 (see Table 5-3 and Figure 5-3) for $CaCO_3$ indicates that the difference between both time scales is not significant for spherical particles addition in the range of concentration studied (2.5-15 wt.%). The linear response of nano-composites under SAOS (Mahi and Rodrigue 2012b) showed that both Rouse and long scale dynamics (terminal zone) did not change significantly with $CaCO_3$ addition (see also Figure 5-1) and accordingly time temperature superposition (TTS) was properly applied for Ca based nano-composites (results are not shown here). On the other hand, although Rouse dynamics were not altered significantly, the slope of long dynamics region (low frequency region) which is related to reptation dynamics decreased notably with increasing clay concentration, indicating longer relaxation times (τ_d) in the presence of these particles so that it was not possible to apply TTS on clay based nano-composites. Recently, Schneider et al. (2011) used neutron spin echo (NSE) experiments and showed that the Rouse relaxation did not change with spherical silica nano-particles addition. This is not surprising since, beside energetic attraction between the nano-particle and polymer chains, the polymer-filler size

ratio has a strong impact on length scale chain dynamics (Nusser et al. 2010). Considering the short size scales involved in the Rouse region, it is less influenced by nano scale particles than the reptation region which includes longer relaxation times (the size of fillers used in this work is 70 nm for $CaCO_3$ and 100-300 nm for clay). Increased relaxation time for clay means that the difference between τ_d and $2\tau_r$ increased even more and therefore overshoot (parameter a_2 in the model) increased more significantly for platelet particles. Such a higher chain confinement for platelet particle than for spherical ones has been reported elsewhere (Chen and Evans 2006, Harton et al. 2010, Li et al. 2012) and can be related to the higher surface area-volume ratio (Li et al. 2012), as well as higher topological constrain of polymer chains by platelet particles (Harton et al. 2010). Furthermore, for platelet particles, as the concentration increases, the probability of nano-particle network formation also increases. Due to their geometry, the contact ability (a parameter which is highly geometry dependent) of platelet particles is much higher than for spherical ones. As it can be seen in Figure 5-5, while for clay nano-composites a continuous particle network is formed at 5 wt.%, for spherical particle such a continuous network is not formed. In addition, to increased non-linearity resulting from increased chain relaxation time by platelet particles, the networks created can increase the non-linearity even more (this will be validated in the next section via FT-rheology) and therefore the overshoot in shear transient test is expected to increase more strongly with clay concentration. The importance of such network structures on the amount of stress overshoot in shear transient has been extensively discussed for percolated systems (Mohraz and Solomon 2005, Letwimolnun et al. 2007, Pujari et al. 2009). The main reason for the inability of the MSF model to predict the non-linear response of clay nano-composites at concentrations higher than 2.5 wt.% (see Figure 5-4) is also attributed to the formation of such network structures. These network structures were found to dominate the linear response of polymer melts and led to an elastic response in SAOS (see Figure 5-1). Therefore the viscosity curves obtained from LVE do not reach steady state within the experimental time (Figure 5-4). Furthermore, in extension, rigid filler networks cannot be stretched and since most of the polymeric chains are shielded between these networks, consequently a discrepancy between linear data and extensional viscosities occurs (LVE data goes beyond extensional viscosities) and

consequently the model fails to predict their behavior. Recently (Mahi and Rodrigue 2012b), the analysis of the linear and non-linear shear response of nano-composites pointed 5 wt.% as a threshold concentration for the clay studied here. The modulus in the low frequency region (G_0) at 5 wt.% and above showed a temperature independence which indicates that the behavior is mainly controlled by a solid network instead of polymeric chains. This is confirmed here as for clay concentrations higher than 2.5 wt.%, the models which are purely based on chain dynamics, are unable to predict the rheological behavior as they do not consider all the mechanisms involved.

For concentrations lower than percolation, chain confinement is the main mechanism controlling the rheological response and such phenomenon can be included in the tube concept by modifying some of the engaging relaxations like changes in primitive paths and entanglement networks (Riggleman et al. 2009), change in tube length (Picu and Rakshit 2007) and change in relaxation time (Li et al. 2012). In this work, the experimental data were well predicted for composites below percolation threshold by variation of the MSF model parameters (a_2, f_{max} and β), while at higher concentrations, regardless of which mechanisms are considered for chain confinement, the tube concept is no longer able to predict the response properly due to contribution from the particle network and increased non-linearity under large deformation (either shear or extension). The increased non-linearity resulting from such network is discussed in the next section.

5-4-3 LAOS, FT-rheology analysis

In the former section, the inability of the MSF model to predict the extensional behavior of clay nano-composites at high concentration was related to the increased non-linearity due to the formation of particle networks. The percolated structure first would dominate the linear response, and second these networks can also increase the non-linearity under large deformation. These two phenomena together resulted in the inability of the MSF model to predict the response at high platelet concentration. To quantify the increased non-linearity by clay networks, the response under large amplitude oscillatory shear (LAOS) was analysed by FT-rheology. Among the many quantitative methods used for non-linear data analysing, FT-rheology is a very reliable technique due to its increased sensitivity (Wilhelm

et al. 1999) and therefore has been used extensively for different systems like polymer melts (Schlatter et al. 2005, Vittorias and Wilhelm 2007), polymer solutions (Neidhofer et al. 2003, Neidhöfer et al. 2004), and filled systems (Kallus et al. 2001). Reviews on FT-rheology can be found elsewhere (Wilhelm 2002, Hyun et al. 2011). It has been shown that the relative intensity of the third harmonic to its first one ($I_3/I_1 = I_{3/1}$) from FT-rheology quantifies the transition from linear to non-linear response (Hyun and Wilhelm 2009, Hyun et al. 2011). By definition, the value has to be zero in the linear viscoelastic domain and increases with increasing degree of non-linearity.

The I_3/I_1 ratio for EVA and different nano-composites are shown in Figure 5-6. It can be seen that for the neat polymer, the non-linearity increased (typically) with strain. For nano-composites the data reveal that while the effect of spherical particles is not considerable, non-linearity increased significantly with platelet particles addition, especially at higher clay concentration (> 2.5 wt.%). This is especially interesting because the MSF model for such clay concentrations (> 2.5 wt.%) could not predict the transient properties (shear and elongation) from SAOS data.

The increased non-linearity under LAOS (quantified by FT rheology, see Figure 5-6) for clay nano-composites is apart from non-linear viscoelasticity of neat polymer related to chain stretching under rapid deformation (e.g. strain-hardening in elongation and stress overshoot in shear). The MSF model could well predict the nonlinearity of the neat polymer under fast deformation by considering a variable tube length. It should be mentioned that the capability of MSF model to predict the nonlinear response of polymer melts under medium amplitude oscillatory shear (MAOS) (Wagner et al. 2011) and LAOS (Wapperom et al. 2005) has been shown. The increased nonlinearity (higher $I_{3/1}$) for clay at concentrations higher than percolation is related to the contribution of non-linear particle network deformation. The particle network dominates the response under SAOS (Mahi and Rodrigue 2012b) and increases the non-linearity under LAOS and therefore the MSF theory cannot predict the response properly. To improve the prediction, models considering particle-particle interactions in addition to chain dynamics must be used and FT rheology should be able to deliver the needed non-linear parameters.

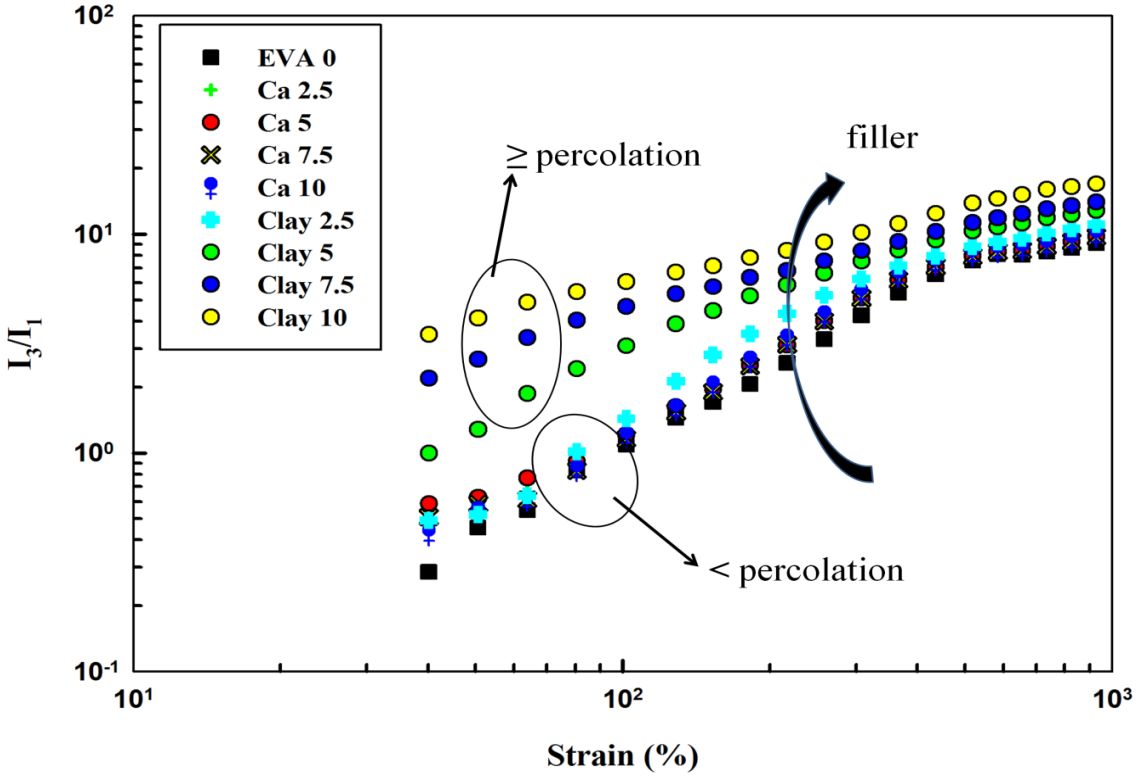

Figure 5-6: Relative intensity of the third harmonic to the first one (I_3/I_1) obtained in LAOS as a function of strain for EVA and different nano-composites at 110°C and 0.05 Hz.

5-5 Conclusion

The rheological response of two different nano-composites based on EVA containing spherical ($CaCO_3$) and platelet (clay) under transient shear and transient extension was investigated by the MSF theory. While for spherical particle, the response was well predicted, for platelet particles at concentration higher than 2.5 wt.% the model could not predict the behavior. When good agreement was observed (for all Ca concentrations and 2.5 wt.% of clay), extensional data showed that the strain-hardening parameter (f_{max}) decreased with increasing concentration which was attributed to the reduction of entropic forces. Shear transient response however showed that while the overshoot parameter (a_2)

did not change significantly for spherical particles, it increased significantly even at the lowest platelet concentration (2.5 wt.%). The results were investigated via the tube theory and differences were related to the stronger effect of platelet particles than spherical ones on chain relaxation time. The inability of the MSF theory to predict the rheological behavior of clay nano-composites for concentrations higher than 2.5 wt.% was attributed to the formation of particle networks which dominate the linear response and therefore increased significantly the non-linearity degree. This increased non-linearity was verified by using FT rheology on data obtained from LAOS experiments. It was then possible to conclude that as long as percolated structures are not formed and the response is dominated by polymer matrix, the MSF model (or any other model which is based on chain dynamics) can predict the response. On the other hand, when a percolated structure is formed, the contribution of particle-particle interactions becomes very important and it is no longer possible to rely on the model which only accounts for polymer chain dynamics.

Acknowledgements

The authors acknowledge the financial support of NSERC (Natural Sciences and Research Council of Canada) and the Quebec Ministry for Economic Development, Innovation and Exportation (MDEIE) for this work. Financial support from the Arboranano center of excellence was also appreciated. Special thanks go to Specialty Minerals Inc. for $CaCO_3$ and Southern Clay Products Inc. for nano-clay samples.

Chapter 6 General Conclusion and Recommendations

6-1 General conclusion

With the aim of understanding the relations between rheology and microstructure in polymer nano-composites, linear and non-linear viscoelastic properties of nano-composites containing cellulose, clay and $CaCO_3$ were studied. Various rheological deformations including dynamic shear (SAOS, LAOS), transient shear and extension were used. The sensitivity of each type of test to the structural variables was discussed with accompanying data from structural analysis (TEM and SEM). As a general remark, it was found that both linear and non-linear data are very important regarding the material structure and both should be considered to have a complete and accurate understanding of the involving dynamics.

Two very important parameters controlling the rheological properties were found to be: polymer-particle interactions which are related to the modification of chain dynamics at the particle surface, and particle-particle interactions which are related to the tendency of the particles to interconnect and to create local fractals and then a continuous network. Other parameters such as state of dispersion, particle size and morphology were found to be important as well, but their contribution can be investigated by considering their effect on the mentioned interactions. Combining all the rheological properties discussed in this work, the relations between morphology development and rheological properties can be investigated in three different situations as shown in figure 6-1 and explained as follows:

1- Concentration Lower than Percolation $m < m_c$

In this situation, the particle concentration is not high enough to form a continuous network. Therefore, even though the longest relaxation time (λ_{max}) is influenced by the presence of the particles, the behaviour is still dominated by polymeric chains. Consequently, the response can be explained within the framework of polymeric systems by considering some modifications. The observed rheological behaviour in this region was as follows:

In SAOS, due to the increased relaxation, the slope of G' and G'' decreased but they were not zero (no plateau yet). Moreover, even though viscosity increased with concentration, the materials showed a measurable η_0. The power-law exponent n in shear transient ($\sigma_{max} \sim \dot{\gamma}^n$) and in SAOS ($G' \sim \omega^n$) for this region is n>0.5 where n decreases with particle concentration. In extensional tests, the linear region of the viscosity curve increased according to SAOS data and strain-hardening (SH) decreased, but not significantly.

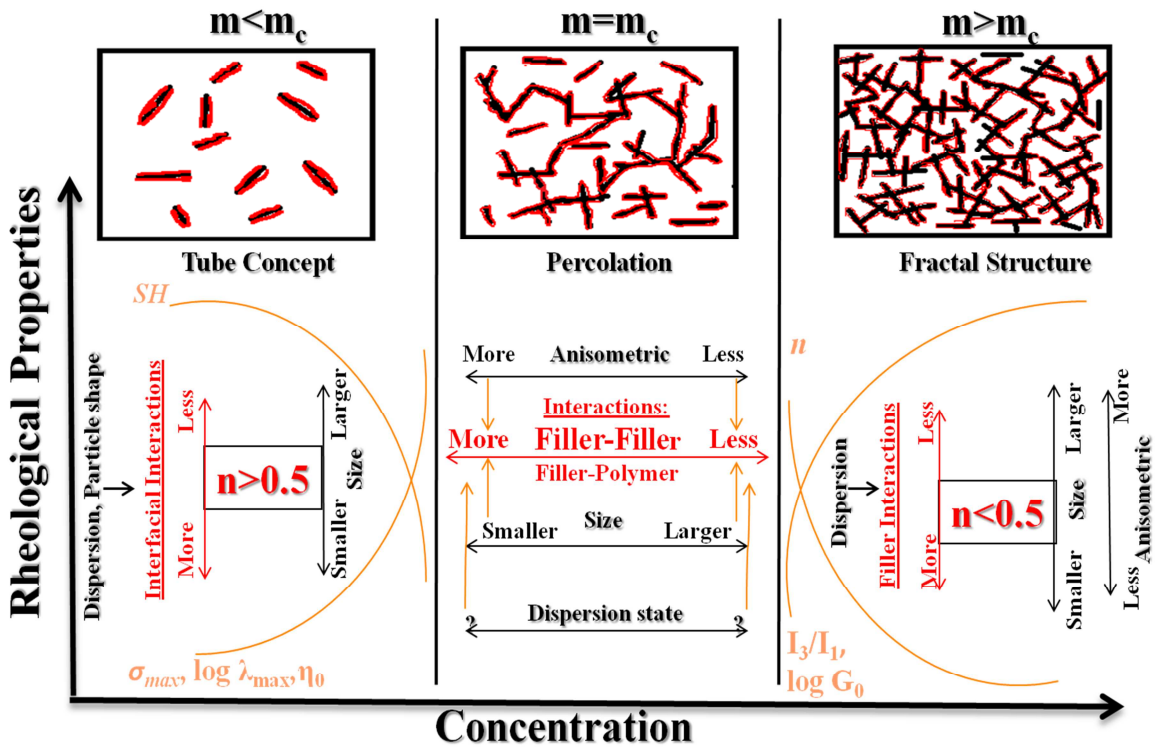

Figure 6-1: Schematic representation of the relations between rheology and microstructure in polymer nano-composites where the effect of morphology development on rheological properties at concentrations lower than percolation, at percolation, and concentration higher than percolation is shown based on the result obtained in this work. The detailed description can be found in the conclusion part.

In LAOS data, the particle effect was not important. All these effects could be explained by chain dynamics in which a model based on the tube theory (MSF) could consider the responses. The effect of different parameters in this region was found to be:

1-1- Particle-particle Interactions

Since for $m < m_c$ the particles are far from each other, the effect of particle-particle interactions is not significant in this case.

1-2- Polymer-Particle Interaction

At concentration lower than percolation the main element is chain interaction at the particle surface which can significantly modify chain dynamics. For all the rheological changes mentioned earlier for this region, the higher the interfacial interactions, the stronger is the effect of particles.

1-3- Particle Shape and Size

Particle-particle and polymer-particle interactions are the key elements in nano-composite structure according to which the effect of the other parameters can be investigated. Since at $m < m_c$, polymer-particle interactions are dominant, the effect of particle characteristics can be investigated in accordance with these interactions. The smaller the size and the more anisometric the shape is, the higher is the interfacial area and the higher is the influence.

1-4- Dispersion State

At $m < m_c$, the effect of dispersion quality can also be interpreted according to the particle-polymer interactions. By increasing the particle dispersion, the interfacial area and consequently the attraction of polymer chains to the particle surface increases, and therefore properties increase by improving dispersion quality.

2- At Percolation $m = m_c$

At percolation, the particles start to interconnect and form a particle network. The contribution of particle interactions in this situation resulted in the appearance of specific behavior. In SAOS data, this was observed in the appearance of a pseudo-plateau in modulus curves (G_0) and the vanishing of η_0 in viscosity curves. The power-law exponent of $(G' \sim \omega^n)$ was found to be $n \sim 0.5$ indicating that at percolation the behavior could be simulated by Rouse dynamic. The scaling behaviour in shear transient $(\sigma_{max} \sim \dot{\gamma}$ was also equal to $n \sim 0.5$. The reduction of strain-hardening was very significant. In LAOS measurements, a jump was observed in the nonlinear parameter I_3/I_1 at low strains which showed the sensitivity of LAOS data in detecting the percolation threshold. Generally, the property changes were so significant that the deviation between predictions of a tube based theory and experimental results started at percolation. The effects of the structural parameters in this region were found to be:

2-1- Particle-particle Interactions

The importance of these interactions comes into play at percolation. Although polymer-particle interactions are also important, the main parameter controlling the behaviour at percolation and at higher concentrations is particle-particle interactions. Therefore, the structural variables improving these interactions would result in the appearance of a lower percolation concentration.

2-2- Polymer-Particle Interaction

These interactions are still important at percolation, and can influence chain dynamic. However, their importance is not as significant as particle-particle interactions.

2-3- Particle Shape and Size

Again, the effect of these parameters can be interpreted on the basis of the above mentioned interactions. At $m = m_c$, both interactions contribute to the system response with a higher input from particle physical contacts. Hence, the particle size and shape characteristic are very important at percolation. The higher the anisometric and the lower the size is, the higher would the contacting capability be, and therefore, the lower would the percolation threshold be. Furthermore, these size characteristics influence the interfacial interactions and chain confinement which encourage more property changes.

2-4- Dispersion State

Although it was mentioned in the introduction chapter that the literature results indicate a paradox for the effect of dispersion on rheological properties, this paradox was explained reasonably and resolved when the interpretation regarding the dispersion state was done based on both types of mentioned interactions. If the particle distribution in the system produces higher particle contact to form a continuous network, the percolation will happen at lower concentration. At the same time, increasing the dispersion quality for anisometric particles would increase the number of particles for the formation of a particle network. To interpret the effect of dispersion state in percolation and higher concentrations, these two phenomena should be considered together.

3- Concentrations Higher than Percolation $m > m_c$

As the concentration increases, the particle networks become stronger and stronger until a 3D network is formed inside the polymer at very high concentrations. In this region then, the response is more solid-like and the behaviour is entirely dominated by particle network. In SAOS data, this would result in the appearance of a terminal plateau in modulus and a yield phenomenon in viscosity curve. The power-law exponent n (of $G' \sim \omega^n$) decreases and

goes to zero ($n \to 0$) as concentration increases. Although the nature of the deformation is different in transient and dynamic shear, similar scaling properties were observed for transient data ($\sigma_{max} \sim ;^{\cdot}$. The extensional properties can no longer be predicted from linear viscoelasticity and no strain-hardening is observed indicating the domination of the behaviour by particle network. In LAOS measurements, the I_3/I_1 parameter increases monotonically with concentration. Due to the contribution of particle networks, tube-based theories could not predict the response and consequently models based on particle fractals were used to understand the behavior.

3-1- Particle-particle Interactions

These interactions become more and more important knowing that the contribution of polymer-particle interactions is not considerable in comparison.

3-2- Polymer-particle Interaction

As mentioned before, although these interactions are still present at $m > m_c$, their contribution on the observed response in all rheological properties is not considerable compared to that of the particle network.

3-3- Particle Shape and Size

Since at $m > m_c$ particle-particle interactions are dominant, particle characteristics are very important. Similar to the case at percolation, in this situation also the higher the anisometry and the lower the size are, the higher would the contacting capability be, and therefore the stronger would the property improvement be.

3-4- Dispersion State

Any dispersion state which results in a better connectivity of the particle would have a higher potential for property improvement.

As a general conclusion, by using rheology, it was possible to get a more comprehensive picture for the rheological behavior of polymer nano-composites. Data agreement between different tests and deformations testified for the applicability and reliability of rheological techniques to understand the structure-property relations in complex structures.

6-2 Recommendations for Future Works

- In many part of this work the importance of particle-particle interactions on rheological properties was discussed analytically based on linear and non-linear viscoelastic properties. A next step would be to design and define models considering such interactions. At first, a modification of the tube theory to consider the dynamics resulted from these interactions must be done. Currently, models based on the tube concept only consider three main issues: deformation of chain segments, relaxation via Brownian motions, and stress for chain orientation distribution. None of these issues are related to the contribution of particle-particle interactions. Therefore additional parameters should be considered in the theory to have better prediction capability for all the mechanisms involved in nano-composites.

- Further work is needed on LAOS measurements of nano-composites since this test is related to nonlinearity as increasing the degree of non-linearity is a primary effect of nano-particles in polymeric systems. Hence, by using LAOS measurements combined with FT-rheology, a classification for nano-composites could be achieved based on the degree of nonlinearity. The evaluation of nonlinearity is very important also to develop models which can consider the role of particle-particle interactions.

- After defining models to describe the rheological properties of nano-composites, the next step can be to use these models to predict the behavior of nano-composites in any melt processing operation. As mentioned, rheology

plays a dual role in polymer nano-composites: rheology for characterization and rheology for processing. While this thesis focused on rheology- characterization issues, the next step can be to predict the flow behavior of the nano-composites from their rheological properties. In this work, two main deformations (shear and extension) were discussed. These two deformations are very common in many melt processing operations like extrusion, injection, foaming, blow molding and so on. Therefore by designing models based on rheological properties, the flow behavior of nano-composites under these common processes in plastic industry can be predicted. But, this will require the development of powerful numerical methods capable of solving the complex nonlinear rheological constitutive equations. This is a complementary work where in the one hand, processing conditions can be controlled so to obtain the desired properties, and on the other hand the nano-composite structure can be tailored to have optimized flow properties in the melt processing technique of interest.

- This work mainly considered the effect of particle characteristics on the rheological properties of nano-composites where a single polymer (EVA) was used for different compositions. However, it is obvious that polymer characteristics also have important effects on the final properties. Regarding polymer structure, three main parameters can be mentioned: chemistry (hydrophilic or hydrophobic), size (MW, Mn), and topology (branching or not). These parameters can influences strongly the flow behavior, particle dispersion, interfacial phenomena, and hence the final rheological properties. Therefore, studying the effect of polymer characteristics is also necessary to design tailor made nano-composites. Especially, the effect of branching is highlighted as such effect has not been studied yet in the field of nano-composites. Many commercial polymers are branched now, especially for applications where high extensibility is required (e.g. foaming, film blowing, fiber spinning, blow molding). Knowing the effect of branching characteristics (amount of

branching, length of branching, and the distribution of branches) on the final properties of nano-composites will provide us with the ability to design appropriate materials for these applications.

- Moreover, finding the relationships between rheological properties and other properties such as mechanical, thermal, and physical would be very interesting. Even though rheological properties are very important, sometimes for the specific end users, other properties like permeability and conductivity are more interesting and more specific. Therefore, models to interpret other properties based on rheological measurements, which are easy to perform, is a very interesting field of study. As a specific case, percolation concentration can be mentioned. For all the above mentioned properties, percolation is very important and, most of the time, an optimum condition. Because of the costs related to raw materials (nano-particles) is important, low particle concentration is desirable. However, for applications such as electrical conductivity and gas permeability, the minimum required is achieved normally at percolation. Therefore, it is important to know the percolation concentration in order to work at the optimum ratio to reduce costs. Hence, finding the relation between rheological properties and other properties as a function of concentrations (more especially at percolation) can open the doors to tailor-made design of nano-composites for different applications.

- Regarding the shape of particles, in this work only anisometric particles (platelet of clay) were compared to spherical particles and the data showed larger property changes for anisometric particles. In addition to platelet, other anisometric particle shapes could be considered such as tubular particles, cubic particles, or cone shaped particles because for anisometric particles, normally percolation happens at lower concentration compared to spherical particles. The comparison of these anisometric shapes will help to better understand the effect of particle shape for percolated systems.

- In this work, in order to validate the statements regarding the nano-composites structure, TEM and SEM images were used to complement rheological measurements. But, several other techniques could also be used for such purpose. While particle-particle contacts and the formation of particle aggregates could be observed by TEM and SEM images, polymer-particle interactions which are very important in polymer nano-composites is not possible to observe by these microscopic techniques. To study such interactions, techniques capturing chain mobility such as solid state nuclear magnetic resonance, dynamic mechanical thermal analysis, quasielastic neutron scattering, spectroscopy, and gas chromatography can be used to "see" how much chain mobility is confined by the presence of nano-particles.

- Finally, as a common suggestion, the general principles of this work can be used to study other advanced macromolecules for which understanding the structure-property relations is the objective. Polymeric foams, liquid crystal polymers and natural macromolecules such as proteins, lipids and DNA, are few examples for which a similar study can be performed to obtain relations between the structural variables and the final properties. The focus of this thesis was on nano-composites, hence only the main structural variables for these systems were considered. But important parameters for other systems and specific to those systems can be investigated using the same analysis as done in this work. By doing so, it would be possible to predict the detailed structure of complex systems by rheology, or to predict the rheological behavior of the system with knowing its structure.

References

Abbasi M, Golshan Ebrahimi N, Nadali M, Khabbazian Esfahani M (2012) Elongational viscosity of LDPE with various structures: employing a new evolution equation in MSF theory. Rheol Acta 51:163-177.

Aguayo JP, Tamaddon-Jahromi HR, Webster MF (2006) Extensional response of the pom-pom model through planar contraction flows for branched polymer melts. J Non-Newt Fluid Mech 134:105-126.

Akcora P, Kumar SK, Sakai VG, Li U, Benicewicz BC, Schadler LS (2010a) Segmental dynamics in PMMA-grafted nanoparticle composites. Macromolecules 43:8275-8281.

Akcora P, Kumar SK, Moll J, Lewis S, Schadler LS, Li Y, Benicewicz BC, Sandy A, Narayanan S, Ilavsky J, Thiyagarajan P, Colby RH, Douglas JF (2010b) Gel-like mechanical reinforcement in polymer nanocomposite melts. Macromolecules 43:1003-1010.

Akcora P, Liu H, Kumar SK, Moll J, Li Y, Benicewicz BC, Schadler LS, Acehan D, Panagiotopoulos AZ, Pryamitsyn V, Ganesan V, Ilavsky J, Thiyagarajan P, Colby RH, Douglas JF (2009) Anisotropic self-assembly of spherical polymer-grafted nanoparticles. Nature Materials 8:354-359.

Allegra G, Raos G, Vacatello M (2008) Theories and simulations of polymer-based nanocomposites: From chain statistics to reinforcement. Prog Polym Sci 33:683-731.

Anderson BJ, Zukoski CF (2010) Rheology and microstructure of polymer nanocomposite melts: variation of polymer segment-surface interaction. Langmuir 26:8709-8720.

Anderson BJ, Zukoski CF (2009) Rheology and microstructure of entangled polymer nanocomposite melts. Macromolecules 42:8370-8384.

Azizi MAS, Alloin F, Sanchez JY, Dufresne A (2004a) Cellulose nanocrystals reinforced poly(oxyethylene). Polymer 45:4149-4157.

Azizi MAS, Alloin F, Sanchez JY, El Kissi N, Dufresne A (2004b) Preparation of cellulose whiskers reinforced nanocomposites from an organic medium suspension. Macromolecules 37:1386-1393.

Batistakis C, Lyulin AV, Michels MAJ (2012) Slowing down versus acceleration in the dynamics of confined polymer films. Macromolecules 45:7282-7292.

Boek ES, Coveney PV, Lekkerkerker HNW, van der Schoot P (1997) Simulating the rheology of dense colloidal suspensions using dissipative particle dynamics. Phys Rev Lett 55:3124-3133.

Bogoslovov RB, Roland CM, Ellis AR, Randall AM, Robertson CG (2008) Effect of silica nanoparticles on the local segmental dynamics in poly(vinyl acetate). Macromolecules 41:1289-1296.

Böhning M, Goering H, Hao N, Mach R, Oleszak F, Schönhals A (2003) Molecular mobility and gas transport properties of polycarbonate-based nanocomposites. Rev Adv Mater Sci 5:155-159.

Bourbigot S, Duquesne S, Jama C (2006) Polymer nanocomposites: how to reach low flammability? Macromol Symp 233:180-190.

Capadona JR, Van den Berg O, Capadona LA, Schroeter M, Rohan SJ, Tyler DJ, Weder C (2007) Self-assembled nanofiber templates for the preparation of well-dispersed polymer nanocomposites. Nat Nanotechnol 2:765-769.

Cassagnau P (2008) Melt rheology of organoclay and fumed silica nanocomposites. Polymer 49:2183-2196.

Cassagnau P (2003) Payne effect and shear elasticity of silica-filled polymers in concentrated solutions and in molten state. Polymer 44:2455-2462.

Cassagnau P, Mélis F (2003) Non-linear viscoelastic behaviour and modulus recovery in silica filled polymers. Polymer 44:6607-6615.

Chatterjee T, Krishnamoorti R (2008) Steady shear response of carbon nanotube networks dispersed in poly(ethylene oxide). Macromolecules 41:5333–5338.

Chauve G, Heux L, Arouini R, Mazeau K (2005) Cellulose poly(ethylene-co-vinyl acetate) nanocomposites studied by molecular modeling and mechanical spectroscopy. Biomacromolecules 6:2025-2031.

Chazeau L, Cavaille JY, Perez J (2000) Plasticized PVC reinforced with cellulose whiskers. II. plastic behavior. J Polym Sci Part B Polym Phys 38:383-392.

Chen B, Evans JRG (2006) Nominal and effective volume fractions in polymer-clay nanocomposites. Macromolecules 39:1790-1796.

Chen DTN, Chen K, Hough LA, Islam MF, Yodh AG (2010) Rheology of carbon nanotube networks during gelation. Macromolecules 43:2048-2053.

Chevigny C, Dalmas F, Di Cola E, Gigmes D, Bertin D, Boué Fo, Jestin J (2010) Polymer-grafted-nanoparticles nanocomposites: dispersion, grafted chain conformation, and rheological behavior. Macromolecules 44:122-133.

Ci L, Suhr J, Pushparaj V, Zhang X, Ajayan PM (2008) Continuous carbon nanotube reinforced composites. Nano Lett 8:2762-2766.

Crosby AJ, Lee JY (2007) Polymer nanocomposites: The nano effect on mechanical properties. Polym Rev 47:217-229.

Dalmas F, Cavaille J-Y, Gauthier C, Chazeau L, Dendievel RM (2007) Viscoelastic behavior and electrical properties of flexible nanofiber filled polymer nanocomposites: influence of processing conditions. Compos Sci Technol 67:829-839.

Dalmas F, Chazeau L, Gauthier C, Cavaille J-Y, Dendievel RM (2006) Large deformation mechanical behavior of flexible nanofiber filled polymer nanocomposites. Polymer 47:2802-2812.

Dealy JM (2010) Weissenberg and Deborah numbers - Their definition and uses. Rheology Bulletin 79:14-18.

Dealy JM, Larson RG (2006) Structure and rheology of molten polymers: from structure to flow behavior and back again. Hanser Gardner Publications, Ohio.

Dealy JM, Tsang WKW (1981) Structural time dependency in the rheological behavior of molten polymers. J Appl Polym Sci 26:1149-1158.

Dealy JM, Wissbrun KF (1990) Melt rheology and its role in plastics processing: theory and applications. Van Nostrand Reinhold, New York.

Doi M, Edwards SF (1989) The theory of polymer dynamics. Clarendon Press, New York

Doi M, (1987) Molecular Theory for the Nonlinear Viscoelasticity of Polymeric Liquids Crystals. In Theory and Applications of Liquid Crystals, J. L. Ericksen & D. Kinderlehrer (Eds.) Springer New York 143-150.

Dong G, Youn J (2007) Application of reptation models to modeling of rheological behavior of polymer nanocomposites. J Cent South Univ Technol 14:50-53.

Du F, Scogna RC, Zhou W, Brand S, Fischer JE, Winey KI (2004) Nanotube networks in polymer nanocomposites: rheology and electrical conductivity. Macromolecules 37:9048-9055.

Durmus A, Kasgoz A, Macosko CW (2007) Linear low density polyethylene (LLDPE)/clay nanocomposites. Part I: structural characterization and quantifying clay dispersion by melt rheology. Polymer 48:4492-4502.

Dutta NK, Choudhury NR, Haidar B, Vidal A, Donnet JB, Delmotte L, Chezeau JM (1994) High resolution solid-state n.m.r. investigation of the filler-rubber interaction: 1. High speed H magic-angle spinning n.m.r. spectroscopy in carbon black filled styrene-butadiene rubber. Polymer 35:4293-4299.

Dykes LMC, Torkelson JM, Burghardt WR (2012) Shear-induced orientation in well-exfoliated polystyrene/clay nanocomposites. Macromolecules 45:1622-1630.

Favier V, Chanzy H, Cavaille JY (1995) Polymer nanocomposites reinforced by cellulose whiskers. Macromolecules 28:6365-6367.

Favier V, Canova GR, Shrivastavas C, Cavaille JY (1997) Mechanical percolation in cellulose whisker nanocomposites. Polym Eng Sci 37:1732-1739.

Galgali G, Ramesh C, Lele A (2001) A rheological study on the kinetics of hybrid formation in polypropylene nanocomposites. Macromolecules 34:852-858.

Giesekus H (1982) A simple constitutive equation for polymer fluids based on the concept of deformation-dependent tensorial mobility. J Non-Newt Fluid Mech 11:69-109.

Goel V, Chatterjee T, Bombalski L, Yurekli K, Matyjaszewski K, Krishnamoorti R (2006) Viscoelastic properties of silica-grafted poly(styrene–acrylonitrile) nanocomposites. J Appl Polym Sci Part B Polym Phys 44:2014-2023.

Goffin AL, Habibi Y, Raquez JM, Dubois P (2012) Polyester-grafted cellulose nanowhiskers: a new approach for tuning the microstructure of immiscible polyester blends. Appl Mater Interfaces 4:3364-3371.

Gray DG (2008) Transcrystallization of polypropylene at cellulose nanocrystal surfaces. Cellulose 15:297-301.

Greco F, D'Avino G, Maffettone PL (2007) Erratum: Stress tensor of a dilute suspension of spheres in a viscoelastic liquid. Phys Rev Lett 98:109904.

Groot RD, Agterof WGM (1995) Dynamic viscoelastic modulus of associative polymer networks: off-lattice simulations, theory and comparison to experiments. Macromolecules 28:6284-6295.

Grunert M, Winter WT (2002) Nanocomposites of cellulose acetate butyrate reinforced with cellulose nanocrystals. J Polym Environ 10:27-30.

Gupta RK, Pasanovic-Zujo V, Bhattacharya SN (2005) Shear and extensional rheology of EVA/layered silicate-nanocomposites. J Non-Newt Fluid Mech 128:116-125.

Guth E, Gold O (1938) On the hydrodynamical theory of the viscosity of suspensions. Phys Rev 53:322.

Habibi Y, Dufresne A (2009) Highly filled bionanocomposites from functionalized polysaccharide nanocrystals. Biomacromolecules 9:1974-1980.

Habibi Y, Goffin AL, Schiltz N, Duquesne E, Duboisand P, Dufresne A (2008) Bionanocomposites based on poly(ε-caprolactone)-grafted cellulose nanocrystals by ring-opening polymerization. J Mater Chem 41:5002-5010.

Habibi Y, Lucia AL, Orlando JR (2010) Cellulose nanocrystals: chemistry, self-assembly, and applications. Chem Rev 110:3479-3500.

Han Z, Fina A (2011) Thermal conductivity of carbon nanotubes and their polymer nanocomposites: A review. Prog Polym Sci 36:914-944.

Handge UA, Pötschke P (2007) Deformation and orientation during shear and elongation of a polycarbonate/carbon nanotubes composite in the melt. Rheol Acta 46:889-898.

Harton SE, Kumar SK, Yang H, Koga T, Hicks K, Lee H, Mijovic J, Liu M, Vallery RS, Gidley DW (2010) Immobilized polymer layers on spherical nanoparticles. Macromolecules 43:3415-3421.

Heinrich G, Klüppel M (2002) Recent advances in the theory of filler networking in elastomers. Adv Polym Sci 160:1-44.

Hobbie, E (2010) Shear rheology of carbon nanotube suspensions. Rheol Acta 49:323-334.

Hornsby PR (1999) Rheology, compounding and processing of filled thermoplastics. Adv Polym Sci 139:155-217.

Huang YY, Ahir SV, Terentjev EM (2006) Dispersion rheology of carbon nanotubes in a polymer matrix. Phys Rev B Cond Matter 73:1254221-1254229.

Huber G (2002) On the mechanism of hydrodynamic reinforcement in elastic composites. Macromolecules 35:9204-9210.

Huh J, Balazs AC (2000) Behavior of confined telechelic chains under shear. J Chem Phys 113:2025-2031.

Hussain F, Hojjati M, Okamoto M, Gorga RE (2006) Review article: polymer-matrix nanocomposites, processing, manufacturing, and application: An Overview. J Compos Mater 40:1511-1575.

Hyun K, Lim H, Ahn K (2012) Nonlinear response of polypropylene (PP)/Clay nanocomposites under dynamic oscillatory shear flow. Korea-Aust Rheol J 24:113-120.

Hyun, K., M. Wilhelm (2009) Establishing a new mechanical nonlinear coefficient Q from FT-rheology: first investigation of entangled linear and comb polymer model systems. Macromolecules 42, 411-422.

Hyun K, Wilhelm M, Klein CO, Cho KS, Nam JG, Ahn KH, Lee SJ, Ewoldt RH, McKinley GH (2011) A review of nonlinear oscillatory shear tests: analysis and application of large amplitude oscillatory shear (LAOS). Polymer 36:1697-1753.

Inoue T, Yamashita Y, Osaki K (2002a) Viscoelasticity of an entangled polymer solution with special attention on a characteristic time for nonlinear behavior. Macromolecules 35:1770-1775.

Inoue T, Uematsu T, Yamashita Y, Osaki K (2002b) Significance of the longest rouse relaxation time in the stress relaxation process at large deformation of entangled polymer solutions. Macromolecules 35:4718-4724.

Introzzi L, Blomfeldt TOJ, Trabattoni S, Tavazzi S, Santo N, Schiraldi A, Piergiovanni L, Farris S (2012) Ultrasound-assisted pullulan/montmorillonite bionanocomposite coating with high oxygen barrier properties. Langmuir 28:11206-11214.

Isichenko MB (1992) Percolation, statistical topography, and transport in random media. Rev Mod Phys 64:961-1043.

Jancar J (2009) Use of reptation dynamics in modelling molecular interphase in polymer nano-composite. In: R Pyrz JC Rauhe (Ed), IUTAM Symposium on Modelling Nanomaterials and Nanosystems. Springer Netherlands, pp. 293-301.

Jancar J, Douglas JF, Starr FW, Kumar SK, Cassagnau P, Lesser AJ, Sternstein SS, Buehler MJ (2010) Current issues in research on structure-property relationships in polymer nanocomposites. Polymer 51:3321-3343.

Jouault N, Vallat P, Dalmas F, Said Sr, Jestin J, Bouè Fo (2009) Well-dispersed fractal aggregates as filler in polymer-silica nanocomposites: long-range effects in rheology. Macromolecules 42:2031-2040.

Kabanemi KK, Hétu J-F (2013) Reptation model for the dynamics and rheology of particle reinforced polymer chains. In Modeling and Prediction of Polymer Nanocomposite Properties. Wiley-VCH Verlag GmbH & Co., pp. 63-94.

Kagarise C, Koelling K, Wang Y, Bechtel S (2008) A unified model for polystyrene-nanorod and polystyrene-nanoplatelet melt composites. Rheol Acta 47:1061-1076.

Kagarise C, Xua J, Wang Y, Mahboob M, Koelling KW, Bechtel SE (2010) Transient shear rheology of carbon nanofiber/polystyrene melt composites. J Non-Newt Fluid Mech 165:98-109.

Kairn, T, Daivis PJ, Ivanov I, Bhattacharya SN (2005) Molecular-dynamics simulation of model polymer nanocomposite rheology and comparison with experiment. J Chem Phys 123:1949051-1949057.

Kalfus J, Jancar J (2007) Immobilization of polyvinylacetate macromolecules on hydroxyapatite nanoparticles. Polymer 48:3935-3937.

Kalfus J, Jancar J (2008) Reinforcing mechanisms in amorphous polymer nanocomposites. Compos Sci Technol 68:3444-3447.

Kallus S, Willenbacher N, Kirsch S, Distler D, Neidhöfer T, Wilhelm M, Spiess HW (2001) Characterization of polymer dispersions by fourier transform rheology. Rheol Acta 40:552-559.

Khatua BB, Lee DJ, Kim HY, Kim JK (2004) Effect of organoclay platelets on morphology of nylon-6 and poly(ethylene-ran-propylene) rubber blends. Macromolecules 37:2454-2459.

Kim H, Abdala AA, Macosko CW (2010) Graphene/polymer nanocomposites. Macromolecules 43:6515-6530.

Kim H, Macosko CW (2008) Morphology and properties of polyester/exfoliated graphite nanocomposites. Macromolecules 41:3317-3327.

Kloser E, Gray DG (2010) Surface grafting of cellulose nanocrystals with poly(ethylene oxide) in aqueous media. Langmuir 26:13450-13456.

Knauert ST, Douglas JF, Starr FW (2007) The effect of nanoparticle shape on polymer-nanocomposite rheology and tensile strength. J Polym Sci, Part B: Polym Phys 45:1882-1897.

Koo CM, Ham HT, Kim SO, Wang KH, Chung IJ, Kim D-C, Zin W-C (2002) Morphology evolution and anisotropic phase formation of the maleated polyethylene-layered silicate nanocomposites. Macromolecules 35:5116-5122.

Koo JH (2006) Polymer nanocomposites - processing, characterization, and applications. McGraw-Hill, New York.

Kota AK, Cipriano BH, Duesterberg MK, Gershon AL, Powell D, Raghavan SR, Bruck HA (2007) Electrical and rheological percolation in polystyrene/MWCNT nanocomposites. Macromolecules 40:7400-7406.

Krishnamoorti R, Chatterjee T (2011) Rheology and Processing of Polymer Nanocomposites. In Applied Polymer Rheology, John Wiley & Sons, Inc. Hoboken, 153-177.

Krishnamoorti R, Giannelis EP (1997) Rheology of end-tethered polymer layered silicate nanocomposites. Macromolecules 30:4097-4102.

Krishnamoorti R, Yurekli K (2001) Rheology of polymer layered silicate nanocomposites. Curr Opin Colloid Interf Sci 6:464-470.

Lee KM, Han CD (2003) Rheology of organoclay nanocomposites: effects of polymer matrix/organoclay compatibility and the gallery distance of organoclay. Macromolecules 36:7165-7178.

Lee SH, Kim SY, Youn JR (2009) Rheological behavior and theoretical modeling of uniaxial elongational flow properties of polypropylene/layered silicate nanocomposites. Polym. Compos 30:1426-1436.

Letwimolnun W, Vergnes B, Ausias G, Carreau PJ (2007) Stress overshoots of organoclay nanocomposites in transient shear flow. J Non-Newt Fluid Mech 141:167-179.

Li Y, Kröger M, Liu WK (2012) Nanoparticle geometrical effect on structure, dynamics and anisotropic viscosity of polyethylene nanocomposites. Macromolecules 45:2099-2112.

Likhtman, AE, Milner ST, McLeish TCB (2000) Microscopic theory for the fast flow of polymer melts. Phys Rev Lett 85:4550-4553.

Lim HT, Ahn KH, Hong JS, Hyun K (2013) Nonlinear viscoelasticity of polymer nanocomposites under large amplitude oscillatory shear flow. J Rheol 57:767-789.

Lin CW, Huang LC, Ma CCM, Yang ACM, Lin CJ, Lin LJ (2008) Nanoplastic flows of glassy polymer chains interacting with multiwalled carbon nanotubes in nanocomposites. Macromolecules 41:4978-4988.

Litvinov VM, Spiess HW (1991) 2H NMR study of molecular motions in polydimethylsiloxane and its mixtures with aerosils. Makromol Chem 192:3005-3019.

Liu H, Liu H, Yao F, Wu Q (2010) Fabrication and properties of transparent polymethylmethacrylate/cellulose. Biores Technol 101:5685-5692.

Ljungberg N, Bonini C, Bortlussi F, Boisson C, Heuex L, Cavaille JY (2005) New nanocomposite materials reinforced with cellulose whiskers in atactic polypropylene: effect of surface and dispersion characteristics. Biomacromolecules 6:2732-2739.

Ma P-C, Liu M-Y, Zhang H, Wang S-Q, Wang R, Wang K, Wong Y-K, Tang B-Z, Hong S-H, Paik K-W, Kim J-K (2009) Enhanced electrical conductivity of nanocomposites containing hybrid fillers of carbon nanotubes and carbon Black. ACS Appl Mater Interfaces 1:1090-1096.

Mahi H, Rodrigue D (2012a) Linear and non-linear viscoelastic properties of ethylene vinyl acetate/nanocrystalline cellulose composites. Rheol Acta 51:127-142.

Mahi H, Rodrigue D (2012b) Relationships between linear and nonlinear shear response of polymer nanocomposites. Rheol Acta 51:991-1005.

Manitiu M, Horsch S, Gulari E, Kannan RM (2009) Role of polymer-clay interactions and nanoclay dispersion on the viscoelastic response of supercritical CO_2 dispersed polyvinylmethylether (PVME)-Clay nanocomposites. Polymer 50:3786-3796.

Mansoutre S, Colombet P, Van Damme H (1999) Water retention and granular rheological behavior of fresh C_3S paste as a function of concentration. Cement Concrete Rec 29:1441-1453.

Marcovich NE, Auad ML, Bellesi NE, Nutt S, Aranguren MI (2006) Cellulose micro/nanocrystals reinforced polyurethane. J Mater Res 21:870-881.

Marrucci G, Ianniruberto G (2004) Interchain pressure effect in extensional flows of entangled polymer melts. Macromolecules 37:3934-3942.

Marrucci, G., N. Grizzuti (1988) Fast flow of concentrated polymers: predictions of the tube model on chain stretching. Gazz Chim Ital 118:179-185.

Mathew AP, Chakraborty A, Oksman K, Sain M (2006) The Structure and Mechanical Properties of Cellulose Nanocomposites Prepared by Twin Screw Extrusion. In Cellulose Nanocomposites, American Chemical Society 114-131.

McLeish TCB, Larson RG (1998) Molecular constitutive equations for a class of branched polymers: the pom-pom polymer. J Rheol 42:81-110.

Matteucci S, Kusuma VA, Swinnea S, Freeman BD (2008) Gas permeability, solubility and diffusivity in 1,2-polybutadiene containing brookite nanoparticles. Polymer 49:757-773.

Mead, DW, Larson RG, Doi M (1998) A molecular theory for fast flows of entangled polymers. Macromolecules 31:7895-7914.

Menezes JD, Siqueira A, Curvelo G, Dufresne A (2009) Extrusion and characterization of functionalized cellulose whiskers. Polymer 50:4552-4563.

Merabia S, Sotta P, Long DR (2008) A microscopic model for the reinforcement and the nonlinear behavior of filled elastomers and thermoplastic elastomers (Payne and Mullins effects). Macromolecules 41:8252-8266.

Mi Y-n, Liang G, Gu A, Zhao F, Yuan L (2013) Thermally conductive aluminum nitride-multiwalled carbon nanotube/cyanate ester composites with high flame retardancy and low dielectric loss. Ind Eng Chem Res 52:3342-3353.

Mobuchon C, Carreau P, Heuzey M-C (2007) Effect of flow history on the structure of a non-polar polymer/clay nanocomposite model system. Rheol Acta 46:1045-1056.

Mobuchon C, Carreau PJ, Heuzey M-C (2009) Structural analysis of non-aqueous layered silicate suspensions subjected to shear flow. J Rheol 53:1025-1048.

Mohraz A, Solomon MJ (2005) Orientation and rupture of fractal colloidal gels during start-up of steady shear flow. J Rheol 49:657-681.

Moniruzzaman M, Winey KI (2006) Polymer nanocomposites containing carbon nanotubes. Macromolecules 39:5194-5205.

Morgan AB (2006) Flame retarded polymer layered silicate nanocomposites: a review of commercial and open literature systems. Polym Adv Technol 17:206-217.

Morin A, Dufresne A (2002) Nanocomposites of chitin whiskers from riftia tubes and poly(caprolactone). Macromolecules 35:2190-2199.

Mu M, Winey KI (2007) Improved load transfer in nanotube/polymer composites with increased polymer molecular weight. J Phys Chem C 111:17923-17927.

Muenstedt H, Katsikis N, Kaschta J (2008) Rheological properties of poly(methyl methacrylate)/nanoclay composites as investigated by creep recovery in shear. Macromolecules 41:9777-9783.

Muthukumar M (1989) Screening effect on viscoelasticity near the gel point. Macromolecules 22:4656-4658.

Naderi G, Lafleur PG, Dubois C (2007) Dynamically vulcanized nanocomposite thermoplastic elastomers based on EPDM/PP (rheology & morphology). Inter Polym Proc 22:284-292.

Nagase Y, Okada K (1986) Heterogeneous behavior after yielding of solid suspensions. J Rheol 30:1123-1143.

Nair KG, Dufresne A, Gandini A, Belgacem MN (2003) Crab shell chitin whiskers reinforced natural rubber nanocomposites. 3. Effect of chemical modification of chitin whiskers. Biomacromolecules 4:1835-1842.

Nan C-W, Shen Y, Ma J (2010) Physical properties of composites near percolation. Ann Rev Mater Res 40:131-151.

Neidhöfer T, Sioula S, Hadjichristidis N, Wilhelm M (2004) Distinguishing linear from star-branched polystyrene solutions with fourier-transform rheology. Macromol Rapid Commun 25:1921-1926.

Neidhöfer T, Wilhelm M, Debbaut B (2003) Fourier-transform rheology experiments and finite-element simulations on linear polystyrene solutions. J Rheol 47:1351-1371.

Nusser K, Neueder S, Schneider GJ, Meyer M, Pyckhout-Hintzen W, Willner L, Radulescu A, Richter D (2010) Conformations of silica−Poly(ethylene−propylene) nanocomposites. Macromolecules 43:9837-9847.

Nusser K, Schneider GJ, Richter D (2011) Microscopic origin of the terminal relaxation time in polymer nanocomposites: an experimental precedent. Soft Matter 7:7988-7991.

Odegard GM, Pipes RB, Hubert P (2004) Comparison of two models of SWCN polymer composites. Compos Sci Technol 64:1011-1020.

Ojijo V, Sinha Ray S, Sadiku R (2012) Effect of nanoclay loading on the thermal and mechanical properties of biodegradable polylactide/poly[(butylene succinate)-co-adipate] blend composites. Appl Mater Interfaces 4:2395-2405.

Okamoto M, Nam PH, Maiti P, Kotaka T, Hasegawa N, Usuki A (2001a) A house of cards structure in polypropylene/clay nanocomposites under elongational flow. Nano Lett 1:295-298.

Okamoto M, Nam PH, Maiti P, Kotaka T, Nakayama T, Takada M, Ohshima M, Usuki A, Hasegawa N, Okamoto H (2001b) Biaxial flow-induced alignment of silicate layers in polypropylene/clay nanocomposite foam. Nano Lett 1:503-505.

Osaki K, Inoue T, Uematsu T, Yamashita Y (2001) Evaluation methods of the longest relaxation time of an entangled polymer in semidilute solution. J Polym Sci Part B Polym Phys 39:1704-1712.

Palermo E, Si M, Occhiogrosso R, Berndt C, Rudomen G, Rafailovich M (2001) Effects of supercritical carbon dioxide on phase homogeneity, morphology, and mechanical properties of poly(styrene-blend-ethylene-stat-vinyl acetate). Macromolecules 38:9180-9186.

Park J, Kim J, Kim D, Ahn K, Lee S, Cho K (2006) Rheological behavior of polymer/layered silicate nanocomposites under uniaxial extensional flow. Macromolecular Research 14:318-323.

Pattamaprom C, Driscroll JJ, Larson RG (2000) Nonlinear viscoelastic predictions of uniaxial-extensional viscosities of entangled polymers. Macromol Symp 158:1-14.

Paul DR, Robeson LM (2008) Polymer nanotechnology: nanocomposites. Polymer 49:3187-3204.

Pearson D, Herbolzheimer E, Grizzuti N, Marrucci G (1991) Transient behavior of entangled polymers at high shear rates. J Polym Sci Part B: Polym Phys 29:1589-1597.

Pearson DS, Kiss AD, Fetters LJ, Doi M (1989) Flow-induced birefringence of concentrated polyisoprene solutions. J Rheol 33:517-535.

Picu RC, Rakshit A (2007) Dynamics of free chains in polymer nanocomposites. J Chem Phys 126:144909.

Pluta M, Jeszka JK, Boiteux G (2007) Polylactide/montmorillonite nanocomposites: structure, dielectric, viscoelastic and thermal properties. Eur Polym J 43:2819-2835.

Prince E, Rouse J (1953) A theory of the linear viscoelastic properties of dilute solutions of coiling polymers. J Chem Phys 21:1272-1280.

Pujari S, Rahatekar SS, Gilman JW, Koziol KK, Windle AH, Burghardt WR (2009) Orientation dynamics in multiwalled carbon nanotube dispersions under shear flow. J Chem Phys 130:214903.

Rajabian M, Naderi G, Carreau PJ, Dubois C (2010) Flow-induced particle orientation and rheological properties of suspensions of organoclays in thermoplastic resins. J Polym Sci, Part B: Polym Phys 48:2003-2011.

Ren J, Krishnamoorti R (2003) Nonlinear viscoelastic properties of layered-silicate-based intercalated nanocomposites. Macromolecules 36:4443-4451.

Ren J, Silva AS, Krishnamoorti R (2000) Linear viscoelasticity of disordered polystyrene-polyisoprene block copolymer based layered-silicate nanocomposites. Macromolecules 33:3739-3746.

Riggleman RA, Toepperwein G, Papakonstantopoulos GJ, Barrat J-L, Pablo JJd (2009) Entanglement network in nanoparticle reinforced polymers. J Chem Phys 130:244903.

Robertson CG, Roland CB (2002) Nonlinear rheology of hyperbranched polyisobutylene. J Rheol 46: 307-320.

Robertson CG, Roland CM (2008) Glass transition and interfacial segmental dynamics in polymer-particle composites. Rubber Chem Technol 81:506-522.

Roland CM, Archer LA, Mott PH, Sanchez-Reyes J (2004) Determining rouse relaxation times from the dynamic modulus of entangled polymers. J Rheol 48:395-403.

Rolón-Garrido V, Wagner M (2007) the MSF model: relation of nonlinear parameters to molecular structure of long-chain branched polymer melts. Rheol Acta 46:583-593

Rolón-Garrido V, Pivokonsky R, Filip P, Zatloukal M, Wagner M (2009) Modelling elongational and shear rheology of two LDPE melts. Rheol Acta 48:691-697.

Rouse PE (1953) A Theory of the linear viscoelastic properties of dilute solutions of coiling polymers. J. Chem. Phys 21:1272-1280.

Rueb CJ, Zukoski CF (1997) Viscoelastic properties of colloidal gels. J Rheol 41:197-218.

Sarvestani AS (2008) Modeling the solid-like behavior of entangled polymer nanocomposites at low frequency regimes. Eur Polym J 44:263-269.

Schlatter G, Fleury G, Muller R (2005) Fourier transform rheology of branched polyethylene: experiments and models for assessing the macromolecular architecture. Macromolecules 38:6492-6503.

Schneider, GJ, Nusser K, Willner L, Falus P, Richter D (2011) Dynamics of entangled chains in polymer nanocomposites. Macromolecules 44:5857-5860.

Schroers M, Kokil A, Weder C (2004) Solid polymer electrolytes based on nanocomposites of ethylene oxide–epichlorohydrin copolymers and cellulose whiskers. J Appl Polym Sci 93:2883-2888.

Sentmanat M (2004) Miniature universal testing platform: from extensional melt rheology to solid-state deformation behavior. Rheol Acta 43:657-669.

Shih W-H, Shih WY, Kim S-I, Liu J, Aksay IA (1990) Scaling behavior of the elastic properties of colloidal gels. Phys Rev A 42:4772-4779.

Shweta AP, Simonsen J, Lombardi J (2008) Poly(vinyl alcohol)/cellulose nanocrystal barrier membranes. J Membr Sci 320:248-258.

Siqueira G, Bras J, Dufresne A (2009) Cellulose whiskers versus microfibrils: influence of the nature of the nanoparticle and its surface functionalization on the thermal and mechanical properties of nanocomposites. Biomacromolecules 10:425-432.

Sinha Ray S, Okamoto M (2003) Polymer/layered silicate nanocomposites: a review from preparation to processing. Prog Polym Sci 28:1539-1641.

Smith GD, Bedrov D, Li L, Byutner O (2002) A molecular dynamics simulation study of the viscoelastic properties of polymer nanocomposites. J Chem Phys 117:9478-9489.

Solomon MJ, Almusallam AS, Seefeldt KF, Somwangthanaroj A, Varadan P (2001) Rheology of polypropylene/clay hybrid materials. Macromolecules 34:1864-1872.

Song Y, Zheng Q (2010) Linear viscoelasticity of polymer melts filled with nano-sized fillers. Polymer 51:3262-3268.

Starr FW, Douglas JF, Glotzer SC (2003) Origin of particle clustering in a simulated polymer nanocomposite and its impact on rheology. J Chem Phys 119:1777-1788.

Sternstein SS, Zhu A-J (2002) Reinforcement mechanism of nanofilled polymer melts as elucidated by nonlinear viscoelastic behavior. Macromolecules 35:7262-7273.

Stratton RA, Butcher AF (1973) Stress relaxation upon cessation of steady flow and the overshoot effect of polymer solutions. J Appl Polym Sci 11:1747-1758.

Takahashi S, Goldberg HA, Feeney CA, Karim DP, Farrell M, O'Leary K, Paul DR (2006) Gas barrier properties of butyl rubber/vermiculite nanocomposite coatings. Polymer 47:3083-3093.

Tandon GP, Weng GJ (1984) The effect of aspect ratio of inclusions on the elastic properties of unidirectionally aligned composites. Polym Compos 5:327-333.

Tucker III CL, Liang E (1999) Stiffness predictions for unidirectional short-fiber composites: Review and evaluation. Compos Sci Technol 59:655-671.

Twite-Kabamba E, Mechraoui A, Rodrigue D (2009) Rheological properties of polypropylene/hemp fibre composites. Polym Compos 30:1401-1407.

Twite-Kabamba E, Rodrigue D (2008) The effect of recycling on LDPE foamability: elongational rheology. Polym Eng Sci 48:11-18.

Utracki LA, Jorgensen JL (2002) Dynamic melt flow of nanocomposites based on poly-ε-caprolactam. Rheol Acta 41:397-407.

Utracki LA, Sepehr MM, Carreau PJ (2010) Rheology of Polymers with Nanofillers. In: LAJA Utracki (ed), Polymer Physics:from suspensions to nanocomposites and beyond. John Wiley & Sons, Inc., Hoboken, pp. 639-708.

Van Dusschoten D, Wilhelm M (2001) Increased torque transducer sensitivity via oversampling. Rheol Acta 40:395-399.

Vermant J, Ceccia S, Dolgovskij MK, Maffettone PL, Macosko CW (2007) Quantifying dispersion of layered nanocomposites via melt rheology. J Rheol 51:429-450.

Via, MD, Morrison FA, King JA, Caspary JA, Mills OP, Bogucki GR (2011) Comparison of rheological properties of carbon nanotube/polycarbonate and carbon black/polycarbonate composites. J Appl Polym Sci 121:1040-1051.

Vittorias I, Wilhelm M (2007) Application of FT rheology to industrial linear and branched polyethylene blends. Macromol Mater Eng 292:935-948.

Wagener R, Reisinger TJG (2003) A rheological method to compare the degree of exfoliation of nanocomposites. Polymer 44:7513-7518.

Wagner M, Kheirandish S, Stange J, Münstedt H (2006) Modeling elongational viscosity of blends of linear and long-chain branched polypropylenes. Rheol Acta 46:211-221.

Wagner MH, Bastian H, Hachmann P, Meissner J, Kurzbeck S, Münstedt H, Langouche F (2000) The strain-hardening behaviour of linear and long-chain-branched polyolefin melts in extensional flows. Rheol Acta 39:97-109.

Wagner, M. H, V. Rolón-Garrido (2010) The interchain pressure effect in shear rheology. Rheol Acta 49:459-471.

Wagner, MH, Hepperle J, Munstedt H (2004a) Relating rheology and molecular structure of model branched polystyrene melts by molecular stress function theory. J Rheol 48:489-503.

Wagner, MH, Kheirandish S, Hassager O (2005a) Quantitative prediction of transient and steady-state elongational viscosity of nearly monodisperse polystyrene melts. J Rheol 49:1317-1327.

Wagner MH, Kheirandish S, Koyama K, Nishioka A, Minegishi A, Takahashi T (2005b) Modeling strain hardening of polydisperse polystyrene melts by molecular stress function theory. Rheol Acta 44:235-243.

Wagner MH, Kheirandish S, Yamaguchi M (2004b) Quantitative analysis of melt elongational behavior of LLDPE/LDPE blends. Rheol Acta 44:198-218.

Wagner MH, Rolon-Garrido VH, Hyun K, Wilhelm M (2011) Analysis of medium amplitude oscillatory shear data of entangled linear and model comb polymers. J Rheol 55:495-516.

Wagner MH, Rubio P, Bastian H (2001) The molecular stress function model for polydisperse polymer melts with dissipative convective constraint release. J Rheol 45:1387-1412.

Wagner MH, Schaeffer J (1993) Rubbers and polymer melts: universal aspects of nonlinear stress-strain relations. J Rheol 37:643-661.

Wagner MH, Yamaguchi M, Takahashi M (2003) Quantitative assessment of strain hardening of low-density polyethylene melts by the molecular stress function model. J Rheol 47:779-793.

Wang Y, Xu J, Bechtel ES, Koelling KW (2006) Melt shear rheology of carbon nanofiber/polystyrene composites. Rheol Acta 45:919-941.

Wapperom P, Leygue A, Keunings R (2005) Numerical simulation of large amplitude oscillatory shear of a high-density polyethylene melt using the MSF model. J Non-Newt Fluid Mech 130:63-76.

Watanabe, H (1999) Viscoelasticity and dynamics of entangled polymers. Prog Polym Sci 24:1253-1403.

West AHL, Melrose JR, Ball RC (1994) Computer simulations of the breakup of colloid aggregates. Phys Rev 49:4237-4249.

Wilhelm M (2002) Fourier-transform rheology. Macromol Mater Eng 287:83-105.

Wilhelm M, Maring D, Spiess HW (1998) Fourier-transform rheology. Rheol Acta 37:399-405.

Wilhelm M, Reinheimer P, Ortseifer M (1999) High sensitivity fourier-transform rheology. Rheol Acta 38:349-356.

Whittle M, Dickinson E (1997) Stress overshoot in a model particle gel. J Chem Phys 107:10191-10200.

Winter HH, Chambon F (1986) Analysis of linear viscoelasticity of a crosslinking polymer at the gel point. J Rheol 30:367-383.

Winter H, Mours M (1997) Rheology of polymers near liquid-solid transitions neutron spin echo spectroscopy viscoelasticity rheology. Adv Polym Sci 134:165-234.

Wohlfarth C (2001). Chapter 6, PVT Data of Molten Copolymers. In CRC Handbook of Thermodynamic Data of Copolymer Solutions, CRC Press.

Xu L, Nakajima H, Manias E, Krishnamoorti R (2009) Tailored nanocomposites of polypropylene with layered silicates. Macromolecules 42:3795-3803.

Xu L, Reeder S, Thopasridharan M, Ren J, Shipp DA, Krishnamoorti R (2005) Structure and melt rheology of polystyrene-based layered silicate nanocomposites. Nanotechnology 16:S514-S521.

Yoonessi M, Gaier JR (2010) Highly conductive multifunctional graphene polycarbonate nanocomposites. ACS Nano 4:7211-7220.

Yziquel F, Carreau PJ, Tanguy PA (1999) Non-linear viscoelastic behavior of fumed silica suspensions. Rheol Acta 38:14-25.

Zeng QH, Yu AB, Lu GQ (2008) Multiscale modeling and simulation of polymer nanocomposites. Prog Polym Sci 33:191-269.

Zhang Q, Archer LA (2002) Poly(ethylene oxide)/silica nanocomposites: structure and rheology. Langmuir 18:10435-10442.

Zhao J, Morgan AB, Harris JD (2005) Rheological characterization of polystyrene-clay nanocomposites to compare the degree of exfoliation and dispersion. Polymer 46:8641-8660.

Zheng X, Xu Q (2010) Comparison study of morphology and crystallization behavior of polyethylene and poly(ethylene oxide) on single-walled carbon nanotubes. J Phys Chem 114:9435-9444.

Zheng X, Xu Q (2010) Comparison study of morphology and crystallization behavior of polyethylene and poly(ethylene oxide) on single-walled carbon nanotubes. J Phys Chem 114:9435-9444.

Zhou T, Zha J-W, Hou Y, Wang D, Zhao J, Dang Z-M (2011) Surface-functionalized MWNTs with emeraldine base: preparation and improving dielectric properties of polymer nanocomposites. Appl Mater Interfaces 3:4557-4560.

Zhu A-J, Sternstein SS (2003) Nonlinear viscoelasticity of nanofilled polymers: interfaces, chain statistics and properties recovery kinetics. Compos Sci Technol 63:1113-1126.

Zhu Z, Thompson T, Wang S-Q, von Meerwall ED, Halasa A (2005) Investigating linear and nonlinear viscoelastic behavior using model cilica-particle-filled polybutadiene. Macromolecules 38:8816-8824.

Appendix A

In order to examine the no-slip boundary condition, shear transient tests were performed with different gaps (1.2, 1.7, 2.4 mm) at a shear rate of 0.1 s^{-1}. From the data shown in fig. A-1, it is clear that there is no significant deviation between the data. Usually, significant slip occurs at Weissenberg (Wi) numbers much higher than unity which is not the case in our work (the highest value was 0.67). Also, considering the sticky nature of EVA, it is believed that wall slip is not happening (significantly) at least for the shear rates that were used here (up to 5 s^{-1}). Although edge fracture can be happening in some samples, our tests did not present such effect which limits the maximum shear rate that can be applied.

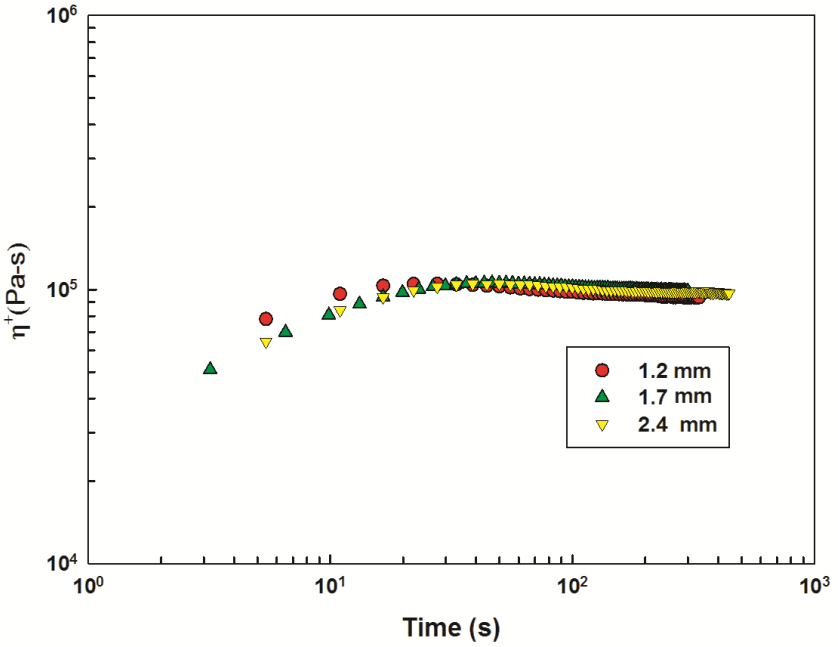

Figure A-1: Transient shear viscosity of EVA 0 at a shear rate 0.1 s^{-1} and 110°C with different gaps.

Appendix B

Time sweep tests performed on clay nano-composites (see figure B-1) show a continuous modulus evolution within the experimental time frame (about 4500 s). However, after the initial time (5–10 min), the rate of increase was very small.

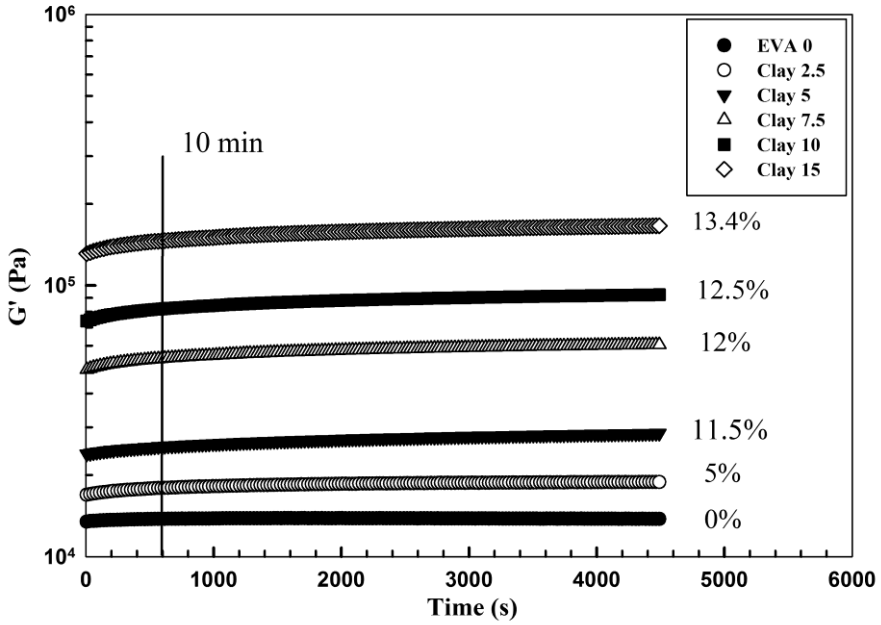

Figure B-1: Modulus evolution of EVA and clay nano-composites in a time sweep test (ω = 0.5 rad/s, T = 110°C, γ = 2%).

Appendix C

From equations (5-6a) and (5-6b), the shear and uniaxial counterparts of the MSF model can be written as follow:

Shear:

$$\frac{\partial f_s}{\partial \gamma} = f_s \left(S_{12} - \frac{f_s (f_s^3 - 1)}{\lambda} \right) \tag{C-1}$$

$$\frac{\partial f^2}{\partial \gamma} = \beta f^2 \left(S_{12} - \frac{(f^2 - 1)}{2\left(f_{\max}^2 - 1\right)} \sqrt{S_{11} + S_{22}} - \frac{a_2 (f^2 - 1)}{2} \sqrt{|S_{11} - S_{22}|} \right) - (\beta - 1) \frac{\partial f_s^2}{\partial \gamma} \tag{C-2}$$

Uniaxial:

$$\frac{\partial f_s}{\partial \varepsilon} = f_s \left(S_{11} - S_{33} - \frac{f_s (f_s^3 - 1)}{\lambda} \right) \tag{C-3}$$

$$\frac{\partial f^2}{\partial \varepsilon} = \beta f^2 \left(S_{11} - S_{33} - \frac{f^2 - 1}{f_{\max}^2 - 1} \sqrt{S_{11} + \frac{1}{2} S_{33}} \right) - (\beta - 1) \frac{\partial f_s^2}{\partial \varepsilon} \tag{C-4}$$

Figure C-1 shows the numerical solution of Eq. (C-1) in shear flows. As seen, f_s has a maximum around a shear strain of 3.5. At large strains, f_s goes back to the initial value of one. This means the molecule is simply oriented in the flow direction and, due to dissipative constraint release, the tube diameter returns to its equilibrium value a_0. Also, increasing *De* has no significant effect on f_s in shear flows.

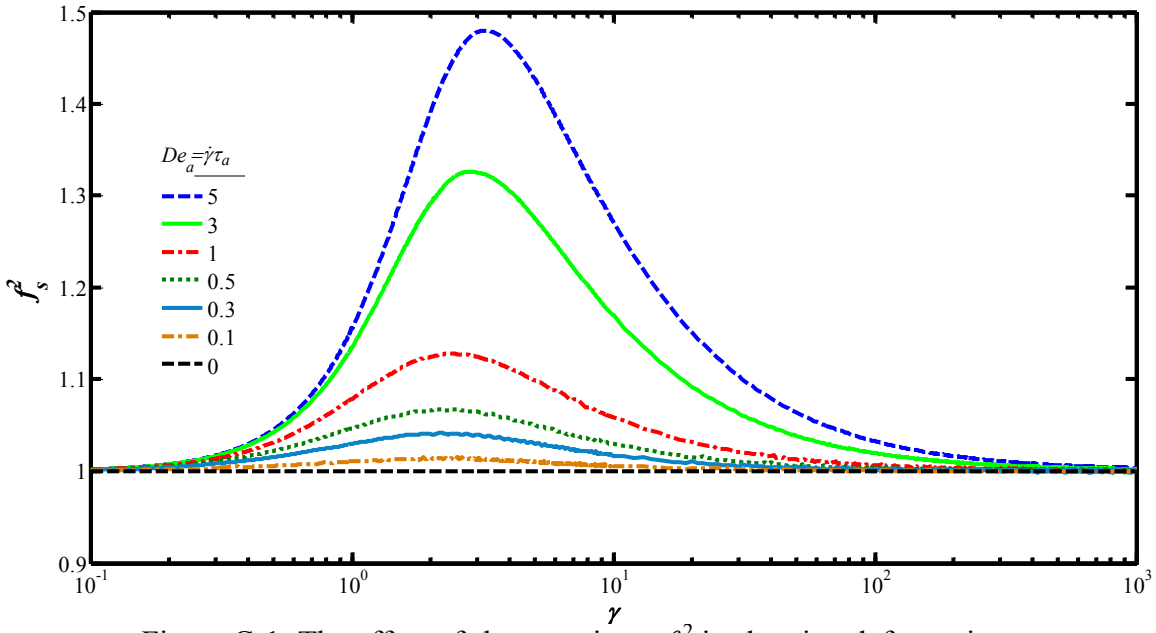

Figure C-1: The effect of shear strain on f_s^2 in shearing deformation.

Figure C-2 illustrates the numerical solution of Eq. (C-2) at different Deborah numbers. As expected, f_s^2 grows monotonically and reaches a constant value of $f^2_{s,max}$ for Deborah numbers higher than 0. At $De_a = 0$ no stretching is imposed to the side chains and $f_s = 1$.

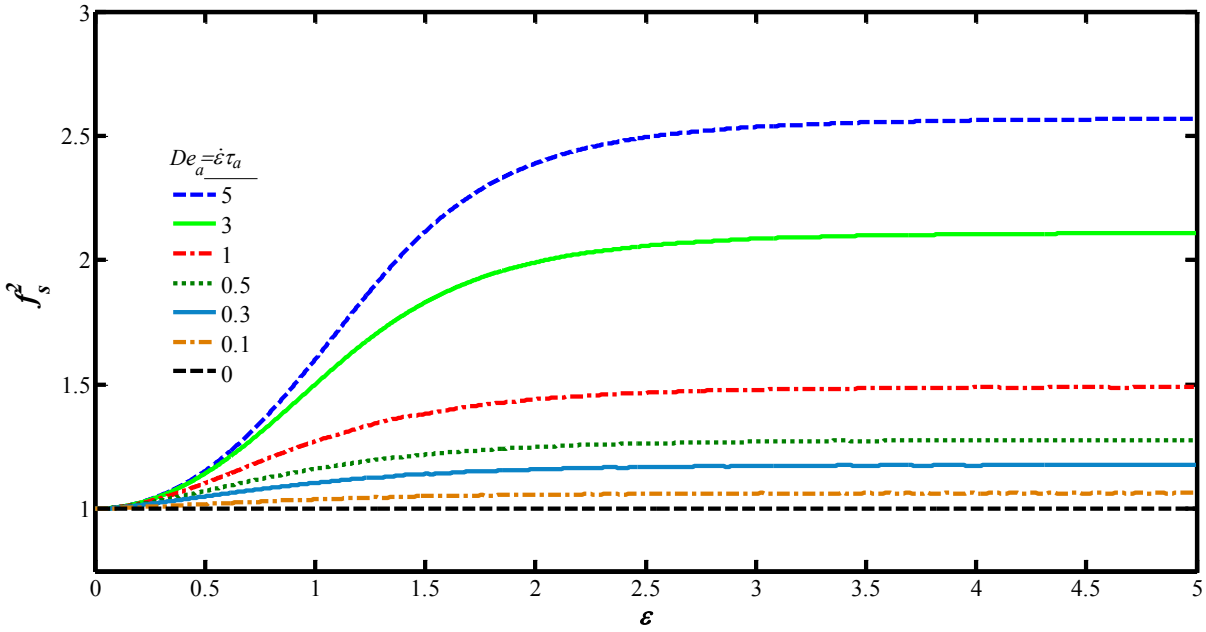

Figure C-2: f_s^2 versus uniaxial strain at different Deborah numbers.